DESIGN, FABRICATION AND DELIVERY OF AN IMPROVED SINGLE ELASTIC LOOP MOBILITY SYSTEM (ELMS)

Volume II

Technical Report

July 1972

HREC-7737-2
LMSC-HREC D225600-II

COPY NO.

LOCKHEED MISSILES & SPACE COMPANY, INC.
HUNTSVILLE RESEARCH & ENGINEERING CENTER
HUNTSVILLE RESEARCH PARK
4800 BRADFORD DRIVE, HUNTSVILLE, ALABAMA

DESIGN, FABRICATION AND DELIVERY OF AN IMPROVED SINGLE ELASTIC LOOP MOBILITY SYSTEM (ELMS)

Volume II

Technical Report

July 1972

Contract NAS8-27737

Prepared for National Aeronautics and Space Administration
Marshall Space Flight Center, Alabama 35812

by

W. Trautwein

APPROVED: T.R. Beal

T. R. Beal, Manager
Dynamics & Guidance Department

George D. Rogers for J. S. Farrior

Resident Director

FOREWORD

This final report documents the results of a 10-month effort to finalize the design and fabricate an improved version of Lockheed's Elastic Loop Mobility System (ELMS). This effort was performed under Contract NAS8-27737 by Lockheed's Huntsville Research & Engineering Center for the National Aeronautics and Space Administration, George C. Marshall Space Flight Center (MSFC), Alabama, and it was sponsored by the Advanced Development Office, Advanced Manned Missions, NASA Headquarters. Dr. N. C. Costes of the Space Sciences Laboratory was the MSFC Contracting Officer's Representative (COR), with Mr. C. S. Jones, Jr., of the MSFC Astrionics Laboratory as the alternate COR.

Dr. W. Trautwein was the project engineer at Lockheed. He was assisted by Dr. C. J. Chang and Mr. G. P. Gill in engineering and design and by Mr. K. R. Leimbach in structural analysis.

Substantial support in manufacturing and metallurgical testing was obtained from the Process Engineering Laboratory's Research & Process Technology Division under Mr. W. Angele and, in particular, by Mssrs. J. R. Williams, P. G. Parks, E. A. Hasemeyer, V. H. Yost, and H. P. Irwin.

The assistance provided by Messrs. F. J. Nola and E. H. Berry of the Advanced Technology Branch, MSFC Astrionics Laboratory in providing high-performance electric drive motors and controllers for the test vehicle is gratefully acknowledged.

This report is divided into two volumes:

Volume I – Executive Summary Report
Volume II – Detailed Technical Report

Design details are documented in the form of engineering-type drawings, a reproducible set of which is submitted under this contract.

PROPRIETARY NOTICE

CONTENTS

CONTENTS (Continued)

CONTENTS (Continued)

Section 1
INTRODUCTION

The development rationale of an improved version of Lockheed's Elastic Loop Mobility System (ELMS) was based on soil mechanics and wheel-soil interaction data obtained during the Apollo lunar manned missions (Refs. 1 through 11). Under this contract, the detailed design and fabrication requirements were set forth for the following major systems and components:

- Elastic loop and associated new manufacturing tools.
- Major drive system components including the integration of new electric drive motors (GFE) and frictionless drive drums.
- Chassis design with provisions for integrating remote control and telemetry data system provided GFE.
- Grousers for improved traction.
- Adjustable shock absorbers.
- Support trailer.
- Instrumentation for performance testing.

According to the Work Statement, shown in part in Appendix A, the test vehicle had to be compatible with the mobility testing apparatus of the U. S. Army Engineer Waterways Experiment Station (WES). The onboard instrumentation required checkout and calibration before delivery to the Marshall Space Flight Center.

This detailed technical report documents the design rationale, engineering analyses, and manufacturing approach chosen to achieve the program objectives. Complete design details are documented in the form of engineering type drawings, a reproducible set of which is submitted under the contract.

Finally, preliminary test results from the Acceptance Test Program performed at WES are presented here and compared with data from the performance evaluation tests conducted at WES on the first-generation ELMS (Ref. 12).

Section 2
ELASTIC LOOP FABRICATION FOR UNIFORM PRESSURE DISTRIBUTION AND HIGHER LOAD CAPABILITY

2.1 FIRST-GENERATION LOOP FABRICATION AND PERFORMANCE

A first-generation ELMS test vehicle had been built in 1970 under Lockheed's Independent Development program and was tested under NASA Defense Purchase Request H-74660A at the U. S. Army Engineer Waterways Experiment Station (WES) in Vicksburg, Miss. (Ref. 12).

First-generation elastic loops had been fabricated from annealed Ti-6Al-4V titanium alloy in the following steps:

1. Weld cylindrical ring of 1.3 mm (0.050 in.) sheet.
2. Anneal in vacuum furnace at 1400°F for 15 minutes, furnace cool to 800°F, aircool.
3. Trim to width of w = 35.6 cm (14 in.).
4. Rollform to obtain transverse curvature in straight loop sections of radius $r \approx w$.

The rollforming was performed in a single-stand rollforming machine built by Lockheed-Huntsville for manufacturing elastic loops. As shown in Fig. 2-1, the loop is held in an oval shape and laterally guided by two pairs of guide rolls. In the middle of the upper straight section the loop passes through a set of three spherical rolls (one driven roll below, two passive rolls above loop), emerging from the rolls with a uniaxial bend radius in the longitudinal direction. After each loop revolution the roll stand is shifted laterally by a fixed amount (4 to 5 mm). After the complete width is bent by this process, the loop assumes the shape of Fig. 2-2.

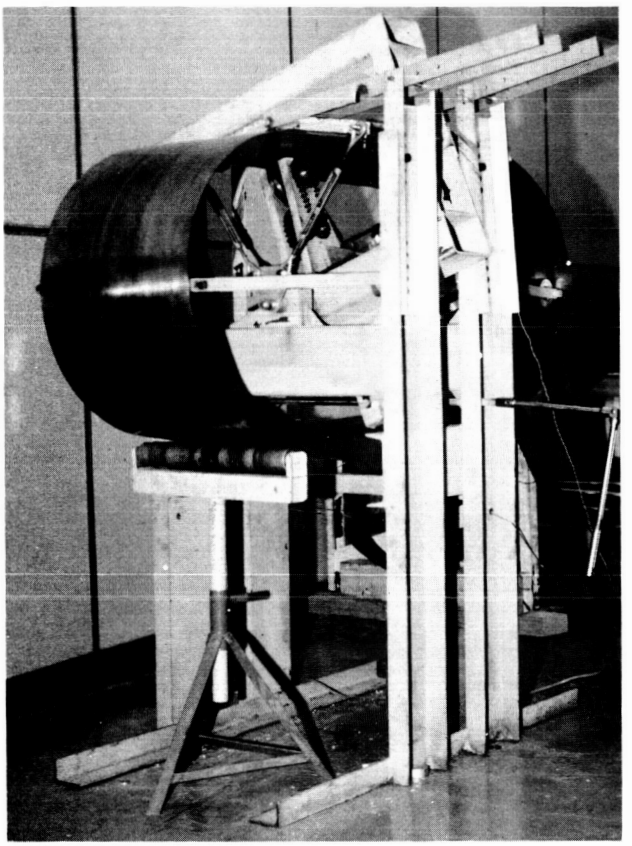

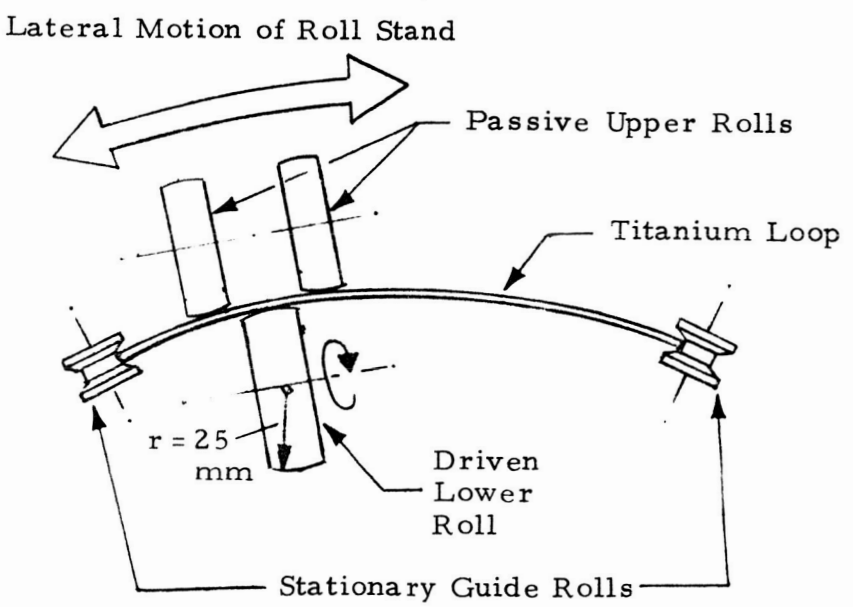

Fig. 2-1 - Single-Stand Rollforming Machine to Bend Transverse Curvature into Welded Elastic Loops

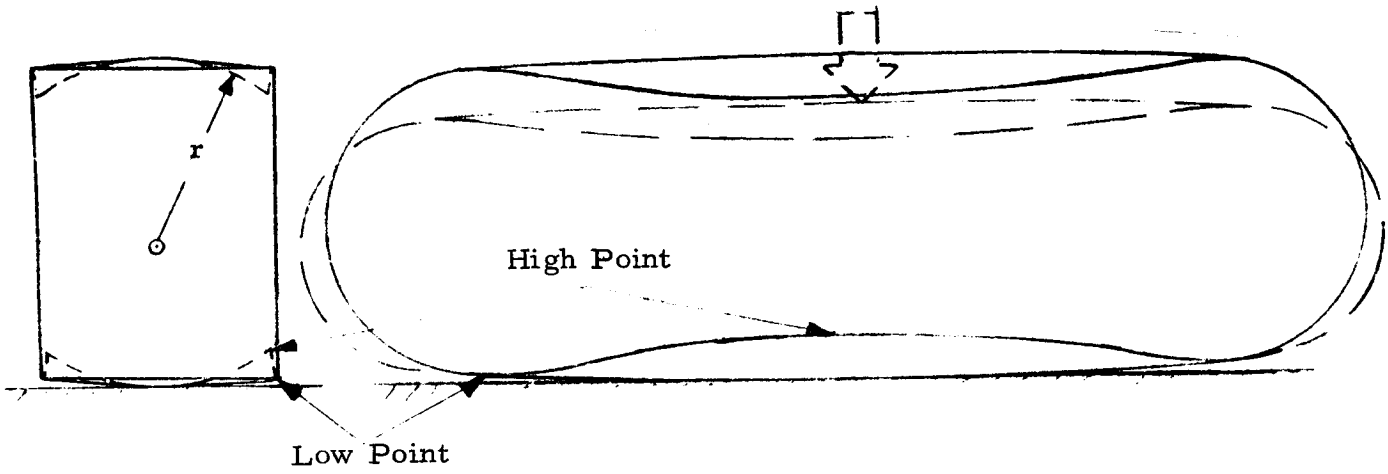

Fig. 2-2 - First-Generation Elastic Loop "A" Formed from Flat Ring ($r \approx r_b$). Note concave bow of edges along the straight sections.

The edges along the straight sections are curved longitudinally with a high point at the center and low points at the ends of the bottom section. The resulting footprint in soil exhibits strong variations in contact pressure with large areas of zero or near zero pressure under the loop's mid section which contribute nothing or very little to the tractive effort.

Treading the outer surface by installing large grousers would not improve the footprint significantly because the load would be concentrated at the front and rear grousers with no or little load shared by the grousers located in the mid section. This unfavorable footprint was the main reason why the first-generation ELMS did not show the high pull characteristics typical for tracks.

2.2 SECOND-GENERATION LOOP DESIGN

Upon completion of the first-generation ELMS, another independent development effort was started to improve the footprint characteristics of elastic loops and to increase the load-carrying capability of loop/soil systems. A new forming concept resulted (Ref. 2) which involved two major manufacturing steps:

1. Bulge Forming of a cylindrical metal ring.
2. Bending or rollforming in the longitudinal direction.

Small-scale model loops were manufactured to verify the concept using annealed Ti-6Al-4V material. A spherical or near-spherical bulge in the previously flat ring as shown in Fig. 2-3 was expected to shorten the loop's circumference edge sections by the amount necessary to straighten the lower edges under load.

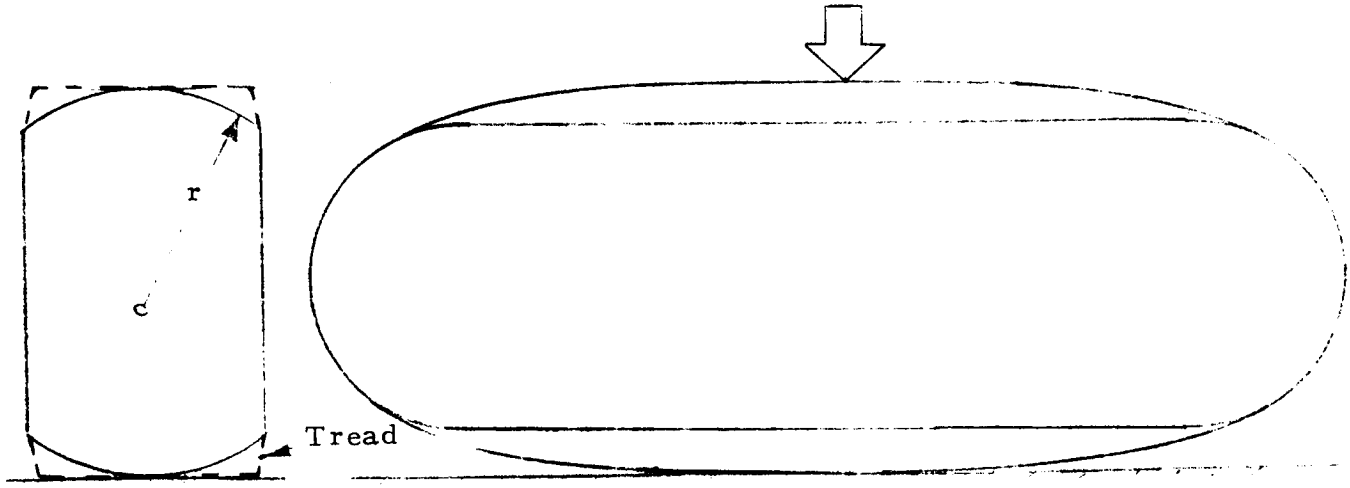

LOOP "B" FORMED FROM STRETCHED RING ($D_0 > D_1$)

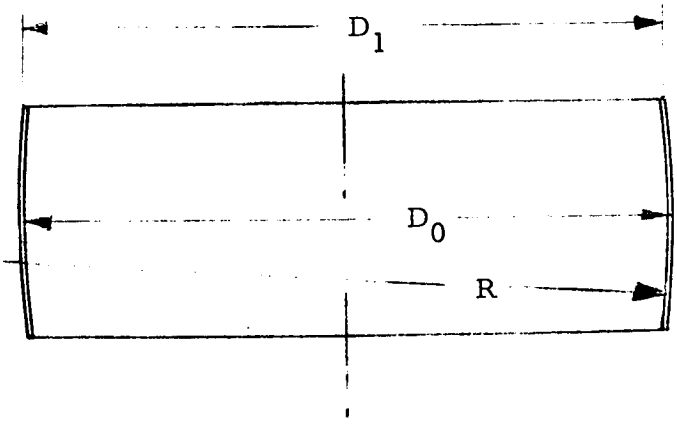

$D_0 - D_1$ = 4 mm (0.160 in.)

R/r = 6

Fig. 2-3 - Bulge Forming of Second-Generation Elastic Loop and Additional Rollforming Results in Constant Height of Edges above Ground. Uniform ground pressure distribution can be achieved by treading outer surface.

The model fabrication experiments were successful. Near-linear edge sections were obtained which permitted the installation of large grousers for near-planar footprint characteristics. Based on these model loops, the major design parameters for full-scale loops could be readily derived by scaling up all linear dimensions.

The spring and stress characteristics of bulge- and rollformed loops were derived and verified by testing available loops under load (Appendix B).

2.2.1 Material Selection for Elastic Loops

Due to the higher load capability desired for second-generation loops, the high fatigue life required in future loops after welding and cold forming operations, several advanced materials were evaluated for possible use as loop material. The screening of high strength-to-weight materials centered around recently developed titanium alloys with improved cold formability and higher ultimate tensile strength than the previously used Ti-6Aℓ-4V alloy in the annealed condition. Two titanium alloys were selected on the basis of available physical properties listed in Table 2-1, and shown in Fig. 2-4, with the standard Ti-6Aℓ-4V alloy for comparison which must be used in the annealed condition to avoid water quenching. To reduce the risk of late delivery, both "Beta III" and "Transage 129" sheets, 0.065 inches thick, were ordered from different sources.

The Beta III material arrived first and was therefore used for fabricating the first loop. The test certificate is shown in Fig. 2-5.

2.2.2 Elastic Loop Sizing

Based on test results from models and the first-generation loop, the loop size was modified to accommodate higher loads. At the same time, an effort was made to increase available spring travel and reduce the maximum tensile stresses. The following loop dimensions were chosen (dimensions of first-generation ELMS in parentheses):

Table 2-1

PHYSICAL PROPERTIES OF EVALUATED TITANIUM ALLOYS
(0.063 in./0.050 in. sheet)

		Ti-6Al-4V Annealed	Ti-11.5Mo-6.5Zr-4.6Sn (Beta III)		Ti-2Al-11.5V-2Sn-11.3Zr (Transage 129)	
			Mill S.T.	Age Hardened 950-8hr-AC**	Mill S.T.	Age Hardened 1200°F-1hr-AC 800°F-24hr-AC
Base Metal	Tensile Yield Stress, σ_{ty} (ksi)	120	113	178.5		186 (160)*
	Ultimate Tensile Stress, σ_{tu} (ksi)	130	127.7	196	109	203 (173)
	Elongation, $\Delta\ell/\ell$ (%)	8	16.7	5.5	16	6 (8)
	σ_{max} for $\geq 10^6$ cycles to failure of notched specimen (Fig. 2-4) (ksi)	41				58
	Modulus of Elasticity, E (psi)	16×10^6	10×10^6	15×10^6	10.5×10^6	14.2×10^6
	Min. Bend Ratio r/t (t = thickness)	4	2		2	
Butt Welded	σ_{ty} (ksi)	127		162.4		162.5
	σ_{tu} (ksi)	140		174.5		165.5
	Elong. (%)	8		4.9 (Ref. 14) 0.5 to 1.5 (tested)		2.5
	Density (g/cm^3)	4.4	5.1		4.8	

*Values in parentheses refer to age hardening at 1350°F, 15 min, AC; 1200°F, 1 hr, AC; 900°F, 4 hr, AC.

**AC = air cooled.

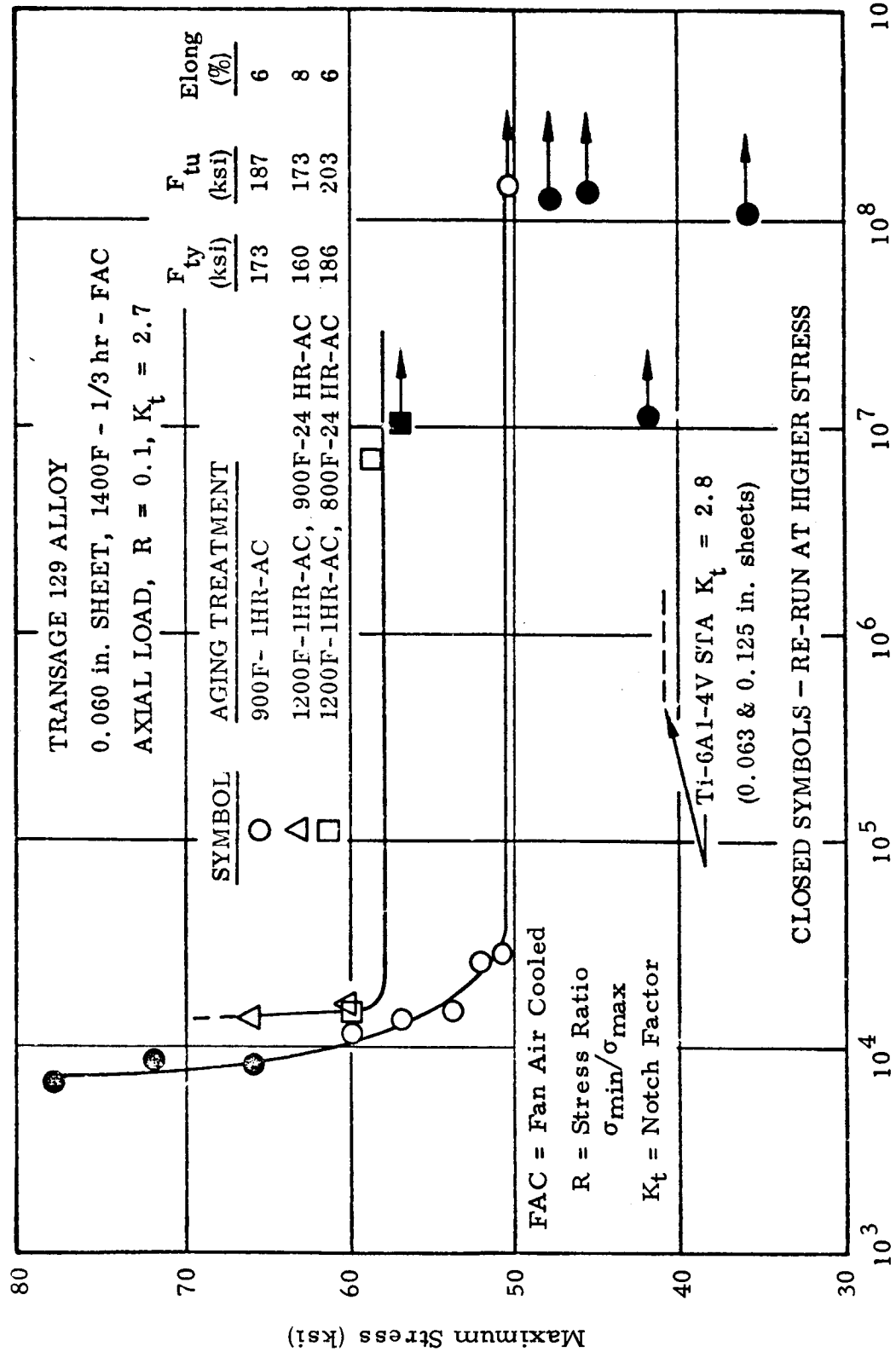

Fig. 2-4 - Axial Fatigue Data (R = 0.1) for Center Hole Notch Sheet Specimen of Transage 129 Compared with STA Ti-6Al-4V Alloy

Crucible SP 25 500 REV 4 71

Colt Industries **Crucible Inc** 412 - 643 1100

STAINLESS STEEL DIVISION, MIDLAND, PA. 15059 091

GRADE	PROD	MPG	CUSTOMER CODE	SHIPPED FROM	DATE SHIPPED	INSTRUCTIONS
60123	15	245	8432783-01	MIDLAND PA	06/16/1	

SOLD TO: LOCKHEED MISSILES & SPACE CO
4800 BRADFORD DRIVE
HUNTSVILLE ALABAMA 35807

SHIP TO: S

412 - 643 - 1100

PAPERS		BL	SN	CT	INV	HA	HRD	NTZ
	SOLD	1	1	3	3	Y	Y	Y
	SHIP					N		

ITEM	CUSTOMER ORDER NO.	OUR ORDER NO.	DESCRIPTION	SIZE
	H-6037 1 05-19	7P4100381	BETA III CR A SOL TRT & WATE - R QUENCHED	18 X .066 165 IN

HEAT NO.	C	O	H	SN	~~BO~~ N	FE	MO	ZR
K50403	.01	.112	.0077	4.6	.012	.05	11.5	6.5

HEAT #	COIL #	QUANTITY	GRAIN	HARDNESS	YIELD	TENS.	BND	DG&FAC	ELONG %&GL	RA %	CHAR	IZOD
K50403	925703	0			XL 113325	127762		OK	16.7			
K50403	925703	80			XT 108275	124550		OK	17.0			

MARGARET G. MORRIS Notary Public
MIDLAND BEAVER COUNTY
MY COMMISSION EXPIRES
JANUARY 14, 1974

JUN 1971 PROCUREMENT

SWORN TO AND SUBSCRIBED BEFORE ME

THIS 18TH DAY OF JUNE 19 71

Margaret G. Morris
NOTARY PUBLIC

Colt Industries **Crucible Inc**

CERTIFICATE OF TEST

THE TEST RESULTS SHOWN IN THIS REPORT ARE CORRECT TO THE BEST OF OUR KNOWLEDGE AND BELIEF.

COLT INDUSTRIES CRUCIBLE Inc

CERTIFIED BY: A. J. Zebrowsky
REPRESENTATIVE

Fig. 2-5 - Manufacturer's Test Data for Loop Material

Loop Width: b = 38.8 cm (35.6 cm)

Loop Thickness: t = 1.6 mm (1.27 mm)

Loop Circumference: L = 3.68 m (4.06 m)

Overall Loop Length
Under Nominal Load: 1.6 m (1.78 m)

Bulge Radius: 15 m

2.2.3 Prediction of Spring Characteristics and Stresses for Elastic Loop

For the selected loop size the following spring and stress characteristics were calculated using the formulas derived in Appendix B.

Assumed Nominal Load W_o:

$$W_o = 557 \text{ N } (125 \text{ lb})$$

Nominal Load F_o to be Carried by Loop under the Assumption that the Lower Half of the Loop Rests on the Ground:

$$F_o \approx W_o - \frac{1}{2} W_{Loop}$$

where

W_{Loop} = weight of assembled loop (incl. grousers)

= 148 N (33 lb)

Thus

F_o = 557 - 74

= 483 N (108.5 lb)

Beta III Data (Table 2-1):

Modulus of Elasticity $E = 10.3 \times 10^6 \text{ N/cm}^2$ $(15 \times 10^6 \text{ psi})$

Poisson's Ratio $\nu = 0.3$

According to Eq. (B-3), Appendix B, the bending rigidity of the loop is:

$$B = \frac{Et^3}{12(1-\nu^2)} = 3840 \text{ N-cm}$$

The load-deflection law is given by Eq. (B-10), Appendix B:

$$F = \pi b B K_b^{(1)2} \left[1 - \frac{K_b^{(0)} + \nu(K_b^{(1)} - K_b^{(0)})}{K_b^{(1)}} \right]$$

where K_b is the longitudinal curvature in the bent loop section (Fig. B-1), superscript (0) denotes no load, superscript (1) denotes load F. Under no load:

$$K_b^{(0)} = 0.0236 \text{ cm}^{-1}$$

Thus

$$F = 4.69 \times 10^5 K_b^{(1)2} \left[1 - \frac{0.0236 + 0.3(K_b^{(1)} - 0.0236)}{K_b^{(1)}} \right] \quad \text{(N)}$$

$$= 4.69 \times 10^5 K_b^{(1)} \left[(1 - 0.3) K_b^{(1)} - (1 - 0.3) 0.0236) \right] \quad \text{(N)}$$

$$\boxed{F = 4.69 \times 10^5 K_b^{(1)} \left[0.7 K_b^{(1)} - 0.0166 \right] \quad \text{(N)}}$$

This spring-deflection characteristic is plotted in Fig. 2-6.

Maximum stress, σ_{max}, can be predicted using Eq. (B-11), Appendix B:

$$\sigma_{max} = \frac{6B}{t^2} \left[K_b^{(1)} - K_b^{(c)} - K_q^{(c)} \right],$$

where superscript (c) denotes "loop in circular form." For

$$K_b^{(c)} = 0.0171 \text{ cm}^{-1}, \qquad K_q^{(c)} = 0.0002 \text{ cm}^{-1},$$

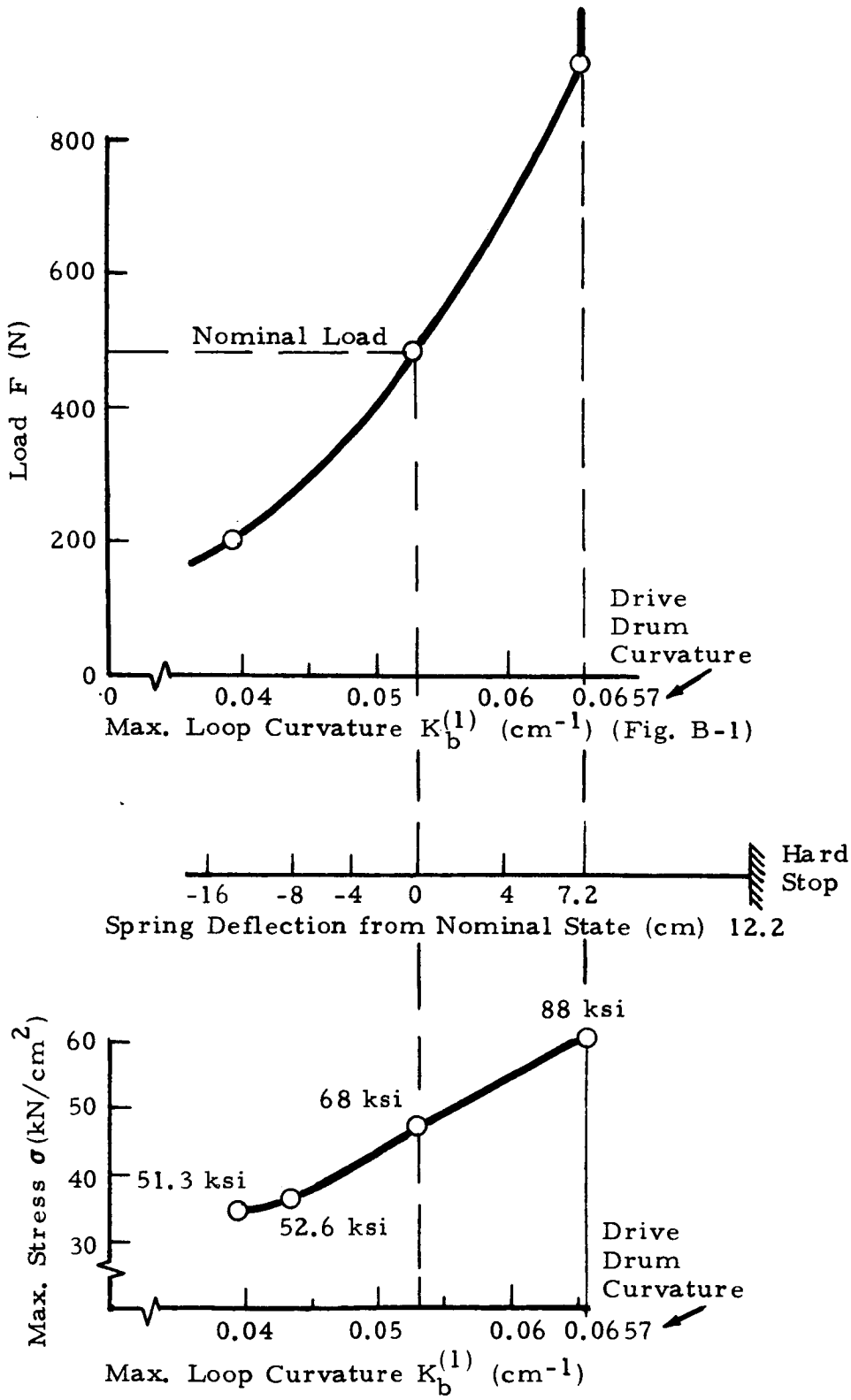

Fig. 2-6 - Predicted Spring-Deflection and Stress Characteristics of Second-Generation Elastic Loop of Beta III

one obtains,

$$\sigma_{max} = 8.7 \times 10^5 \left[K_b^{(1)} - 0.0173 \right] \frac{N}{cm^2} ,$$

which is also plotted in Fig. 2-6. The curves indicate that the new loop can well carry loads between 270 N and 670 N (60 and 150 lb) as specified in the Work Statement. The maximum stresses under nominal load (557 N = 125 lb) of 47 kN/cm^2 (68,000 psi) would be far too high for long fatigue life of Ti-6Aℓ-4V loops and is even 17% too high if the new Transage alloy were used which has 58,000 psi safe stress levels for infinite fatigue life (10^6 cycles to fatigue of notched specimens, see Table 2-1).

By an empirical formula for the available spring deflection, x, of a loop:

$$x = \frac{2}{K_b} - D_d + 5 \text{ cm} ,^*$$

where D_d = drive drum diameter, the loop curvature in Fig. 2-6 can be related to vertical spring deflection as shown by the additional scale.

2.3 TOOL DESIGN FOR LOOP MANUFACTURE

In a small-scale pilot study the new forming concept of Ref. 13 was tried out which also helped in tool design for full-scale loop fabrication. Due to the short length of the strips for model loops of 65 cm, the transverse curvature could be achieved by multiple brake bending of the flat strip before welding instead of rollforming the welded loops.

The required bulge shown in Fig. 2-3 was formed by trapped-rubber forming using a female contoured die sketched in Fig. 2-7. This manufacturing experiment was successful. The model loops made had the desired virtually straight lower edge sections. One model loop was subsequently delivered to MSFC's Space Sciences Laboratory for performance testing under the direction of Dr. N. C. Costes.

*Additional 5 cm spring deflections are gained in the transition region from curvature K_b to the straight section.

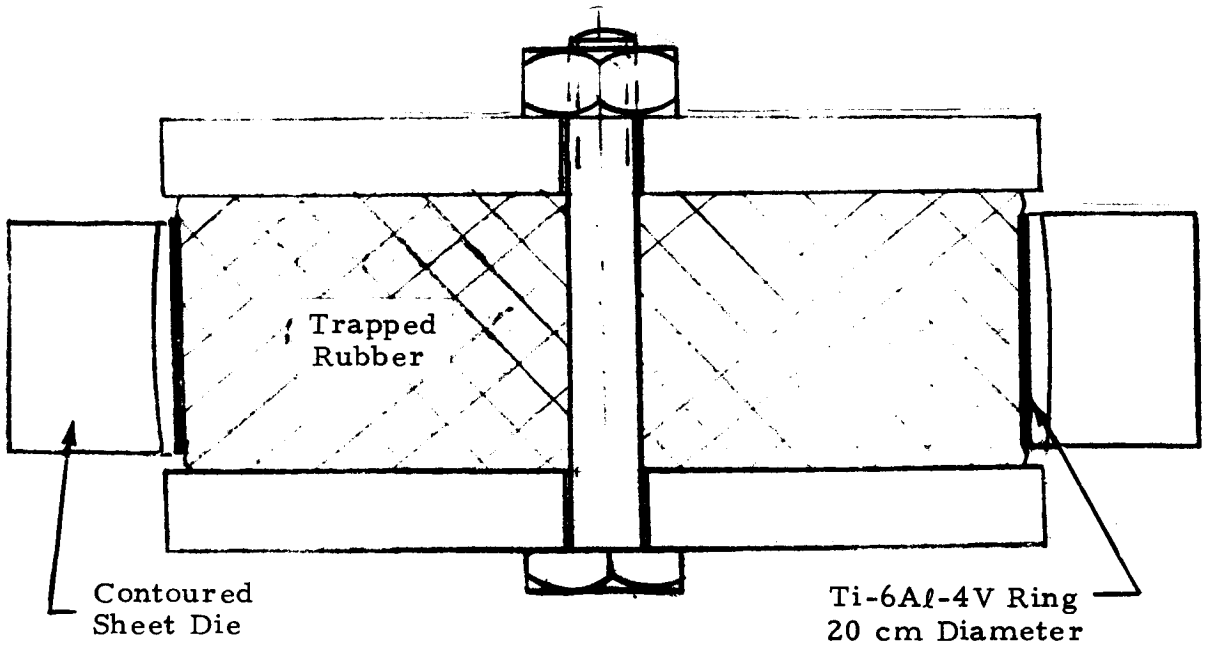

Fig. 2-7 - Bulge-Forming Tool Used in Pilot Study to Manufacture Second-Generation Elastic Loops

In designing a scaled-up bulge-forming tool for manufacturing loops of 1.2 m diameter, an effort was made to copy the model forming process as closely as practical. The first design shown in Fig. 2-8 was based on the trapped rubber process where the rubber was to be deformed in a hydraulic press with several hundred tons capacity.

In the final tool design a suggestion by Mr. J. R. Williams, S&E-PE-M, was followed to replace the big rubber pad by a solid core surrounded by a water-filled bladder (truck inner tube) as sketched in Fig. 2-9 and shown in partially opened condition in Fig. 2-10.

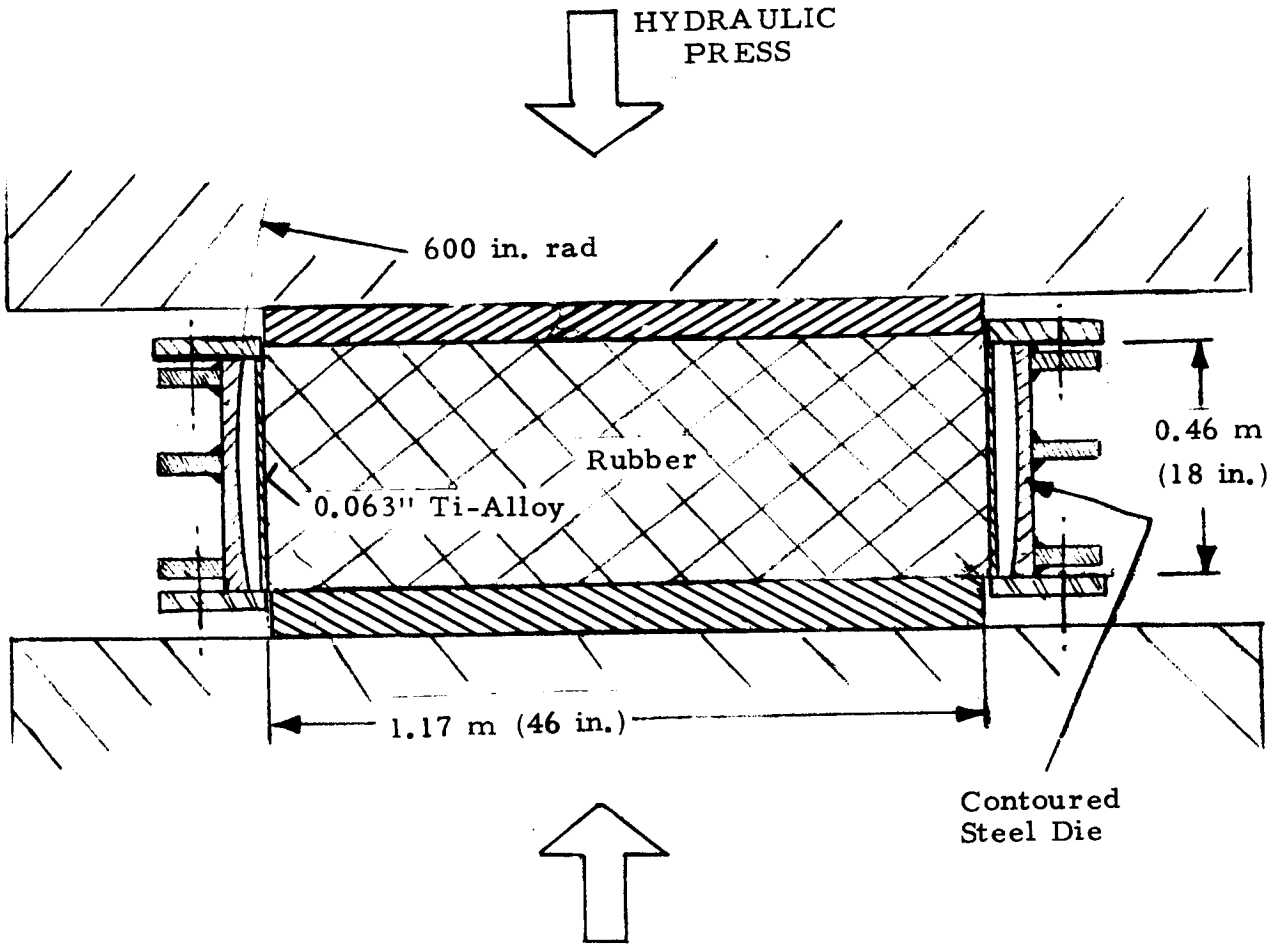

Fig. 2-8 - First Tool Design for Bulge Forming of Full-Scale Second-Generation Loops

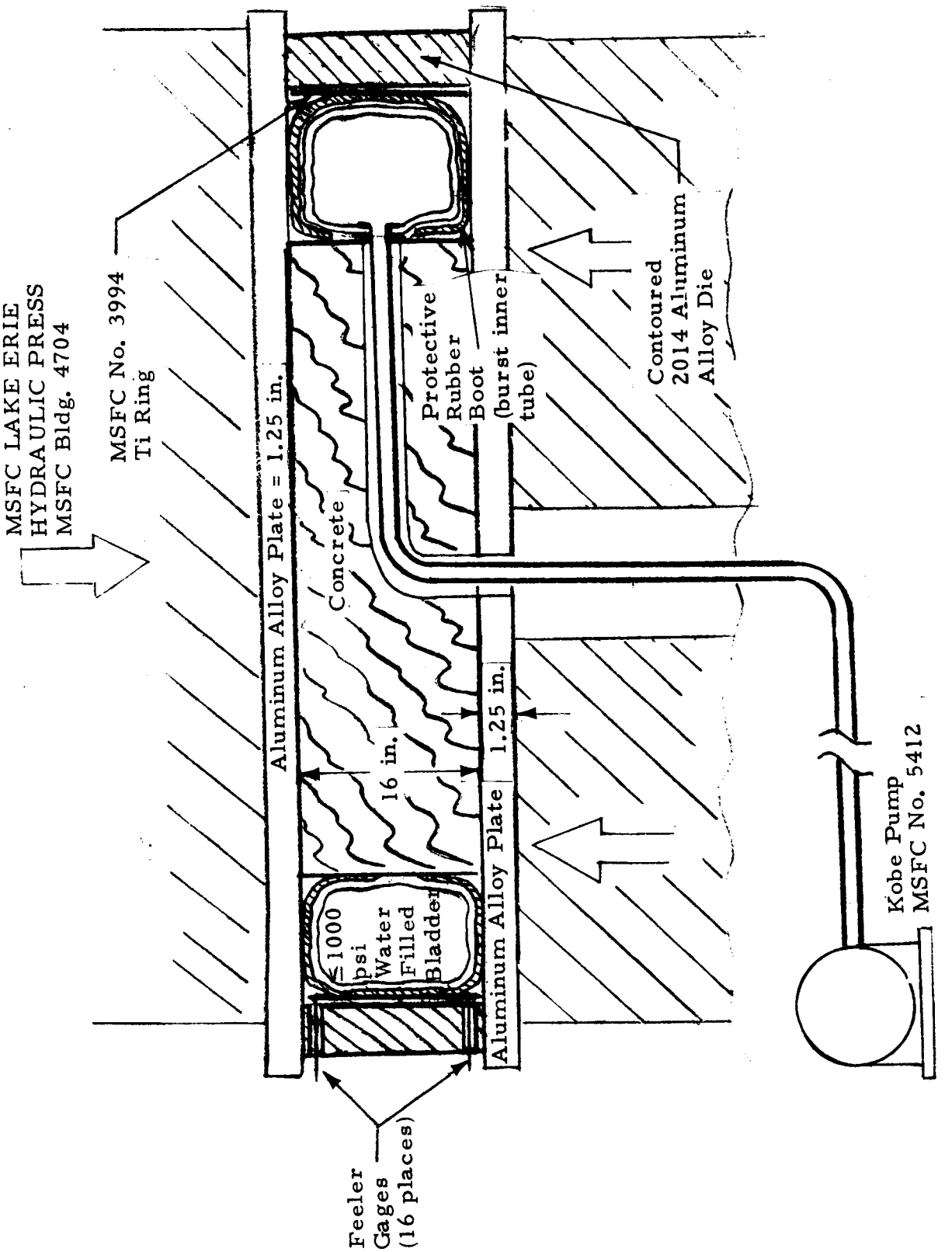

Fig. 2-9 - Schematic View of Final Design of Bulge Forming Tool

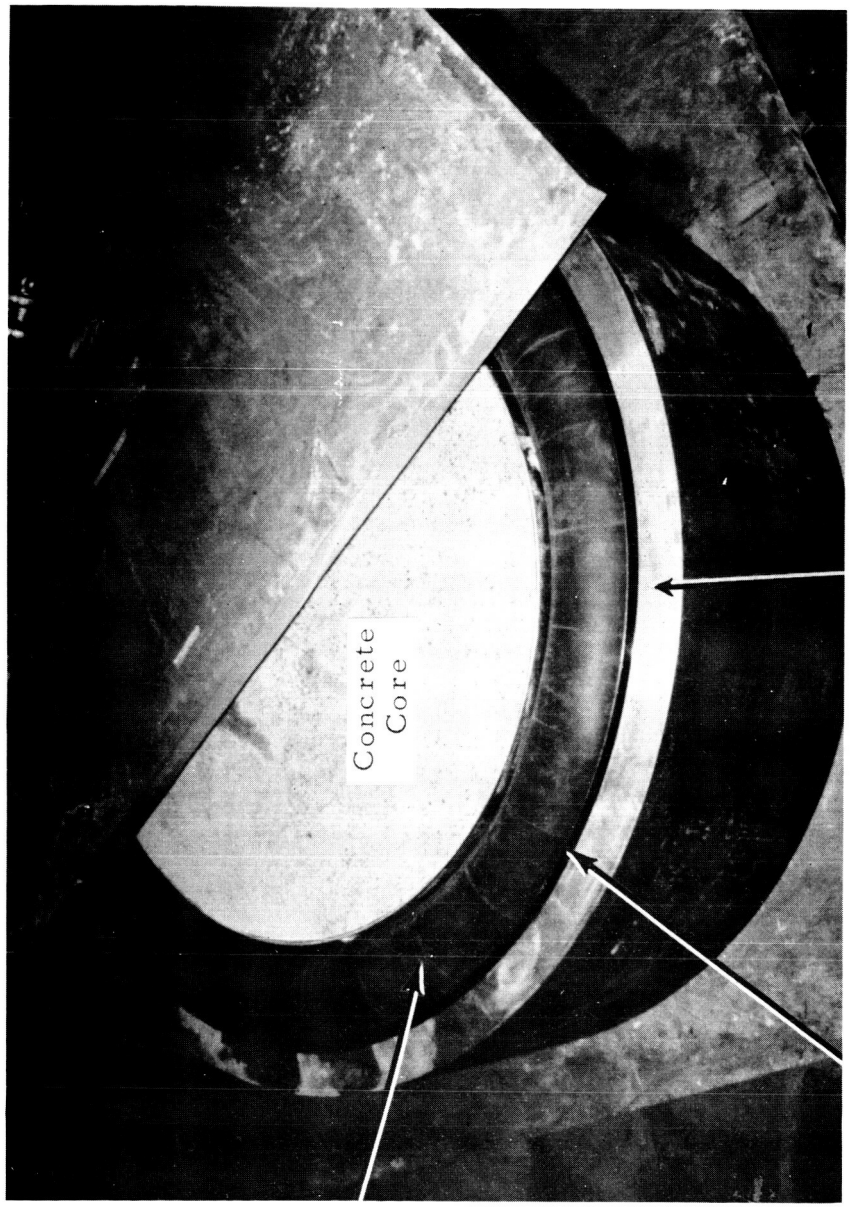

Fig. 2-10 - Bulge Forming Tool for Elastic Loop Manufacturing

2.3.1 Design of Outer Die

The required pressure and die size to cold form the loop can be estimated by analyzing the loop stress-strain relationships as follows:

Beta III Data, Mill Annealed:

$$\sigma_{ty} = 78 \text{ kN/cm}^2 \qquad (113.3 \text{ ksi})$$

$$E = 6.9 \times 10^3 \text{ kN/cm}^2 \quad (10 \times 10^3 \text{ ksi})$$

Approximate Strain, ϵ_y, at Yield Point:

$$\epsilon_y = \sigma_{ty}/E$$

$$= 0.0113 = 1.13\%$$

Selected Total Strain when Loop Makes Contact with Die:

$$\epsilon_{total} = 2.5\%$$

This strain level was used to size die inside diameter (I.D.) (47.377 in.) based on specified loop outside diameter (O.D.) (46.221 in.).

Internal Pressure Required to Reach Yield Stress in Loop (thin wall hoop stress formula):

$$\frac{t\sigma_y}{r} \leq p < \frac{t\epsilon_y E}{r} ,$$

where r is loop radius (23.077 in.) and t thickness (0.063 in.). Thus,

$$450 \text{ N/cm}^2 \leq p < 985 \text{ N/cm}^2$$

$$(310 \text{ psi} \leq p < 680 \text{ psi})$$

The required pressure should be closer to the lower estimate because the stress-strain curve flattens substantially once the yield point is reached. For design purposes it was assumed that up to $p = 2180\ N/cm^2$ (1500 psi) may be applied during forming.

2.3.2 Die Material Selection

Aluminum Alloy 2219-T87

$\sigma_{ty} = 35\ kN/cm^2$ (51 ksi) Elong. = 6%

$\sigma_{tv} = 44\ kN/cm^2$ (64 ksi) $E = 7.25 \times 10^3\ kN/cm^2$ $(10.5 \times 10^3\ ksi)$

Weld Joint Strength: $\sigma_{tv} = 23.5\ kN/cm^2$ (34 ksi)

The availability of the required amount and size for the die as GFE had been confirmed by MSFC's Technical Materials Division before start of contract. When material was requested, this material was no longer available. Instead, plate of alloy 2014 was offered as replacement. In the heat-treated condition-T6, it has the same listed weld joint strength of 23.5 kN/cm^2 (34 ksi) and was, therefore, accepted to avoid a program delay.

Required Wall Thickness for Die, Using Hoop Stress Formula for Thin Wall Cylinder:

$$t \geq \frac{p D}{2\sigma_{Die}}$$

Assuming as a worst case a fractured titanium loop, the total bladder pressure acts on the die. Thus

$$t \geq \frac{1500 \times 47.1}{2 \times 34{,}000} = 1.04 \text{ in.}$$

Safety Factor: 2

Selected: $t = 2\frac{5}{16}$ in. (including allowance for machining inner wall)

Engineering drawings are shown in Figs. 2-11 and 2-12.

To be Rolled, Welded, Heat Treated

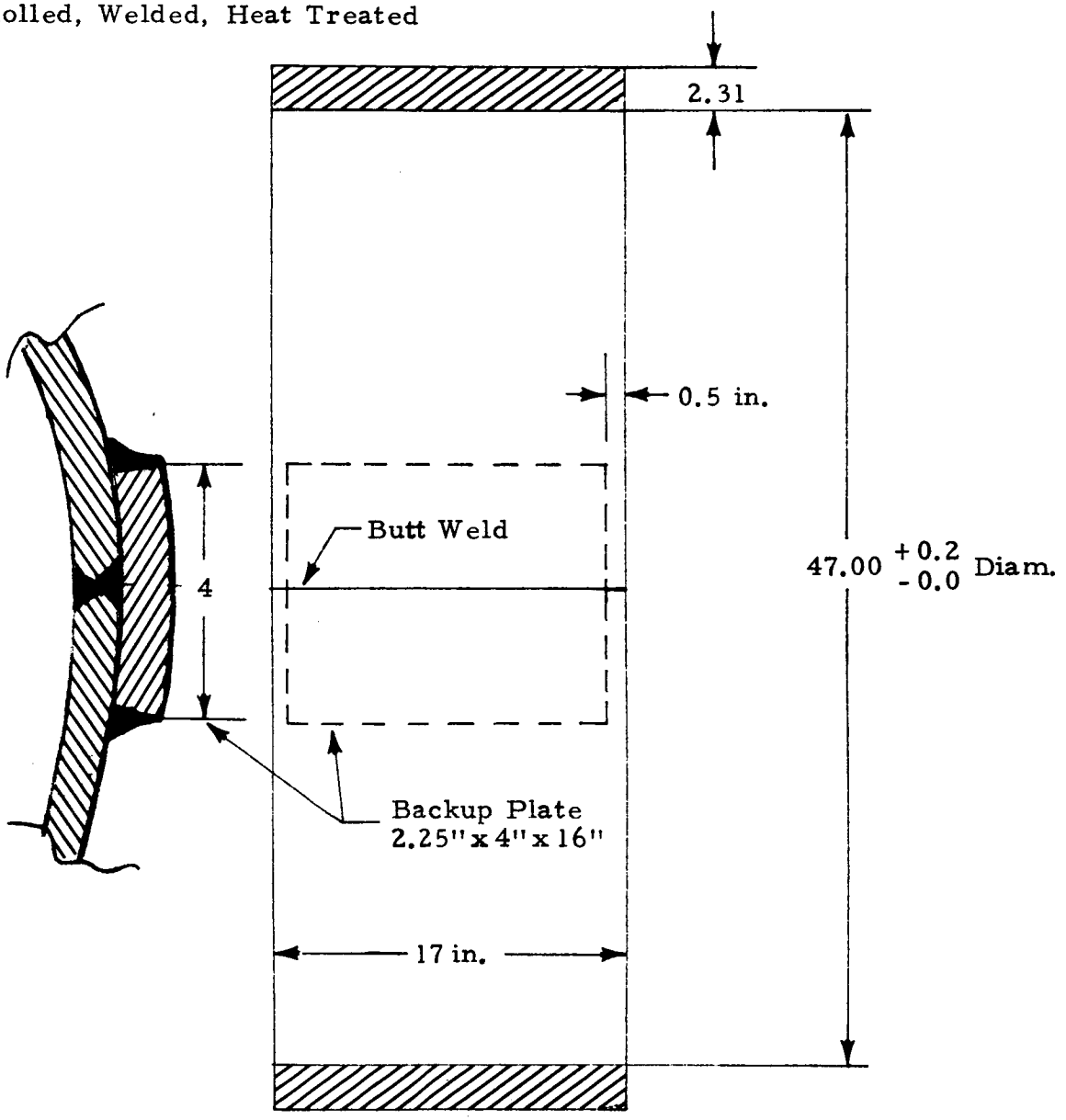

Material	17" x 171" x 2.31 thick
Replaced by 2014-T6	16" x 4" x 2.31 thick

Material above furnished GFE.

Fig. 2-11 - Drawing for Rolling and Welding Die from Flat Plate Stock

Outer Ring Inner Contour (Not to Scale)

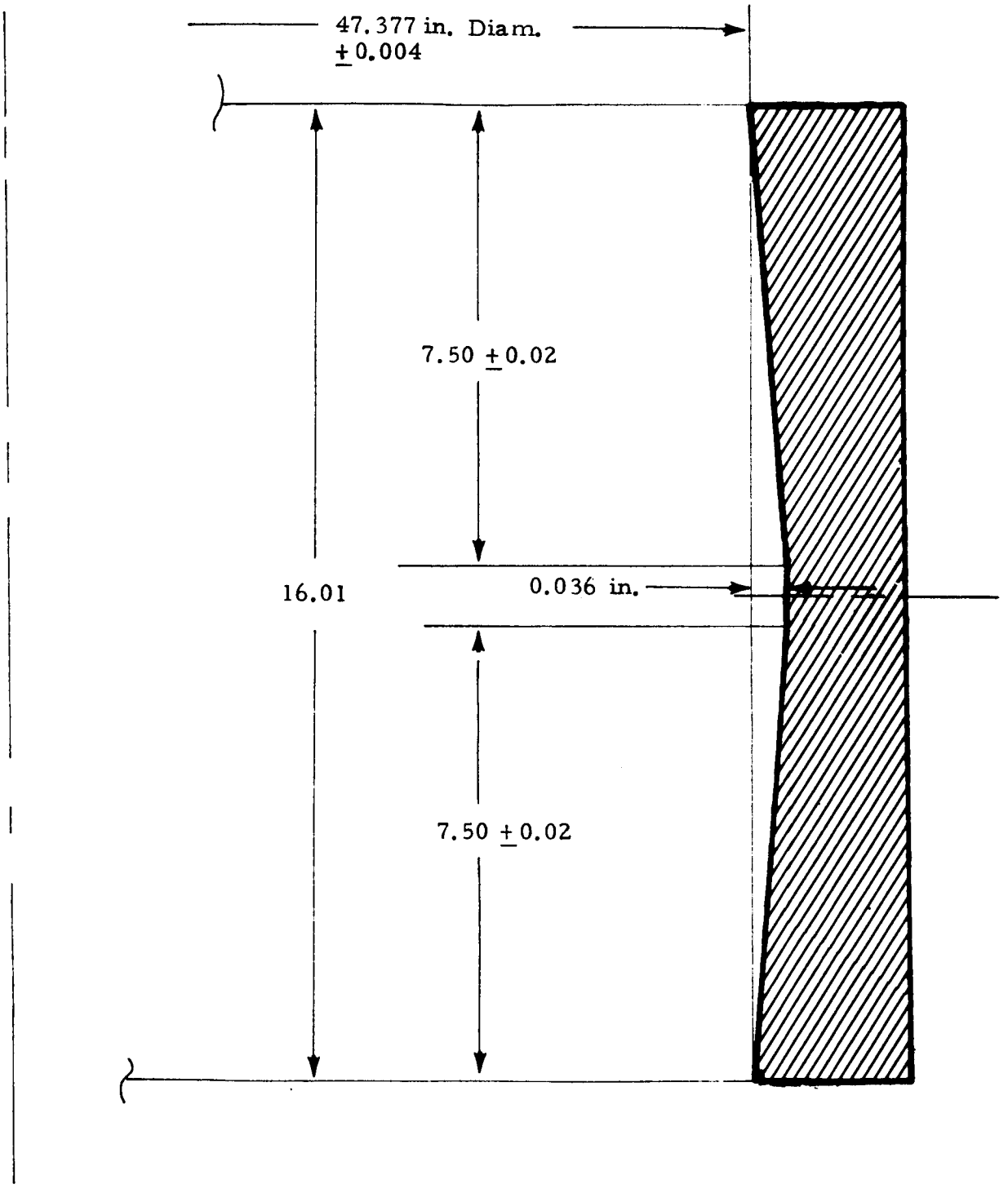

Fig. 2-12 - Contour of Bulge Forming Die

2.3.3 Fixture for Loop Machining and Heat Treatment

Figure 2-13 shows a fixture constructed for the purpose of: trimming elastic loops to width; drilling and holding loops in circular form during heat treatment. This fixture was built with two circular machined rings of 0.75 inch width and twelve machined pads to support the loop.

2.4 ELASTIC LOOP MANUFACTURING

A major effort under this contract was devoted to the manufacture of a titanium alloy elastic loop with uniform ground pressure distribution. A total of three loops were manufactured as shown in Table 2-2 and described in more detail in subsequent sections.

2.4.1 Welding

A 45-degree weld joint was chosen for the loops to minimize any adverse effects which welded cross sections might have in the area of maximum bending stresses at the front and rear. The ends were milled to 45-degree angles. TIG-welding and subsequent X-ray examination were performed by the PE Laboratory's Product Development Division. The weld was found to be acceptable.

2.4.2 First Bulge Forming

In cooperation with the Research & Process Technology Division, procedures for bulge forming in MSFC's Lake Erie Press No. 3994, located in Bldg. 4704, were worked out (Appendix C) for proper setup and operation of all equipment. After several procedural problems had been resolved and after some experience was gained in pressurizing and depressurizing the system without rupturing the bladder, the first loop was bulge formed. The bulge followed closely the contour of the die except in a section extending about 90 degrees angle from the loop center, where an excessive curling was encountered as sketched in Fig. 2-14. In that section, the loop appeared to have been prevented from uniform expansion. The major reasons for this irregularity was believed to be a lack of sufficient clearance in height between the upper and lower plates closing the die, sharp corners of the loop edges and too soft plate material (aluminum alloy 2219).

Table 2-2

LOOP PROCESSING DATA

	Loop Number			
	1	2	Reworked 1	3
Material Data, Alloy Temper, etc.	Ti-11.5 Mo-6.5 Zr-4.6 Sn (Beta III) Detailed Data in Fig. 2-5			Ti-2 Al-11.5V-2 Sn-11.3 Zr (Transage 129), Mill Annealed
Welding Data	TIG Welded by MSFC, S&E-PE-DF		TIG Welded by S&E-PE-DF, Repair TIG Welded by S&E-PE-MW	TIG Welded by S&E-PE-DF
Length, Width, Thickness before Bulge Forming	L = 144.13 in. W = 16.0 in t = 0.064 in.	L = 143.96 in. W = 16.0 in, t = 0.064 in.	L = 143.96 in. (cut and rewelded) W = 15.85 t ≈ 0.064 ± 0.001	L = 143.96 in. W = 16.0 in. t = 0.064 ± 0.001
Length, Width after Bulge Forming and Heat Treatment	L = 145.85 in. W ≥ 15.85	Catastrophic failure during bulge forming	L = 146.24 in. W ≥ 15.335 in.	L = 146.4 in. W ≥ 15.5 in.
Width after Trimming	W = 15.85 in.		W = 15.335 in.	W = 15.335
Heat Treatment Data			1. 950°F, 4 hr; AC* 2. 950°F, 4 hr; AC 3. 950°F, 3 hr; AC	1. 1350°F, 15 min., AC 2. 1200°F, 1 hr, AC 3. 900°F, 4 hr, AC
Rollforming Data			6 in. long crack near completion of roll forming	Sufficient transverse curvature $K_q = 0.004\ cm^{-1}$ achieved. No defects visible in X-ray of weld after roll forming.
Remarks	Irregular edge section encountered in bulge forming (see Fig. 2-14, Vol II)	Failure analysis in Appendix D, Vol. II	Crack was analyzed (see App. E), TIG repair welded and X-rayed by S&E-PE-MW	Loop was severely distorted during heat treatment; however, feasibility of roll forming after age-hardening was successfully demonstrated

*AC = Air Cooled

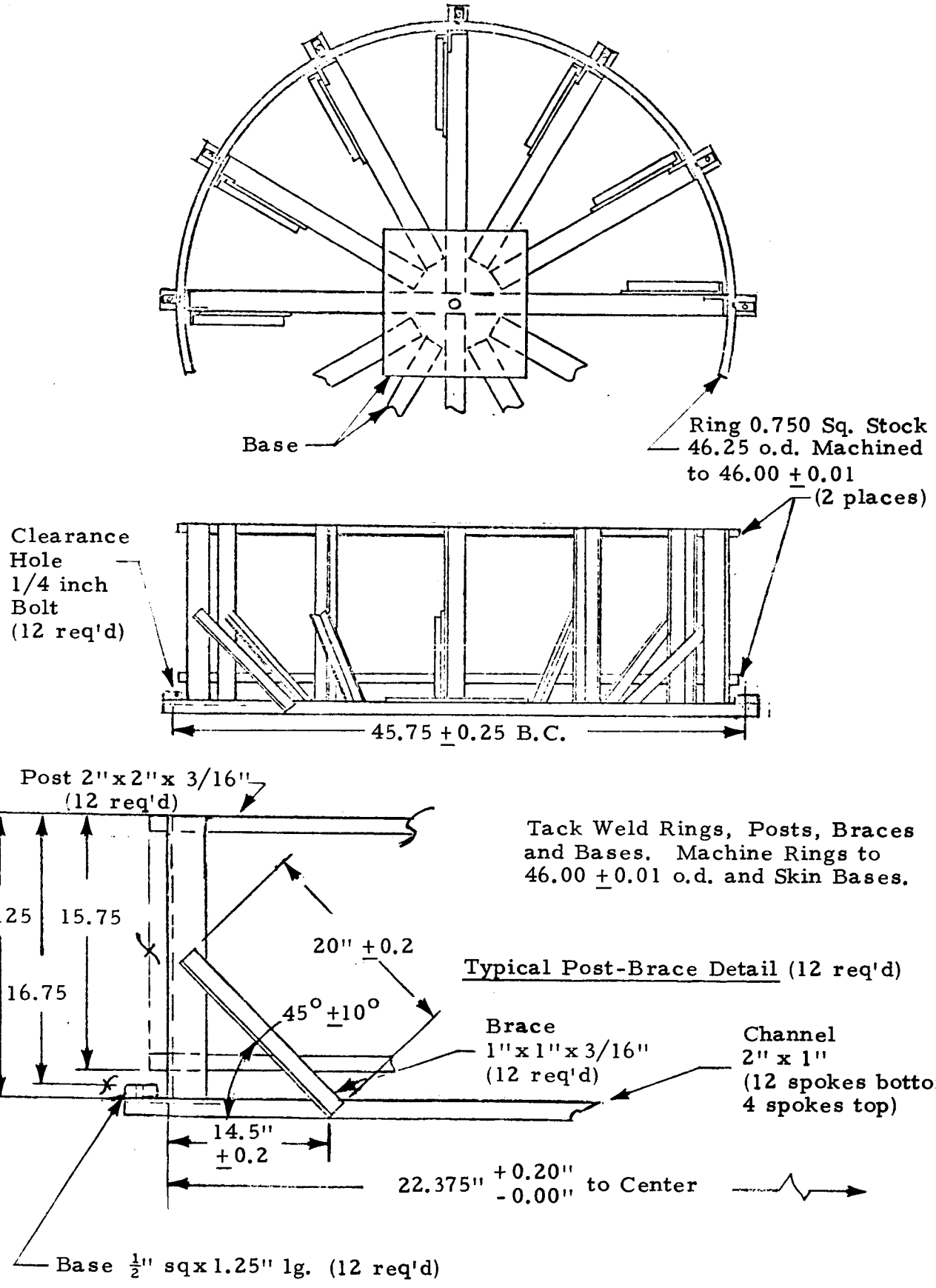

Fig. 2-13 - Fixture for Loop Machining and Heat Treatment

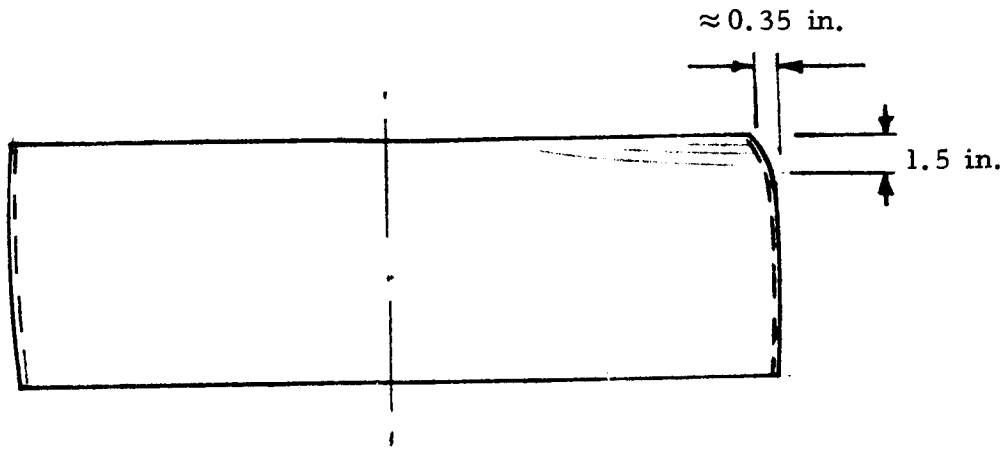

Fig. 2-14 - Sketch of Irregularity Encountered over a 90-Degree Section after First Bulge Forming

The following measures were taken to prevent this irregular forming from recurring:

1. Increase clearance in height to $\geq$0.020 in. plus 0.006 in. of anticipated compression of die under the press.
2. Install cold rolled carbon steel plates of hard and smooth surface finish on top and bottom of die.
3. Lubricate top and bottom plates and bladder/loop interface carefully with rubber lubricant (Permatex Company).

An additional modification to the die was made to adjust the final loop circumference closer to the desired length of 145 inches. The die was shimmed by a 0.125-inch thick aluminum sheet of soft condition (6061-0).

2.4.3 Second Bulge Forming (Loop No. 2)

A second sheet of "Beta III" titanium alloy was prepared for welding, TIG-welded, and trimmed to width. Before bulge forming of the loop was performed, the aluminum shim ring was formed to fully adhere to the inner contour of the die and to permit inspection for possible irregularities at the seam before bulge forming the loop.

When a bladder pressure of about 500 psi was applied, the outer die was fractured at one of the two welds. (A second weld had been made by the subcontractor after an unsuccessful attempt to cold roll the 2014 aluminum alloy without annealing.) The crack (sketched in Fig. 2-15) showed a complete lack of penetration of weld and base material. Since time and cost did not permit fabrication of a new die, the broken die was repaired as shown in Fig. 2-16. A total of six flat steel bars (AISI 4130) of the following dimensions

3 ea 1 x 3 x 48 in.

3 ea 0.75 x 2 x 48 in.

were provided by MSFC as GFE. They were rolled to match the die o.d., match drilled, and bolted to the die to bridge the two welds. The bolt heads and the crack region were subsequently covered by an aluminum fill epoxy (Devcon F-2) and sanded using two templates (one for axial, one for circumferential checking of contour).

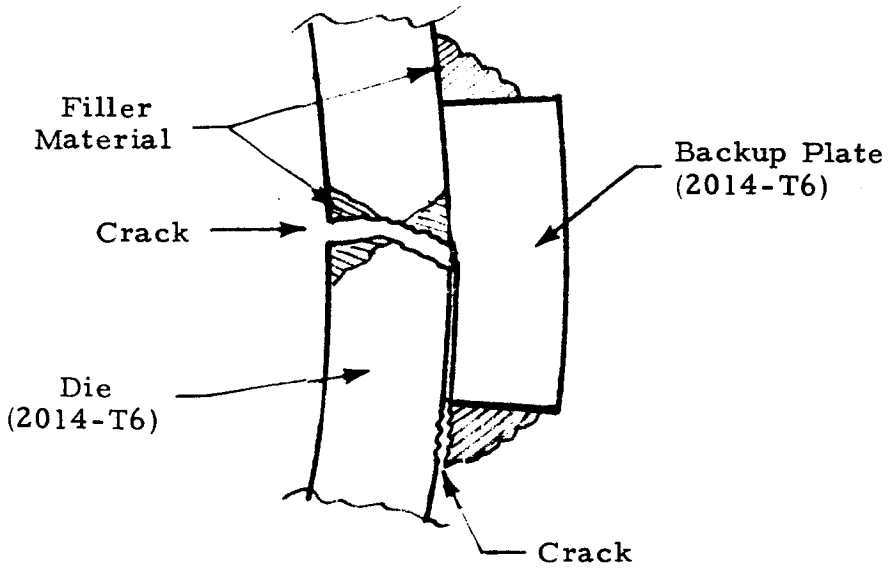

Fig. 2-15 - Sketch of Brittle Fracture of Weld at Approximately 4000 psi Tensile Stress in Die

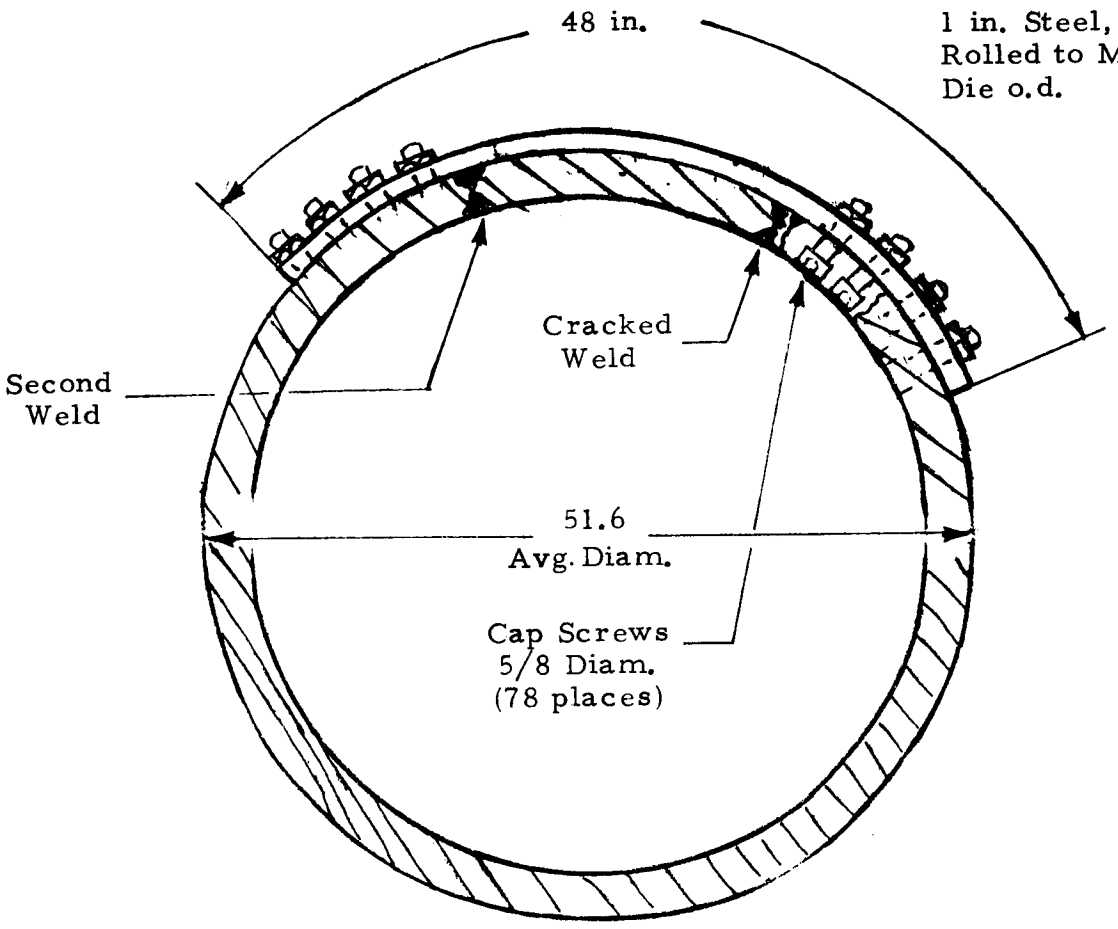

Repair Operations:

1. Remove both aluminum backup plates.
2. Close gap by chain and block and tackle.
3. Drill bolt holes and countersink heads.
4. Cover bolt heads and crack by aluminum-fill epoxy (Devcon F-2)

Fig. 2-16 - ELMS Bulge Form Die Steel Reinforcement

Upon completion of this repair work, the second loop was bulge formed. Near the point of maximum bladder pressure the loop broke. A failure analysis was performed by MSFC's Metals Joining Development Branch. The results were documented as Lab Report No. S&E-PT-MW-72-9, which is presented in narrative form in Appendix D. The failure was attributed to damage to the edge of the titanium loop close to the weld by a hammer-type blow. No instructions had been given to the machine shop personnel to use a hammer in any work on the loop. Nevertheless, precautions were taken to make shop personnel fully aware of the severe consequences of rough handling of highly stressed titanium parts.

Loop No. 2 showed again a section with excessive curvature at the edge almost identical to the first loop's irregularity sketched in Fig. 2-14. This apparent binding between an edge section of the loop and the top cover of the die recurred despite the larger vertical clearance, steel sheet used to provide a harder surface for sliding and careful lubrication of top and bottom. It was concluded that large vertical shear forces must be exerted by the bladder to the titanium when the bladder is filled with water from a completely empty condition. This was verified by observing the bladder filling process with the die cover removed. The loop was pushed up by about 3 inches during the bladder filling operation.

The following procedural changes were established to improve the bulge forming operation:

1. Edges of the titanium loop are rounded so that no sharp edges exist which could dig into the cover plate and prevent the loop from expanding into the die.

2. The cover plates used for the first bulge forming operations are replaced by a harder steel, again to prevent binding.

3. Holes were drilled through the die at a sufficient number of circumferential locations and feeler gages installed (see Fig. 2-15) in order to measure outward expansion of the loop during the bulge forming operation. These gages are situated near the top and bottom edges of the die and provide warning of any anomalistic behavior of the loop during the forming operation.

Any unexpected movement as indicated by the gages results in a hold operation until such behavior can be satisfactorily explained and determined not to be detrimental to the success of the operation. Written procedures were expanded to incorporate the monitoring of the gages.

4. Welds are X-rayed routinely prior to bulge forming to ensure against a faulty weld.

5. The bladder will be lubricated with a rubber lubricant to minimize friction between the rubber bladder and the titanium loop.

6. The bladder is filled with water while the cover plate is removed for inspection and possible repositioning of loop and/or bladder before the pressure is increased.

After the catastrophic failure of Loop No. 2, no additional Beta III titanium sheet was available nor could additional material be purchased within a short time. The backup material, Transage 129, was not received until the end of March 1972.

2.4.3 Reworking of Loop No. 1

In view of the difficulties in purchasing additional material without long delays, it was decided to attempt a reworking operation of the first loop which had developed an irregular edge section during bulge forming. Since the bulge forming die had been reduced in inside diameter by shims after the first loop was bulge formed, the loop was cut shorter by eliminating the old weld. The reduction in length was computed on the basis of previous experience with the Beta III alloy, where 0.6% permanent elongation was achieved after springback from a 2.5% total elongation. This resulted in a length (of the neutral fibers before bulge forming) of

$$L_0 = 144.13 \text{ in.}$$

for a final length of

$$L_1 = 145 \text{ in.}$$

The loop was then rewelded, X-rayed and trimmed to a constant width. The reduced width of the loop required shimming of the die at the bottom by steel plates 0.125 inches thick. As an additional procedural change, these shims were chamfered at the outer top edge as sketched in Fig. 2-17 to facilitate outward sliding of the curled edge section. Pinching of the rubber bladder at the loop edges was prevented by strips of fire hose material taped in place to cover the upper and lower corners.

The bulge forming of this rewelded Loop No. 1 reduced the irregularities in the bulge contour to a level which was no longer considered to significantly affect the mobility characteristics of the loop.

2.4.4 Age-Hardening of Loop No. 1

The recommended heat treatment by the manufacturer for high tensile strength is

$$950^{\circ}F \text{ for 4 hours; aircool,}$$

which was performed by MSFC's Process Engineering Laboratory with the loop held in circular form by the fixture of Fig. 2-13. The different coefficients of thermal expansion of

$$6.4 \times 10^{-6} \text{ in/}^{\circ}F\text{-in.} \quad \text{for steel} \quad \text{and}$$
$$4.8 \times 10^{-6} \text{ in/}^{\circ}F\text{-in.} \quad \text{for titanium}$$

amount to an expansion of the fixture relative to the loop of

$$\Delta D_{St/Ti} = (6.4 - 4.8)\, 10^{-6}\, (950-75)\, 46$$

$$= 1.4 \times 10^{-6} \times 875 \times 46 = 0.050 \text{ in.}$$

The clearance between fixture and loop at room temperature was chosen two times the predicted amount or 0.1 inch in diameter. After the aging several mild waves were observed in the otherwise circular upper edge

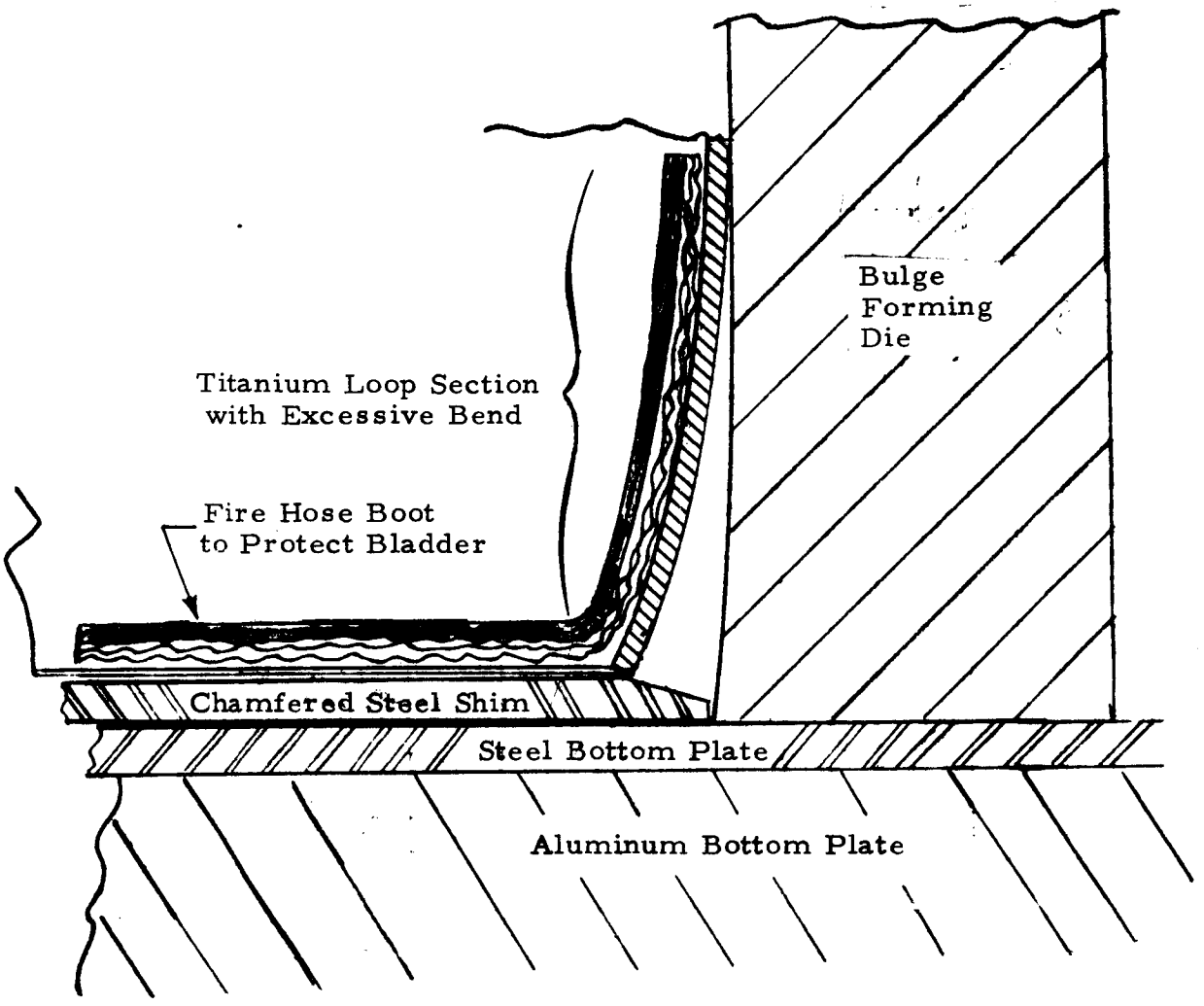

Fig. 2-17 - Chamfering of Steel Shims at Loop Section with Excessive Bend to Facilitate Sliding of Edge During Bulge Forming. Fire hose material protects bladder from pinching.

of the loop. There were indications of a larger difference in thermal expansion of this cold worked titanium alloy sheet and the fixture which had been at high temperature several times prior to this aging operation.

The manufacturer was then consulted whether material properties are adversely affected by a second heating to aging temperature. It was learned that no overaging is obtained if 24 hours are not exceeded.

An attempt was, therefore, made to heat the loop to 950°F again, but with very tight fit in the fixture using steel shim rings between fixture and loop. Very little change was noticed after the second age-hardening at 950°F for another 4 hours. The waviness of the affected edge appeared to be reduced sufficiently to a tolerable level. Further uniformity in loop shape was expected from the subsequent rollforming operation.

2.4.5 Rollforming of Loop No. 1

Shaping of the loop's footprint for uniform longitudinal ground pressure distribution under load required a small amount of rollforming of the age-hardened loop. The Lockheed-built single-stand rollforming machine depicted in Fig. 2-1 was used. The three rolls are sized and located so that the maximum elongation during bending is

$$\epsilon \leq \frac{t}{2R_1}$$

where R_1 is the bulge radius of the lower roll, which is $R_1 = 2$ inches. For the present loop thickness (0.063 in.), the maximum elongation is

$$\epsilon_{max} \leq \frac{0.063}{4} = 0.016$$

which was considered safe when compared with reported properties for "Beta III" (Ref. 3), which after EB welding and aging at 950°F achieved the following properties

σ_{tu} = 174.5 ksi

σ_{ty} = 162.4 ksi

Elongation 4.9%*

Toward the end of the rollforming, a 6-inch long crack developed parallel to the loop edges. It started at the weld which was too brittle to stand a temporary elongation of not quite 1.5%. This was verified in a metallurgical examination performed by MSFC's Metals Joining Development Branch (Appendix E), where between 0.5 and 1.5% elongation was measured in the fractured weldment of a tensile test specimen.

No other defects were found in the loop during the examination. A repair weld was therefore performed by the Metals Joining Development Branch. This repair weld was rated acceptable after X-ray examination. The only adverse side effect of this weldment about 3.5 inches inside the edge was a strong local waveform near the edge which reduced the buckling strength of the loop at that point. An effort was made to remove a sufficient amount of the excess material (which caused the waveform) at the 45 degree weld seam which was only 2 inches away from the wave center. To this end, a V-shaped section was cut out of the weld over about 30% of the loop width, and rewelded (TIG). This reduced the wave in the edge section to a tolerable size.

2.4.6 Descaling of Loop No. 1

After handgrinding of the repair weldments, the blue scale from the heat treatment was removed by sandblasting.

*Fracture in base metal, not in weld.

2.4.7 Loop Drilling and Assembly

Figure 2-18 shows the assembled ELMS with Loop No. 1 equipped with grousers for improved traction. The lower edge is straight over most of the footprint. Thus the major design objective has been accomplished. Ground contact pressure in soft soil can be expected to be fairly uniform over most of the footprint. ELMS weight as shown in Fig. 2-18 is W = 534 N, including battery (20 lb) and part of the trailer weight (6 lb). This amounts to a load of

$$F = W - \frac{1}{2} W_{Loop} = (534 - 72) = 462 \text{ N}$$

According to the calculated spring-deflection characteristic of Fig. 2-6, the loop deflection should be about 12.7 cm (5 in.) away from maximum deflection, where the drive drums provide a hard stop. This is in good agreement with the measured deflection of 11.7 cm for this load. (Torsion springs force the suspension arms outward to provide sufficient contact pressure between drive drums and loop, thereby lowering the loop by a small amount.)

Drive drums and the loop had to be designed simultaneously to ensure proper engagement of the drive lugs mounted on the inside of the loop and the planetary rollers installed in two rows at the drive drum circumference. The drive lug/roller engagement geometry is described in Appendix K. The drive drum design was based on two loop sizes:

(A) Circumference C_A = 3.68 m (145 in.)
Number of Drive Lugs per Side: 69

or

(B) Circumference: C_B = 3.74 m (147.090 in.)
Number of Drive Lugs per Side: 70

In each case the correct spacing of drive lugs was

$$S = 5.3 \text{ cm } (2.089 \text{ in.})$$

After the heat treatment the circumference of Loop No. 1 at the location of the lugs was 3.72 m (146.238 in.), which was nearer to design point (B).

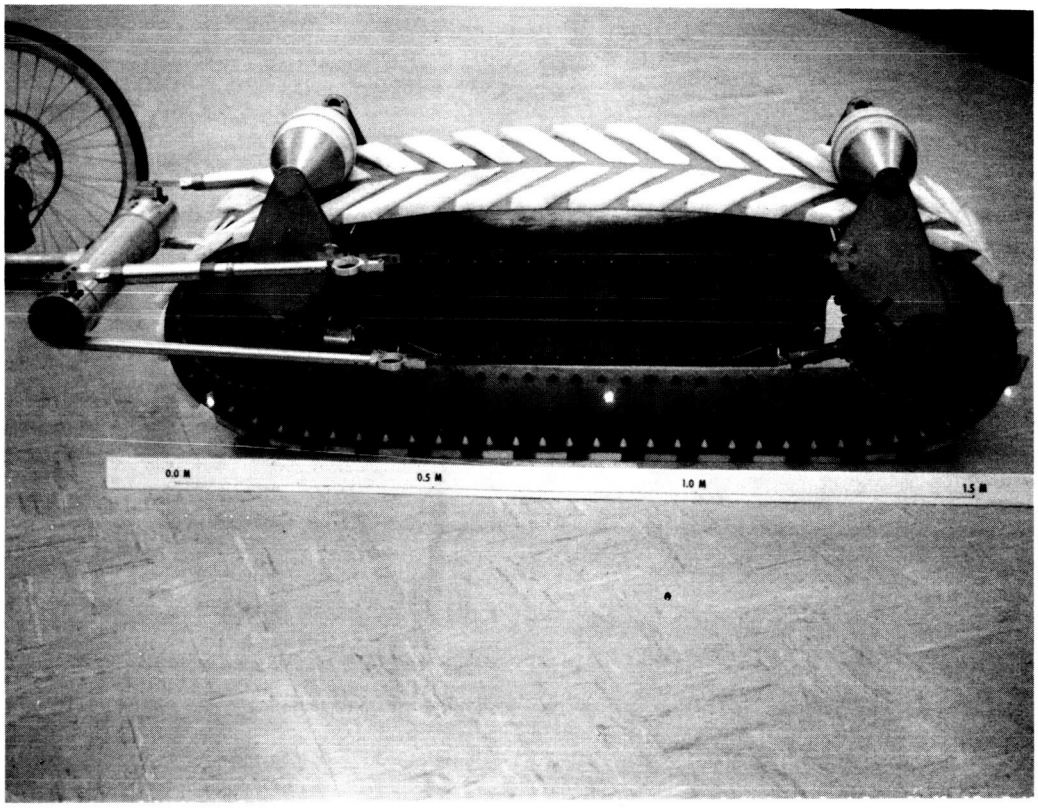

Fig. 2-18 - ELMS Fully Assembled with Loop No. 1 (Beta III Titanium Alloy). Combination of bulge- and rollforming provides uniform ground pressure as indicated by straight lower edge.

Therefore, 70 lugs per side were selected. The error in lug spacing amounts to

$$(C_B - C_{B_{Act.}})/70 = 0.08 \text{ mm } (0.0032 \text{ in.}),$$

which is well within the tolerable range. For equal spacing of the two rows of drive lugs, the fixture of Fig. 2-13 was mounted on a turntable, which was rotated in increments of 360/70 = 5-1/7 degree from hole to hole. The drilling was performed on a milling machine. Holes were located in such a manner that no holes were inside or close to a weldment to reduce notch effects in the weld zone.

2.4.8 Transage-129 Elastic Loop Manufacturing Effort

After the Beta III loop had cracked in a final rollforming operation, the overdue shipment of Transage-129 titanium alloy sheet was received. An effort was therefore started to manufacture a new loop (No. 3) from this new alloy as a backup approach to obtain a satisfactory loop for the test program.

- Welding

Since no weld wire was available, a procedure was worked out by MSFC's Product Development Division, S&E-PE-D, Bldg. 4705, to perform the TIG welding without filler material. After a series of test welds with different forms of butts, the parameters given in Fig. 2-19 were found to yield perfect welds. Metallurgical examinations of pre-production welds were performed by MSFC's Metals Joining Branch, S&E-PE-MW, which showed the weld regions to be of lower R_c hardness (from $R_c = 20$ to 21) than the parent material ($R_c = 24$), whereas Beta III specimens did not have this desirable feature. In Beta III welds, the hardness had been found to be as high as $R_c = 24$ for parent material in the order of $R_c = 20$ to 21.

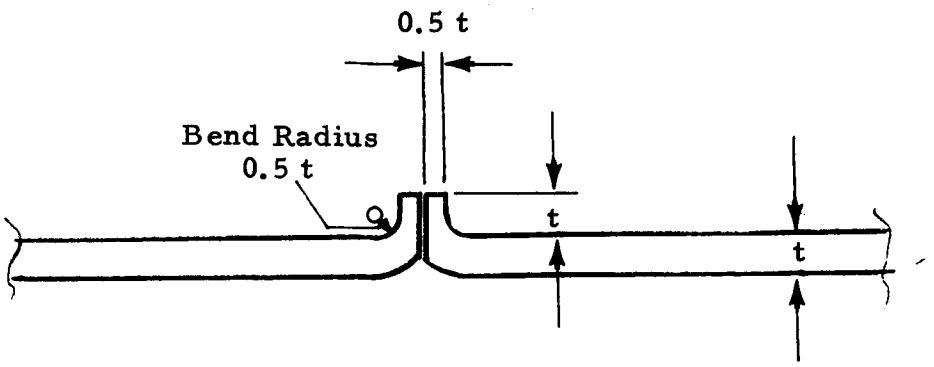

Fig. 2-19 - Preparation of Butts for TIG Welding of Transage-129 Titanium Alloy Without Filler Wire (developed by MSFC's Product Development Division, S&E-PE-D, Bldg. 4705)

A perfect production weld was achieved using the butt form machined according to Fig. 2-19. The weld quality was assured by X-ray examination.

- Bulge Forming

Extreme care was exercised in the preparations for bulge forming. The bladder was filled with water while the die was still open and repositioned after filling was completed to minimize vertical forces exerted by the bladder to the loop. Nevertheless, minor curling of parts of the upper edge was encountered, but was considered small enough to not adversely affect the performance of the finished loop.

- Heat Treatment

The recommended heat treatment to age harden the martensitic Transage-129 titanium alloy is:

1. Hold 15 minutes at 1350°F (+25°F), aircool.
2. Hold 1 hour at 1200°F, aircool.
3. Hold 4 hours at 900°F, aircool.

The fixture shown in Fig. 2-13 was again used to support the loop in the furnace (located in MSFC's Bldg. 4704). Detailed information on thermal expansion characteristics of this new titanium alloy was obtained from LMSC's Palo Alto Research Laboratory where the material had been developed. A shrinkage of 0.5% occurs in sheet when it is solution treated after the last rolling of typically 50% reduction in thickness. It was assumed that during the mill solution treatment this large shrinkage had already taken place. The approximately 3% cold working during bulge forming was believed to result in a shrinkage of approximately 3/50 of 0.5% or 0.03%. A clearance corresponding to twice that amount plus the expected difference in thermal expansion (discussed on page 2-28) was provided between fixture and loop. However, the actual shrinkage experienced was in the order of 0.5%. As a result the Transage loop was stretched by approximately 1/4 inch in diameter in the two edge sections, which eliminated the bulge completely. In this distorted form the loop could not be used.

In order to study the feasibility of rollforming in the aged condition, the loop was rollformed to the required transverse curvature after descaling. No damage of any kind could be found after rollforming and X-ray examination of the weld.

- Conclusions

The experience gained from the three manufacturing efforts has led to a promising new approach that eliminates completely the cold bulge forming operation. A male steel die would be machined to the desired bulge. The welded titanium ring would be of such diameter that it slides over the steel die with minimum clearance. During the heat treatment the loop would shrink sufficiently with respect to the steel die to be hot formed to the shape of the die. Thus, bulge forming and age hardening would be combined to one simple hot forming operation. A preliminary analysis indicates that the loop can be removed from the die without a need for an expensive split die.

Section 3
DRIVE SYSTEM DESIGN AND INSTRUMENTATION

3.1 PERMANENT MAGNET BRUSHLESS DC DRIVE MOTORS*

The propulsion system for each drum of the ELMS consists of a permanent magnet brushless dc motor, a planetary spur gear combination with an 80:1 speed reduction, and an electronic controller. The motor and gear train were initially developed as an alternate drive system for the Lunar Roving Vehicle by the General Electric Company and United Shoe Machinery Company, respectively. The electronic controller was designed specifically for the ELMS by MSFC's Astrionics Laboratory. The propulsion assembly is a high performance system with a combined efficiency of greater than 70% over a wide range of torques and speeds. Complete performance characteristics and system description are documented in Refs. 16 and 17.

The motor-gear combination has two torque-speed ranges and with a nominal battery voltage is capable of developing 80 ft-lb at drum speeds up to 25 rpm and 20 ft-lb at speeds up to 120 rpm. The change in torque-speed range is performed electronically by changing taps on the motor winding. A unipolar tachometer in the motor provides the speed information to the controller required to change ranges. As the drive system accelerates through 25 rpm, the controller automatically switches to the high-speed tap and correspondingly changes the current in the motor so that the output torque remains the same before and after switching. An anomalous condition may occur if the ELMS is forced to accelerate up a grade which requires a total output torque greater than 40 ft-lb. When the motor changes to the high speed tap, the torque is limited to 40 ft-lb and the wheel will slow down and shift back to the low

*This information was contributed by Mr. F. J. Nola of MSFC's Astrionics Laboratory.

speed. The motor will alternate between the high and low speed tap until the speed input command is reduced or the torque requirement is lowered.

The forward and reverse speed of the vehicle is controlled by a single input command which is fed to the two electronic controllers. A given polarity of the input command corresponds to a given direction of rotation while the opposite polarity reverses the direction. The system incorporates proportional regenerative braking which is also controlled by the input command. Reducing the speed command will cause the vehicle to brake proportional to the magnitude of the reduction and is controllable to zero speed. A power supply which can accept energy (such as a battery) must be used to absorb the energy of regenerative braking.

Since speed control was required for testing the ELMS, it was necessary to mount a bipolar tachometer on each motor. The speed signal from each tachometer is fed back and summed with the input command to provide a speed control of 5% of 120 rpm from no load to full load. Since both motors are mechanically coupled by the elastic loop, the tachometer gains have been matched so that both motors produce the same speed for a given input. The system is designed to operate at a nominal battery voltage of $35 \begin{smallmatrix} +5 \\ -7 \end{smallmatrix}$ volts and, due to weight and power limitations, is not protected against battery reversals. The system cannot be damaged by torque overload, overspeed, or by regenerative braking commands which may be applied if power is supplied by a source which cannot accept the braking energy.

Test points are provided for monitoring both the torque and speed. The calibration of the speed voltage is 200 mV/rpm. Curves of output torque versus voltage at various speeds are shown in Figs. 7-6 and 7-7. Also, a control line for inhibiting the drive signal is provided. Applying +12 volts to this line will inhibit the input command signal and stop the motor. This allows a preset speed to be set in, and the vehicle to be stopped by a signal line rather than interrupting the power bus.

The quiescent current drain from the battery for both motors is less than 200 ma. The maximum current drain when delivering 40 ft-lb at 120 rpm is approximately 30 amps. Detailed instructions on the drive motor control are given in Appendix F.

3.2 INSTALLATION OF BRUSHLESS DC-MOTORS

The design goal was to provide a rigid yet lightweight installation for the brushless dc motors which were provided as GFE by the Advanced Research and Technology Branch of the MSFC Astrionics Laboratory. These motors had been built under NASA contract by the General Electric Company to the speed and torque requirements of the Apollo Lunar Roving Vehicle (LRV). Maximum torque requirements for the ELMS test unit were estimated.

A. Slope Climbing

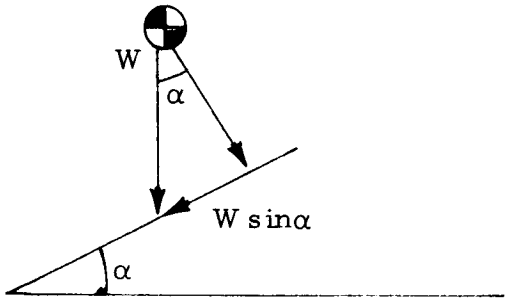

$$T_{max} = \frac{r_e W \sin\alpha}{\eta}$$

Maximum Slope Angle $\alpha = 35$ deg ($\sin\alpha = 0.574$)

Nominal Weight $W = 557$ N (125 lb)

Estimated Efficiency $\eta \geq 0.62$
(First-Generation ELMS $\eta \approx 0.62$)

Effective Radius $r_e \approx 0.16$ m (6.25 in.)

$$T_{slope} \leq \frac{0.16 \times 557 \times 0.574}{0.62} = 82 \text{ Nm } (60 \text{ ft-lb})$$

B. Step Obstacle Climbing

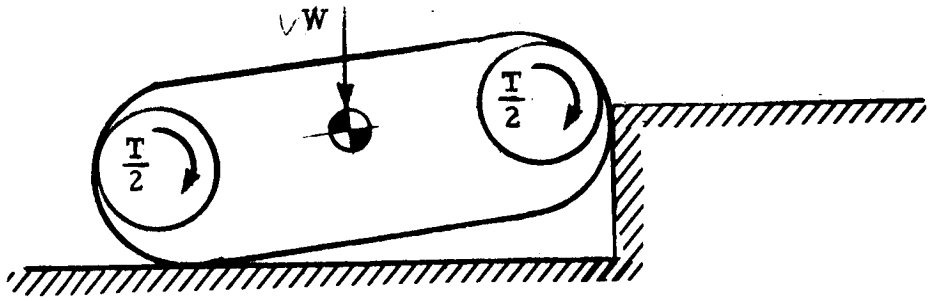

The torque requirements by a single-loop ELMS in climbing a step obstacle have been derived in recent studies under Lockheed's Independent Research program. Good agreement between theoretical results and WES test results as reported in Ref. 1 is obtained. The predicted peak torque during step obstacle climbing was found to be

$$T_{step} = \frac{\mu(1+\mu)}{1+\mu^2} r_e W$$

where μ is the coefficient of friction between the loop and the ground. Assuming $\mu \approx 0.5$, the following range in T_{step} is obtained for ELMS weights considered in the present design:

Nominal Weight

$$T_{step} \leq 0.6\, r_e W = 55.5 \text{ Nm } (41 \text{ ft-lb})$$

Maximum Weight

$$T_{step} \leq 0.6\, r_e W_{max} = 64 \text{ Nm } (47 \text{ ft-lb})$$

The maximum torque was therefore limited to

$$T \leq 82 \text{ Nm } (60 \text{ ft-lb})$$

for the ELMS test unit. This torque limit will protect all components of the drive system, in particular the flexural pivots in the drive drums, from excessive loads.

Unfortunately, a substantial weight penalty results from these big motors which are capable of more than 217 Nm (160 ft-lb) per pair, but only 38% of that torque will be used. Total weight of the two motors, including planetary gear heads, is (80:1 gear reduction):

$$W_M = 99.5 \text{ N } (22.4 \text{ lb})$$

The basic layout of the drive motor assembly is shown in Fig. 3-1. The motor and drive torque to be subassembled is located with its c.g. at the center between the two suspension arms.

A rigged and simple drive system design was obtained by making the gearhead motor unit an integral part of the axle which supports the drum. Magnesium tubes flanged to the motor housing at the left and to the gear housing to the right-hand side support the motor and the ballbearings for the drive drum.

A stress analysis was performed (Appendix G) to size the left and right support tubes and the drive torque tube (Appendix H). The tube walls were kept as thin as practical to provide maximum sensitivity for strain gages which are mounted inside the tubes to measure drive torques at the gearhead output. All strain gages, the tachometer and the wire outlets from the back of the motor are readily accessible for inspection or repair from the side by removal of a cover plate covering the ends of the support tubes.

3.3 DRIVE DRUM DESIGN WITH FRICTIONLESS PLANETARY ROLLERS

The drive drum consists of conical magnesium discs which are flanged to inner cones also of magnesium and a cylinder of rolled magnesium sheet,

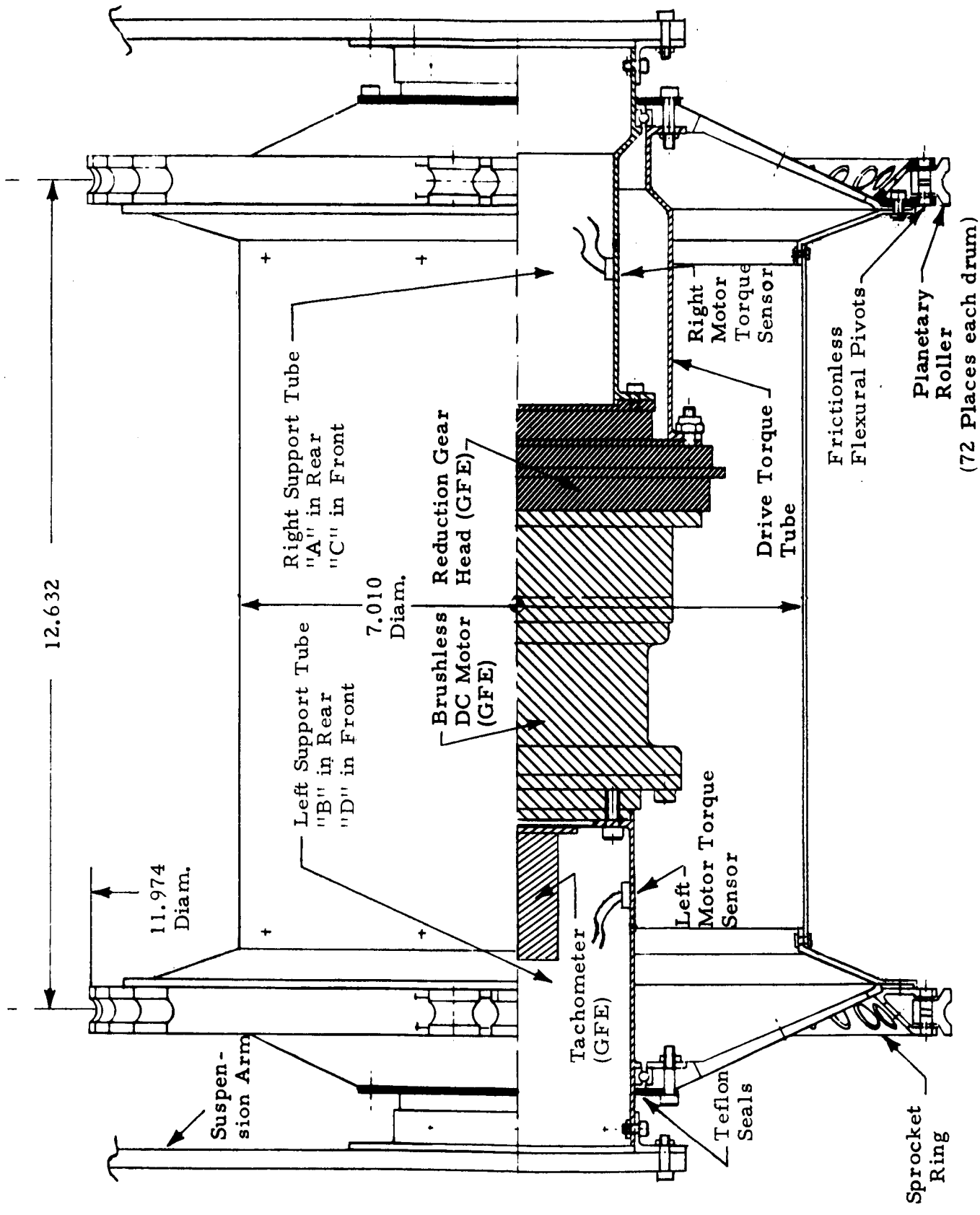

Fig. 3-1 - Layout of Drive Motor Installation and Drive Torque Sensor Locations

as shown in Fig. 3-1. A sizing and stress analysis for the cylinder is given in Appendix I.

At the interface of the discs and inner cones, a sprocket ring is mounted shown in Fig. 3-2. Assembly details are shown in Fig. J-1. Sprocket ring, disc and inner cone are held by the same array of cap screws and can be readily disassembled after the dust cover is removed. Removing this cover also gives access to the flexural pivots which support the planetary rollers discussed below.

A thorough analysis of the engagement geometry between conical drive lugs mounted in two rows to the inside of the elastic loop and an array of rollers at the drive drum circumference was made to ensure perfect engagement and disengagement even under the most adverse loop deflections. The most critical condition is shown in Fig. J-2, where the loop approaches the drum tangentially so that its shape changes from a straight line to the minimum diameter circle around the drum. The minimum cone angle resulting from this study is 25 degrees (to the cone axis). For easy manufacturing and quality control, a ring gage was built (Fig. J-3) to assure good engagement of the actual hardware. The engagement analysis presented in Appendix J also established the number and size of planetary rollers required and their location on the sprocket rings.

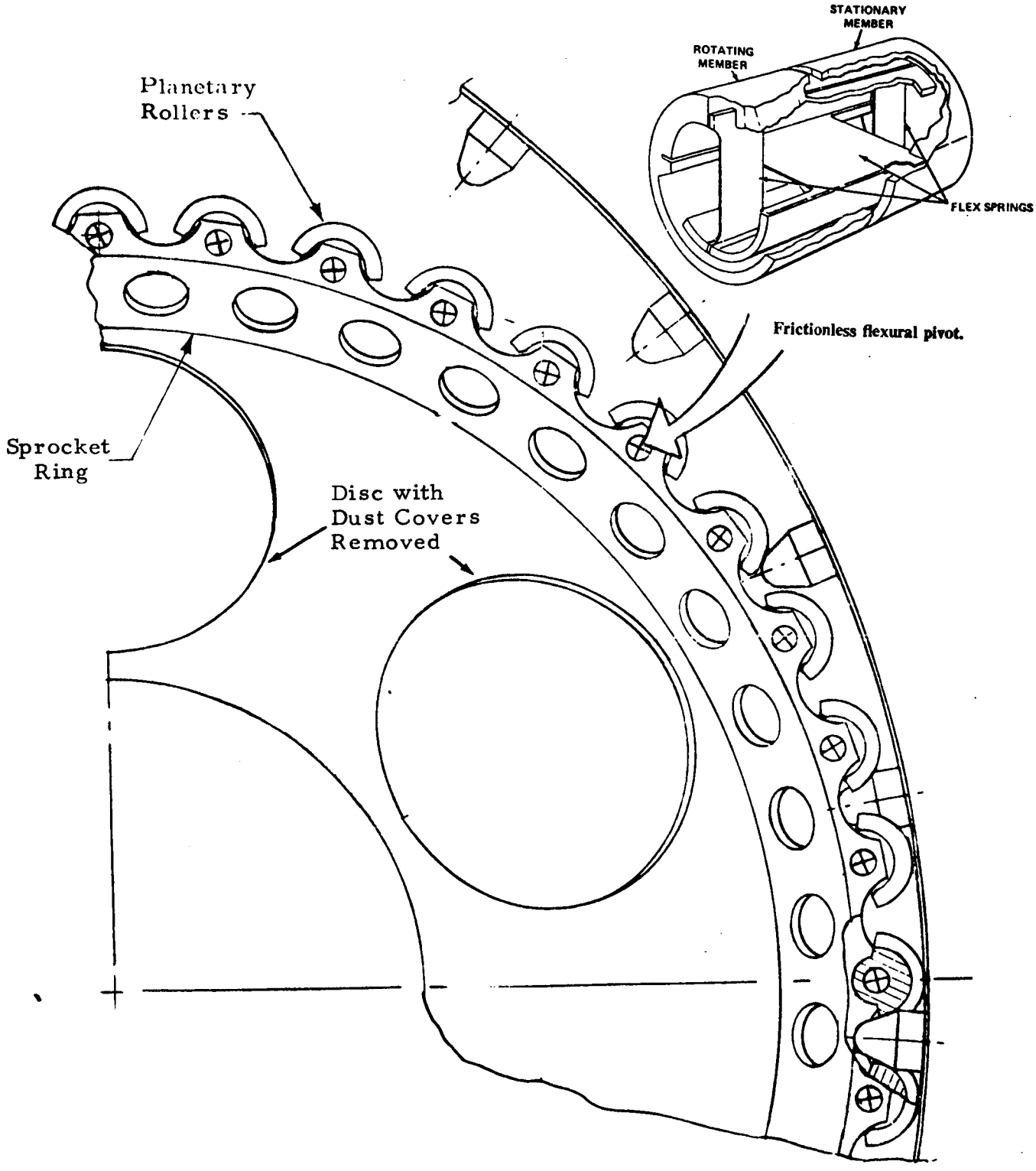

Fig. 3-2 - Sideview of Drive Drum, Planetary Rollers and Flexural Pivots for Frictionless Mounting of Rollers

3.4 PLANETARY ROLLER DESIGN

Lockheed proposed to evaluate planetary rollers mounted in frictionless flexural pivots as an attractive solution to minimize internal losses in the drive train. Flexural pivots are frictionless bearings of limited angular travel, having no backlash and requiring no lubrication. The bearings are made of pairs of flat, crossed springs supporting rotating sleeves. These pivots are available (from Bendix, Utica, N. Y.) in a variety of sizes and pivotal angles. One of the alternative designs that had been considered is shown in Fig. 3-3. It features conventional freely rotating rollers with friction-type radial and axial bearings.

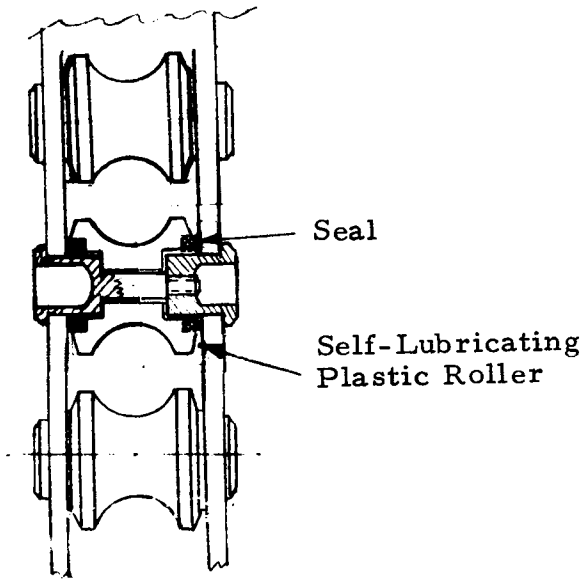

Fig. 3-3 - Alternate Planetary Roller Design with Free 360 Degree Rotation but Friction-Type Bearings

Major factors considered in a tradeoff study were:

Advantages of Conventional Rollers

- Lower Development Risk
- High Structural Strength
- Simple Installation
- Lower Cost

Disadvantages

- Friction Proportional to Load
- Lubrication Required
- Good Sealing from Dirt Required
- Higher Weight of Rollers and Housing

Advantages of Rollers with Limited Rotation and Flexural Pivots

- No Friction
- No Lubrication Required (suitable in hard vacuum)
- Minimum Sealing Required
- Low Weight of Rollers, Pivots and Housing

Disadvantages

- Higher Development Risk (lack of experience in installation and operation)
- Low Safety Margin against Dynamic Loads (of uncertain magnitude) if Standard Catalog Sizes are used
- Higher Cost

The main disadvantage of the flexural pivots shown in Fig. 3-2 is that their built-in restoring torque, which zeros deflections under no load, increases with structural strength. Small restoring torques do not adversely affect the efficiency of the loop-drum drive train since the energy needed to deflect the pivots during engagement is converted into kinetic energy that drives the loop during disengagement. However, very strong flexural pivots of standard catalog sizes require large restoring torques to be overcome during deflection which, in turn, would result in developing sliding friction forces between the drive lugs and the planetary rollers, thus defeating the purpose of these devices. A load analysis was made to determine if standard "off-the-shelf" flexural pivots can take the expected loads (see Appendix K).

Maximum deflection angles required were estimated to be 10 degrees under most adverse conditions (cumulative maximum of all manufacturing tolerances). Stock size pivots provide ±8.5, or ±15, or ±30 degrees deflection. On the basis of this information and the load analysis shown in Appendix K, pivots of the ±15 degree series were considered. The stock size which offered the best compromise in load capability and torsional spring stiffness was Bendix Catalog Number 5006-600, which has the following characteristics per pair:

Diameter	Length	Loads for Leaf Springs Under		Spring Rate
		Compression V_c	Tension V_t	
4.763 mm (3/16 in.)	15.3 mm (0.6 in.)	176 N (36.6 lb)	249 N (54 lb)	7.4 N-cm/rad (0.652 lb-in./rad)

The best orientation of the pivots on the drive drum is shown in Fig. 3-4. Each roller is thus capable of 249 N (56 lb) of radial load. No safe predictions can be made at this time how horizontal impact loads (as a result of hitting a vertical wall) get distributed to the rollers without detailed analysis and testing. In future ELMS designs, special size pivots may be used if the performance tests in the area of drive system efficiency prove successful.

This possible reduction of internal losses by frictionless bearings was the major reason to try flexural pivots as bearings for the planetary rollers. However, the available stock sizes selected have very limited impact load resistance which under adverse conditions (one roller takes all the impact) may be as low as 249 N (56 lb). Under a more likely condition the impact load would be shared by at least three rollers which would increase the radial load resistance to over 500 N (112 lb).

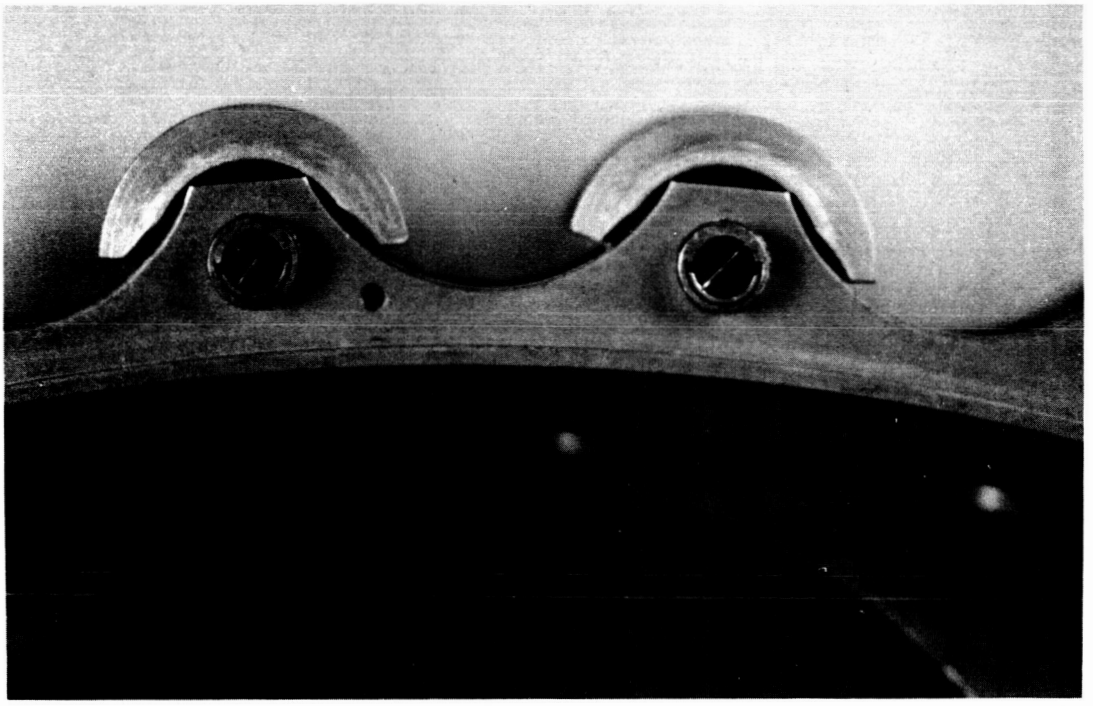

Fig. 3-4 - Frictionless Bearings for Planetary Rollers Oriented for Maximum Strength Against Radial and Near-Radial Loads Directed Toward Drum Axis as Shown Below:

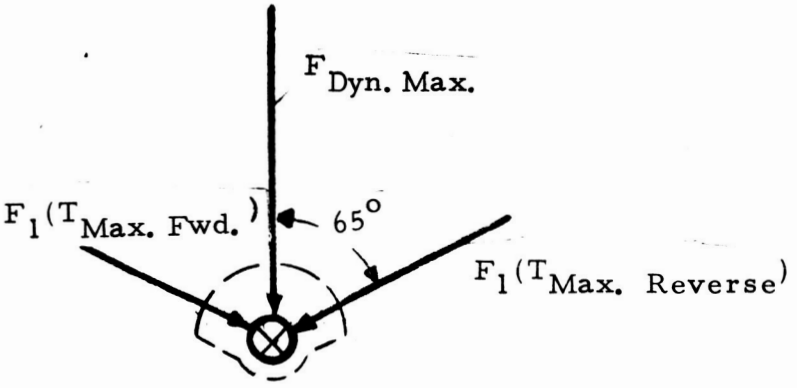

Details of the planetary roller and flexural pivot mount are shown in Fig. 3-5. The two cantilevered pivots are bonded to the sprocket ring and to the roller by an epoxi adhesive ("Loctite 75"). Installation details are discussed in Appendix L. Two plastic washers on both sides of the roller base prevent dust accumulation inside the pivots. The sliding friction caused by these seals is very small because of the low contact pressure between the washers and the adjoining walls. Only if the pivots are installed with an excess amount of adhesive can this friction become larger. Extreme care must therefore be exercised in their installation.

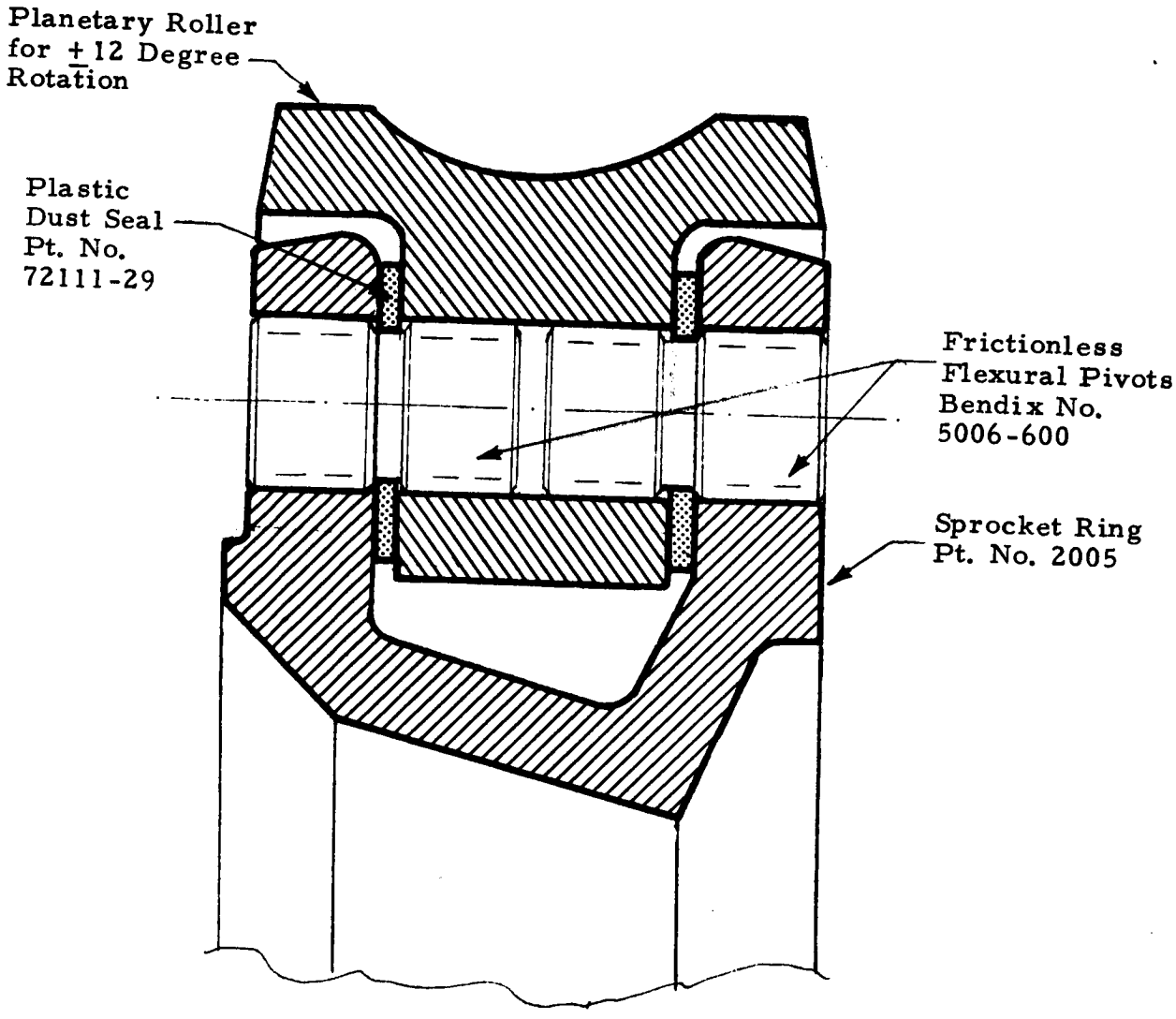

Fig. 3-5 - Detailed View of Planetary Roller, Frictionless Bearing, and Dust Seal Installation

Section 4
CHASSIS DESIGN

4.1 ELASTIC LOOP SUSPENSION

A major advantage of Lockheed's ELMS concept is the dual function of elastic loops: (1) to provide vehicle support and traction over a large footprint, and (2) to provide spring suspension using the 180-degree bends of each loop as suspension springs. To this end, elastic loops are suspended elastically to permit vertical spring deflection under load and dissipation of oscillatory energy. The basic concept of Lockheed's elastic loop suspension is shown in Fig. 4-1.

Vehicle load is transmitted from the chassis to the loop by a pair of upper load wheels (usually passive). At least one of the two load wheels is mounted on the suspension arms which can pivot about a point A of the chassis. At the lower end of the suspension arms, a drive drum is mounted with internal electric drive. Under load, the loop deflects and gets longer in the fore and aft direction. Under the influence of torque Wa, the arm and drive drum rotate outward by an angle α. Under 1-g conditions, this torque is too small to ensure that sufficient contact pressure is maintained between the drum and the loop to transmit drive torques. A spring is, therefore, installed to increase the contact pressure between the drum and the loop. A torsion bar is mounted in the arm pivot bearings "A" extending over the full width of the chassis (43 cm).

The effects of additional torques acting on the suspension arms are illustrated in Fig. 4-2 for a typical ELMS suspension with swing arm drum suspension front and rear. They are torques in reaction to the drive torques applied by the drive drums to the loop and are oriented so that the forward arm is torqued outward causing an increase in contact pressure whereas the rear arm is torqued inward reducing the drum-loop contact pressure. As

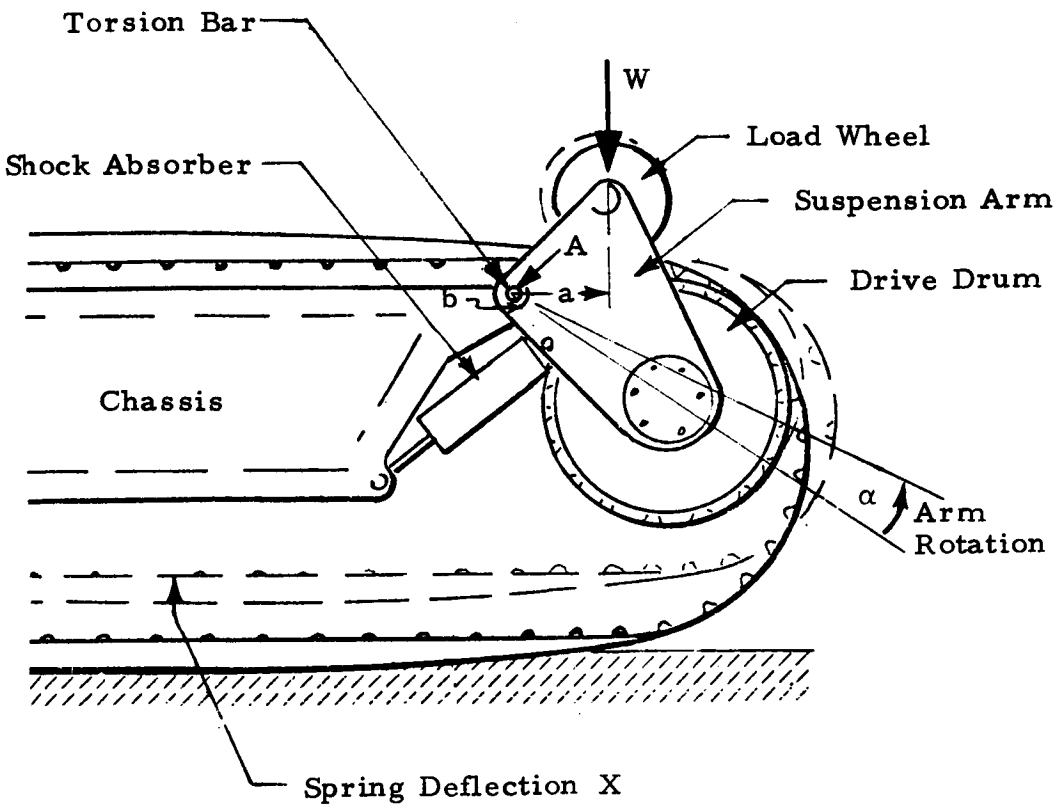

Fig. 4-1 - Typical ELMS Loop Suspension. Vehicle Weight is Transmitted to Loop by Upper Load Wheel. Moment (W·a) keeps drive drum in contact with loop. Spring deflection X results in arm rotation α and damper travel $b\alpha$ to dissipate energy.

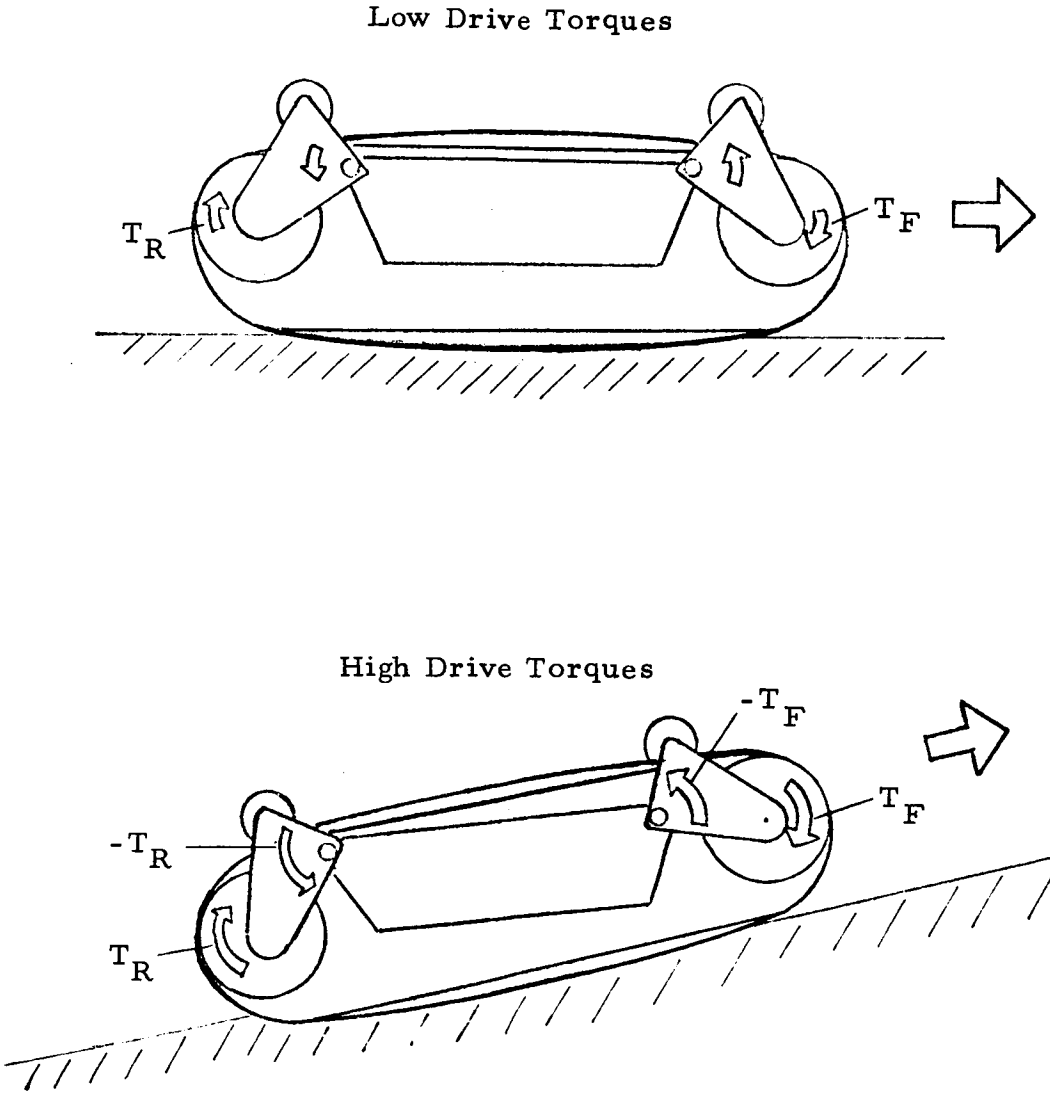

Fig. 4-2 - Front Suspension Arms are Torques Outward, Rear Suspension Arms Inward, in Reaction to Drive Torques Transmitted from Drum's Internal Drive to Loop. Desirable "anti-squat" chassis rotation results.

shown in Fig. 4-2, a desirable "nose-down" rotation of the chassis results which offsets some of the "nose-up" pitching due to load shifts and digging-in of tracks or loops delivering high torques on soft soil.

The inward rotation of the rear arm under maximum drive torque is the critical condition for sizing and adjustment of the torsion springs to a spring rate which must be sufficiently high to ensure that under this critical condition sufficient loop-drum contact pressure is maintained for positive drive torque transmission without separation of loop and drum. Alternate configurations are under study, including rigid rear drum suspension (simplifies design, attractive for low cost, high reliability, automated rovers), or parallelogram suspension of the drive drums which completely eliminates the dependence of the rotation of the suspension arms upon drive torques but increases slightly the mechanical complexity of the system. The latter design appears attractive for high-speed manned rovers.

4.2 CHASSIS STRUCTURE

The main chassis structure which provides stowage for the batteries, electronics telemetry and remote control systems, and supports the loop suspension consists of a rectangular frame of welded aluminum angle as shown in Fig. 4-3. A honeycomb panel provides a mounting base for onboard batteries, remote control and telemetry modules as shown in Fig. 4-4. The skin of the box is made of 0.5-mm magnesium alloy sheet. A curved bumper is mounted under the bottom of the chassis. It provides a stop for the loop when it buckles temporarily under excessive point loads. Friction in the buckled state is minimized by a Teflon molding of semi-circular cross section that covers the bumper. A front and rear access panel is located at the left hand side for quick access to the onboard equipment.

4.3 SUSPENSION ARMS

The suspension arms of the first-generation ELMS as shown in Vol. I, Fig. 2b, were made of 3.2 mm magnesium alloy sheet reinforced by magnesium.

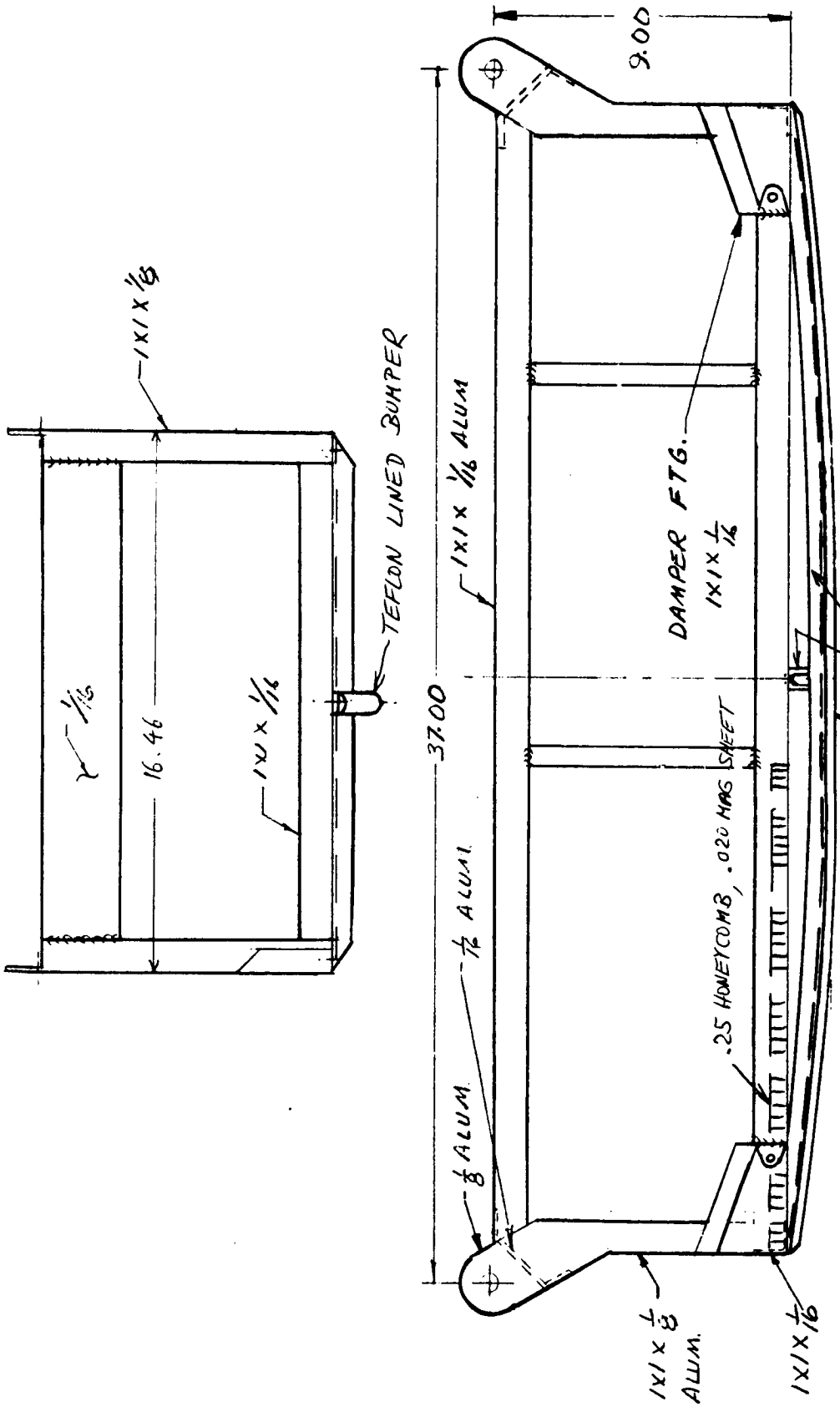

Fig. 4-3 - Chassis Structure Front and Side View

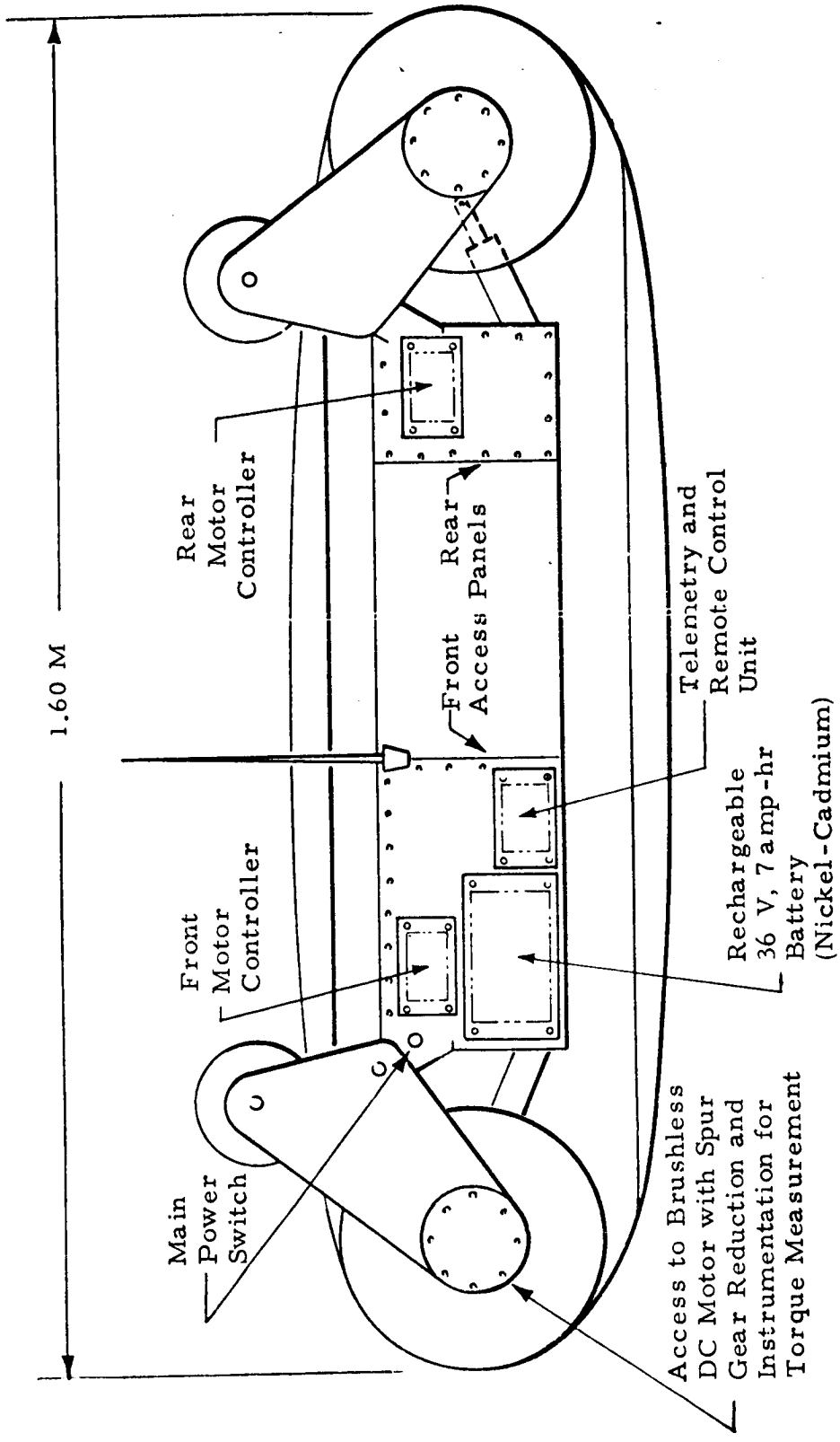

Fig. 4-4 - Location of and Accessibility to Major Subsystems Including Remote Control and Telemetry Units

angles riveted along the edges. A structural analysis (Appendix M) was performed to compare the open section design with a honeycomb core closed section configuration in torsional stiffness which was margional in the previous design. The honeycomb core (Fig. 4-5) with 0.5 mm magnesium alloy panels resulted in a 300% increase in torsional stiffness and a 15% weight reduction. The closed section design was therefore adopted. Bending stresses in the arms as they occur when the ELMS is under high side loads (assumed to be $\leq$650 N or 160 lb) were also checked in Appendix M and found to be within the allowable range for the 6.35 mm core thickness.

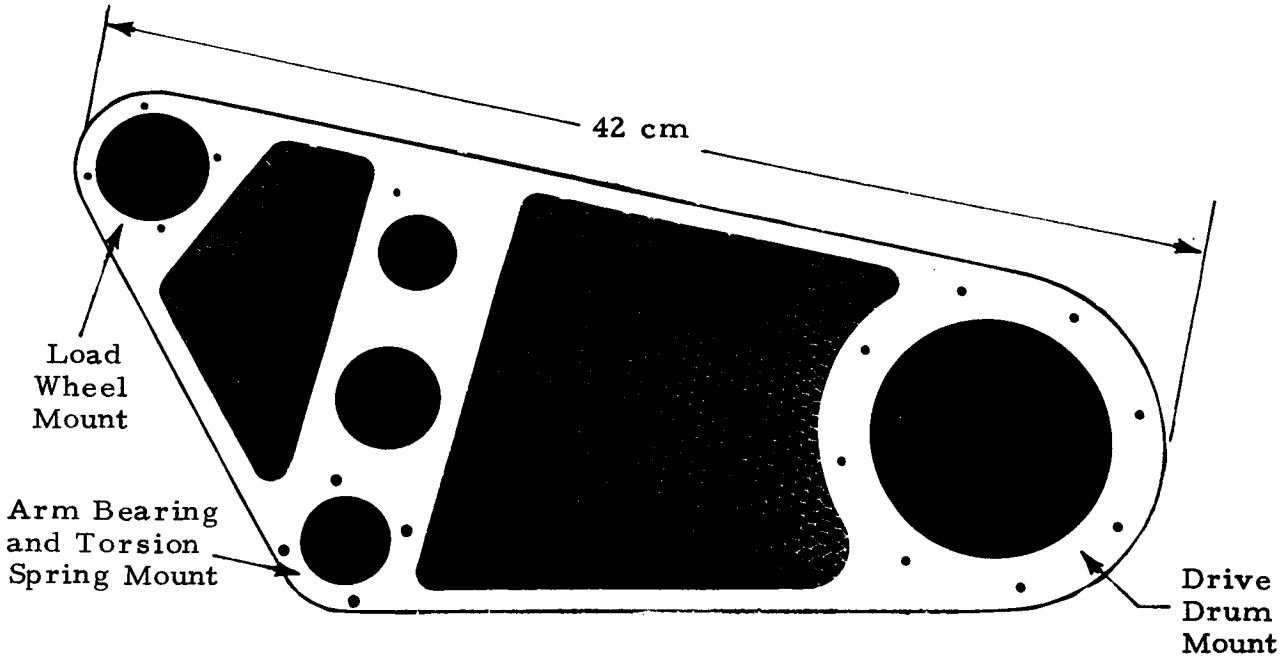

Fig. 4-5 - Core of Closed-Section Suspension Arm for Improved Torsional and Bending Stiffness. Aluminum honeycomb (3/16 in. cells) and magnesium alloy frame (1/4 in. thick).

4.4 DAMPERS

The shock absorbers to damp loop oscillations in pitching and dipping through the coupled suspension arm oscillations as explained in Fig. 4-1 were redesigned to adjust the damping ratio over a wide range (see Fig. 4-6). One-way damping action was required (inward only) to avoid separation of the

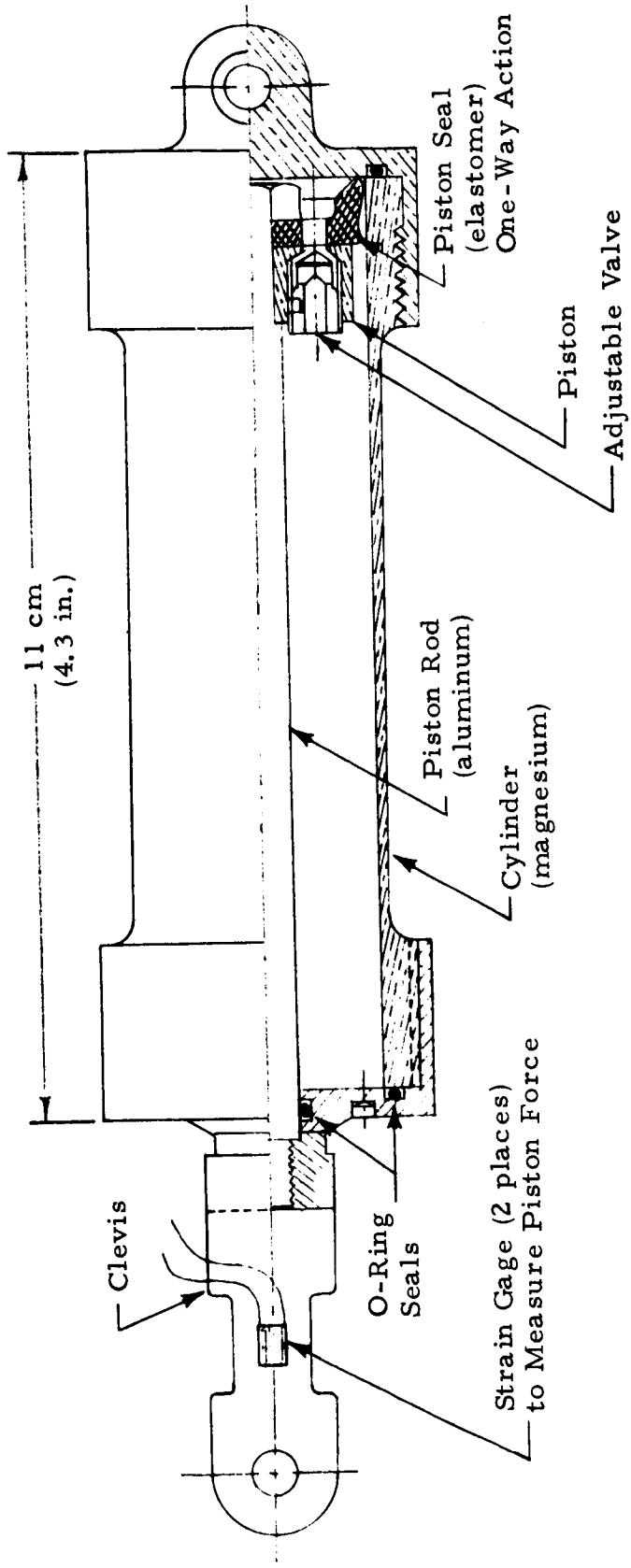

Fig. 4-6 - Lightweight Adjustable Shock Absorber Layout
(Two shock absorbers damp ELMS test unit in
pitch and plunge modes.)

drum from the loop during outward arm rotations. The use of elastomer cap seals for the piston provides a simple means to achieve the desired one-way action. The dampers are filled with a low-viscosity oil (automobile brake fluid).

An analysis of ELMS damping requirements was performed (Appendix N) to establish an approximate range of damping forces required for critical damping (damping ratio ≈ 0.7). The predicted damping coefficient is 2.24 N per deg/sec suspension arm rate. Assuming a maximum rate of 50 deg/sec during an impact load condition, the maximum piston force in the damper was estimated to be 112 N (25 lb).

The damper clevises are equipped with strain gages to measure piston forces. For high sensitivity measurements during operation on smooth terrain, a set of clevises has been reduced in cross section where the sensors are mounted. When rough terrain, high obstacles and steep slopes are negotiated which may require very high drive torques or may lead to high impact loads, the damping forces are measured through an instrumented pair of heavy-duty clevises which stand loads in excess of 3000 N (670 lb).

Once the requirements for damping characteristics are well defined, rotary dampers should be developed that form an integral part of the suspension arm bearing ("A" in Fig. 4-1). Such rotary dampers will not be vulnerable to contamination or damage by soil, dust or rocks.

Section 5
GROUSER DESIGN AND FABRICATION

One of the main improvements incorporated in this second-generation ELMS test unit is the development of uniform footprint of the lower loop section (see Fig. 2-18). This new loop form permits the installation of large grousers which increase substantially the contact area on hard ground, distribute the loads more uniformly across the loop width, and increase the buckling strength of the loop.

5.1 DESIGN

The grouser structure and mounting pattern on the loop is shown in Fig. 5-1. Polyurethane foam was selected as grouser material in a flexible condition:

Brand: Flexipol Urethane Compound FNP-251-8
Mixture Ratio: Prepolymer 67.7 parts by; Activator 100 parts

This hardness results in 7% compression under 6.9 N/cm^2 (1 psi) contact pressure which was considered satisfactory. For sufficient structural integrity and for easy mounting and replacement, a titanium alloy (Beta III) mounting plate was molded in near the base of the grousers. The places were perforated as shown in Fig. 5-2 to improve adhesion to the surrounding foam.

5.2 FABRICATION

A room temperature vulcanizing silicone rubber (RTV) mold was made from four wooden masters mounted on an aluminum sheet which was bent to match the loop curvature. The mounting plates were bolted to this aluminum base with long pins which also provided the access holes to insert the screws in the finished grouser. Four grousers can be molded simultaneously. Mold and foam components were cooled to 15°F before mixing and molding to improve uniformity of the foam.

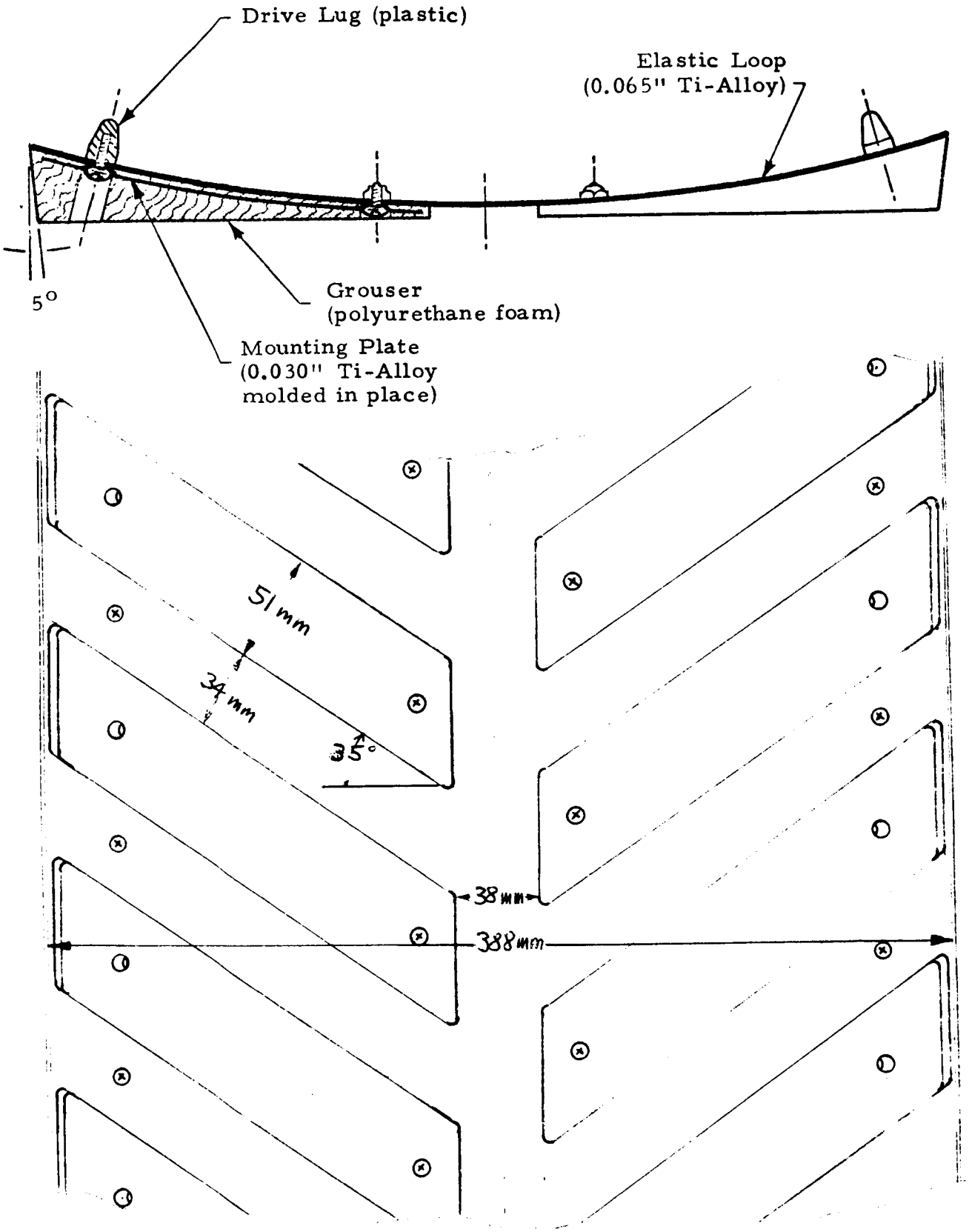

Fig. 5-1 - Grouser Structure and Mounting Pattern

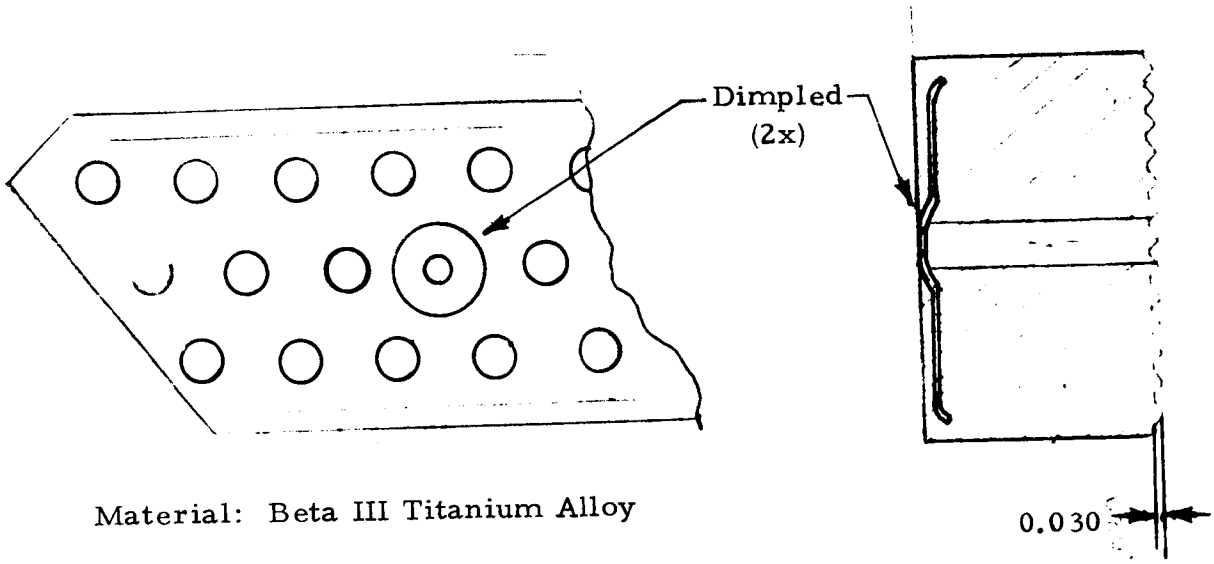

Fig. 5-2 - Titanium Mounting Plate Molded in Place Near Grouser Base to Provide Safe Mounting by Two Bolts and to Improve Structural Strength of Foam Grousers

Section 6
SUPPORT TRAILER DESIGN

As discussed in Volume I, Section 2.5, the major purpose of the trailer is to simulate the interactions of a second articulated ELMS module in a realistic manner. It was found that the various pitch joint configurations to link two ELMS modules together result in basically one of three pitching modes at the articulated pitch joint:

- Locked in pitch
- Spring restrained in pitch
- Free in pitch

The trailer design shown in Fig. 6-1 can simulate all three pitching modes.

6.1 CONSTANT PITCH ANGLE CONFIGURATION

Locking in pitch is achieved by rigid turnbuckle connections of the upper tubes which allow for pitch angle adjustment. The two outer transverse tubes (A) must be locked to the transverse smaller tube (B).

6.2 FLEXIBLE JOINT CONFIGURATION

The spring-restrained articulated joint configuration is obtained by replacing the rigid turnbuckles by the spring connections shown in Fig. 6-2. These units are threaded like turnbuckles with right-hand thread on one end and left-hand thread on the other end, for adjustment of the nominal pitch angle. The springs were sized so that their spring rate simulates two ELMS units in tandem configuration with an articulated joint that is free in pitch. The sizing of the trailer springs is given in Appendix O.

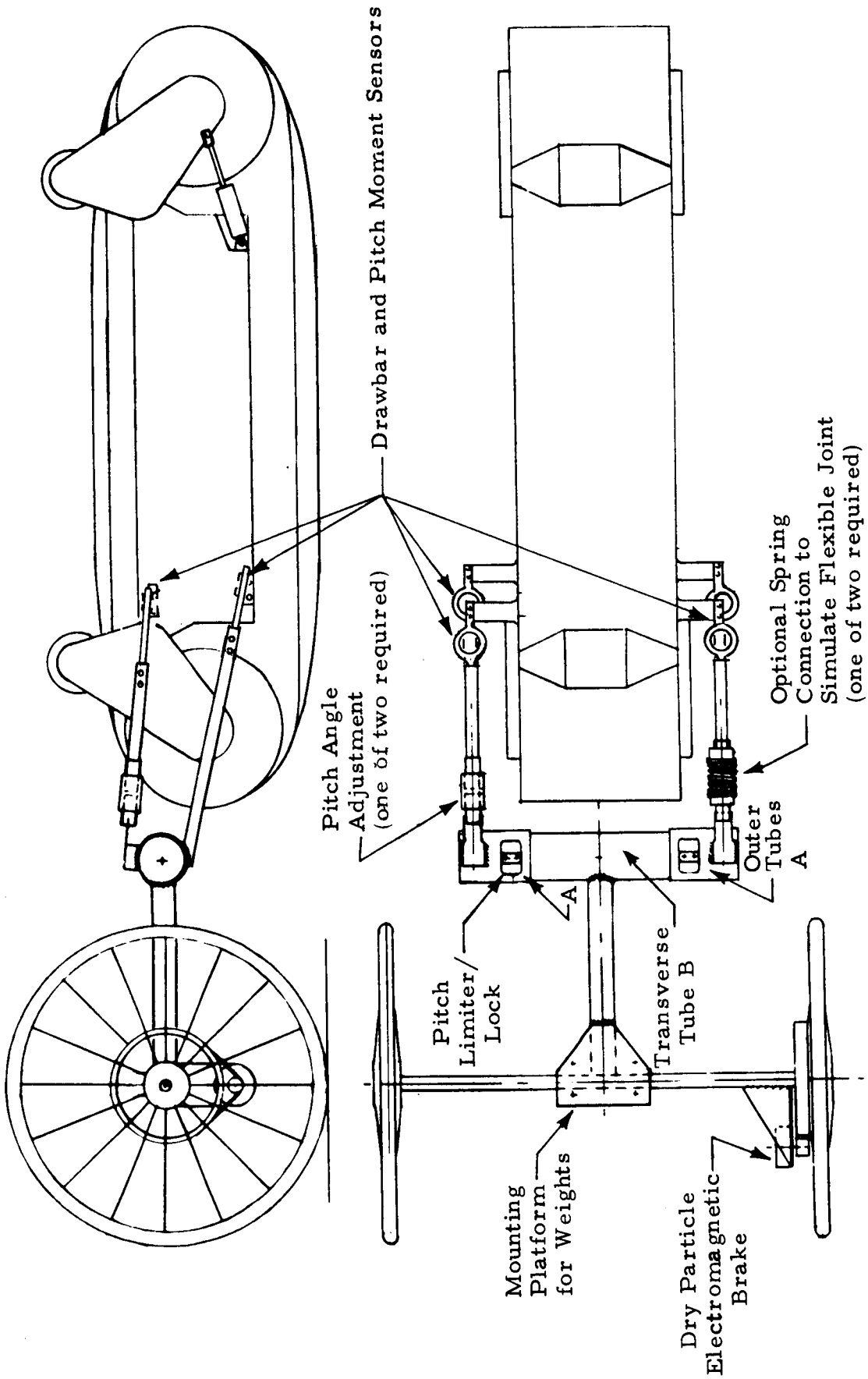

Fig. 6-1 - ELMS Trailer for Stabilization, Measurement of Drawbar Pull, Pitch Torques, Vehicle Speed and Travel and for Generating Specified Drag

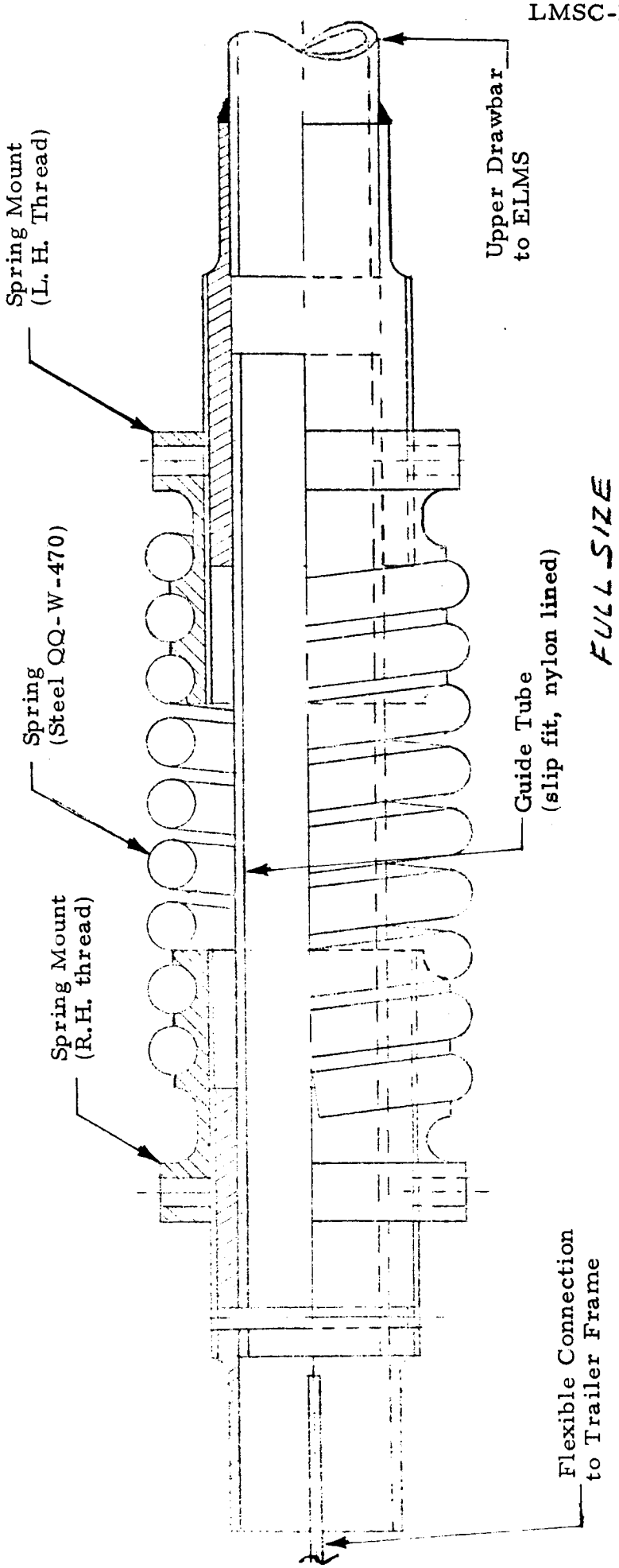

Fig. 6-2 - Spring Connection to be Mounted to Upper Trailer Drawbars in Flexible Pitch Joint Test Configuration

Section 7
INSTRUMENTATION AND CALIBRATION

The contract called for the following parameters to be measured for the performance evaluation of the ELMS, as listed in Section II.B of the Work Statement:

a. Torque requirements at the loop-soil interface.

b. Translational speed.

c. Angular velocity of drums.

d. Slip, including a suitable potentiometer or tachometer for continuous recording of rotary motion of trailer per Fig. 12 of Lockheed Document LMSC D081796-722.

e. Drawbar pull sensors as shown in Fig. 12 of Lockheed Document LMSC D081796-722.

f. Internal energy losses. Instrumentation shall include strain gages bonded to the left and right motor support tubes as shown in Fig. 6a of Lockheed Document LMSC D081796-722.

g. Energy dissipated at shock absorbers and dampers through the measurement of piston force and piston travel by means of appropriate sensors.

h. Distribution of contact pressure. The instrumentation shall consist of thin pressure gages installed in pockets provided in one or two grousers. These pressure gages are approximately 0.040 inches thick and 0.75 inches in diameter. Sufficient wire length shall be provided to make runs of two to three ELMS lengths without difficulty. The details of the pressure gage installation will be worked out in coordination with MSFC and WES personnel.

i. Drive torque and pitching moment sensors attached to the trailer arm per Fig. 12 of Lockheed Document LMSC D081796-722.

j. Dry particle brake attached to the trailer per Fig. 12 of Lockheed Document LMSC D081796-722.

In the following sections the instrumentation selected for measuring each of these parameters is described and the calibration data necessary for performance testing are presented.

A survey of the ELMS instrumentation in tabular form is given in Table 1, p. 19, of Volume I.

7.1 TORQUE REQUIREMENTS AT THE LOOP-SOIL INTERFACE

During the early phase of instrumentation design outlined in Ref. 15, it was assumed that the pitch torques picked up at the ELMS support might be processed so that torques at the loop-soil interface could be derived. A more detailed analysis showed that torques at the loop-soil interface can be isolated from measured pitch torques only if the center of ground contact pressure is precisely known which varies with soil conditions, drive torque, load and speed and is therefore not a practical variable for use in torque computations. A simpler and more reliable way to determine torques at the loop-soil interface is therefore proposed:

$$M_I = M_S - M_H,$$

where

M_I = net torque to overcome the losses at the loop-soil interface

M_S = total torque measured at the drive drums on the specified test soil at the same vehicle speed and drawbar pull

M_H = total torque measured at the drive drums on a hard surface at the same vehicle speed and drawbar pull

Two alternate methods to measure the drive torques delivered by motor and gearhead to the drive drums are described in Section 7.6.

7.2 TRANSLATIONAL SPEED

The ELMS trailer gear train assembly is shown in Fig. 7-1. Pulley A has 84 teeth and is connected to Pulley B of the magnetic particle brake which has 13 teeth. Pulley C of the magnetic particle brake has 20 teeth and is connected to Pulley D which has 128 teeth.

A calibration curve for the sensor output voltage versus trailer travel is shown in Fig. 7-2. The effective radius of the trailer wheel is 32.3 cm, with a tire pressure of 20.65 Newton/square centimeter (30 psi).

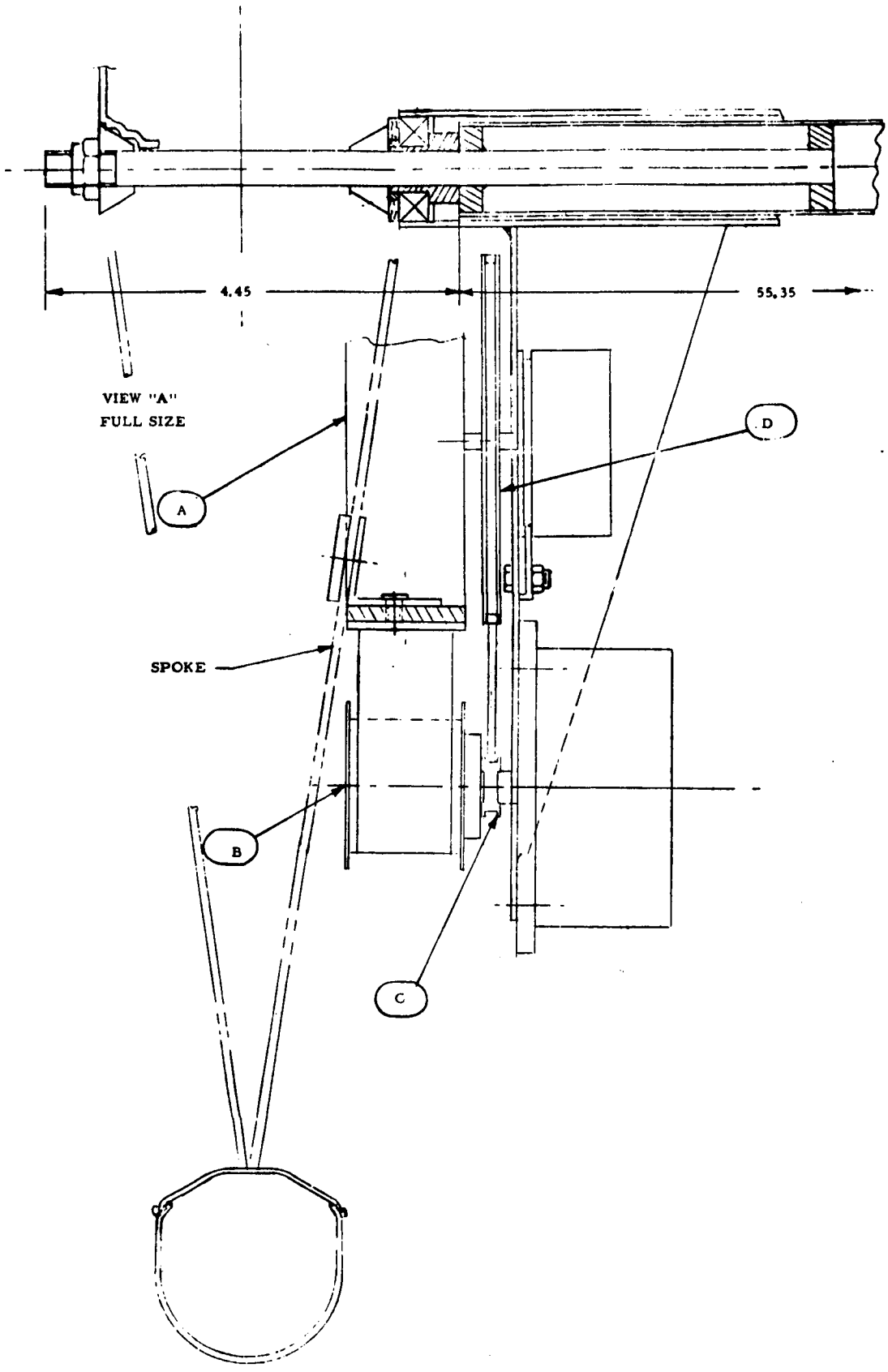

Fig. 7-1 - ELMS Trailer Gear Train Assembly

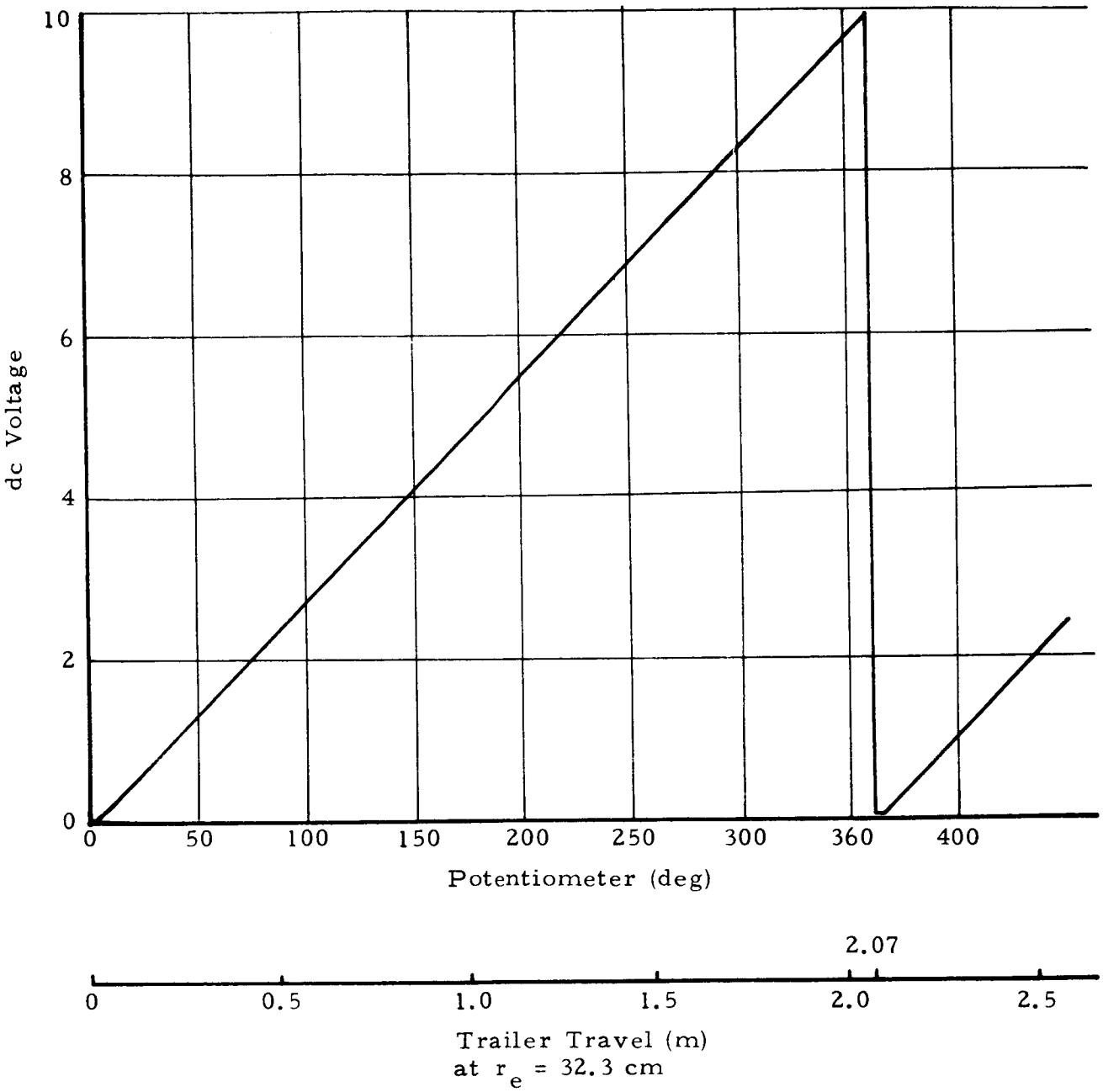

Fig. 7-2 - Voltage vs Trailer Travel

7.3 MEASUREMENT OF ANGULAR VELOCITY OF DRUMS

A calibration curve for the sensor output voltage versus angular velocity of drums is shown in Fig. 7-3. It was obtained by an end-to-end calibration of counted and timed drum revolutions versus output voltage.

7.4 MEASUREMENT OF SLIP AND TRAILER TRAVEL

Slip can be determined by the following formula:

$$\text{Slip} = \frac{V_L - V_T}{V_T}$$

where

V_L = velocity of the ELMS

V_T = velocity of the trailer (assuming that the wheel slip of the trailer is zero)

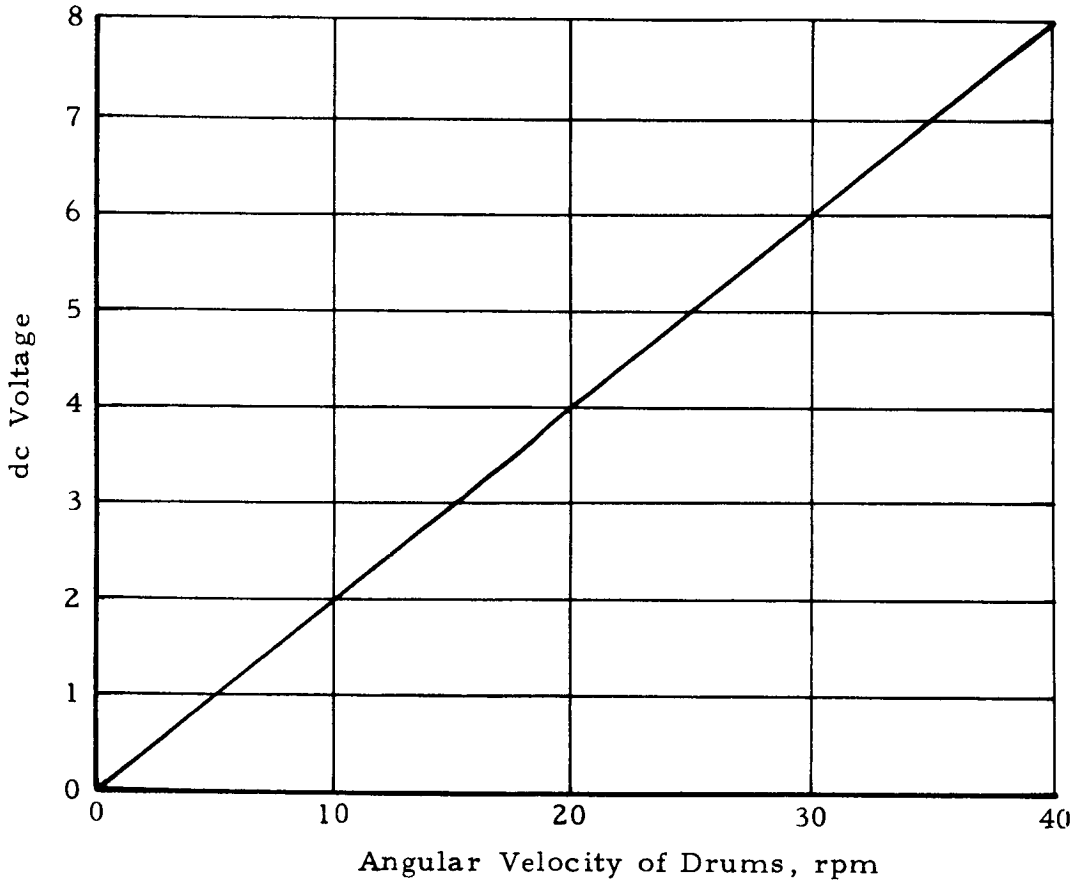

Fig. 7-3 - Voltage vs Angular Velocity of Drums

7.5 DRAWBAR PULL AND PITCH TORQUE MEASUREMENTS

As shown in Fig. 7-4, the upper and lower trailer drawbars are mounted to the ELMS chassis by means of ring-shaped strain gaged sensors that measure drawbar pull by summing all the signals where tension signals are positive, compression signals negative. Pitch torques acting between trailer and ELMS are obtained by subtracting the upper from the lower forces and multiplying by the distance between upper and lower ring sensors. The sensor design is shown in Fig. 7-4. The critical ring dimensions were established by a stress analysis given in Appendix P, to ensure maximum sensitivity within the expected range of drawbar pull and superimposed pitching torques, which was predicted to be 2770 N (620 lb).

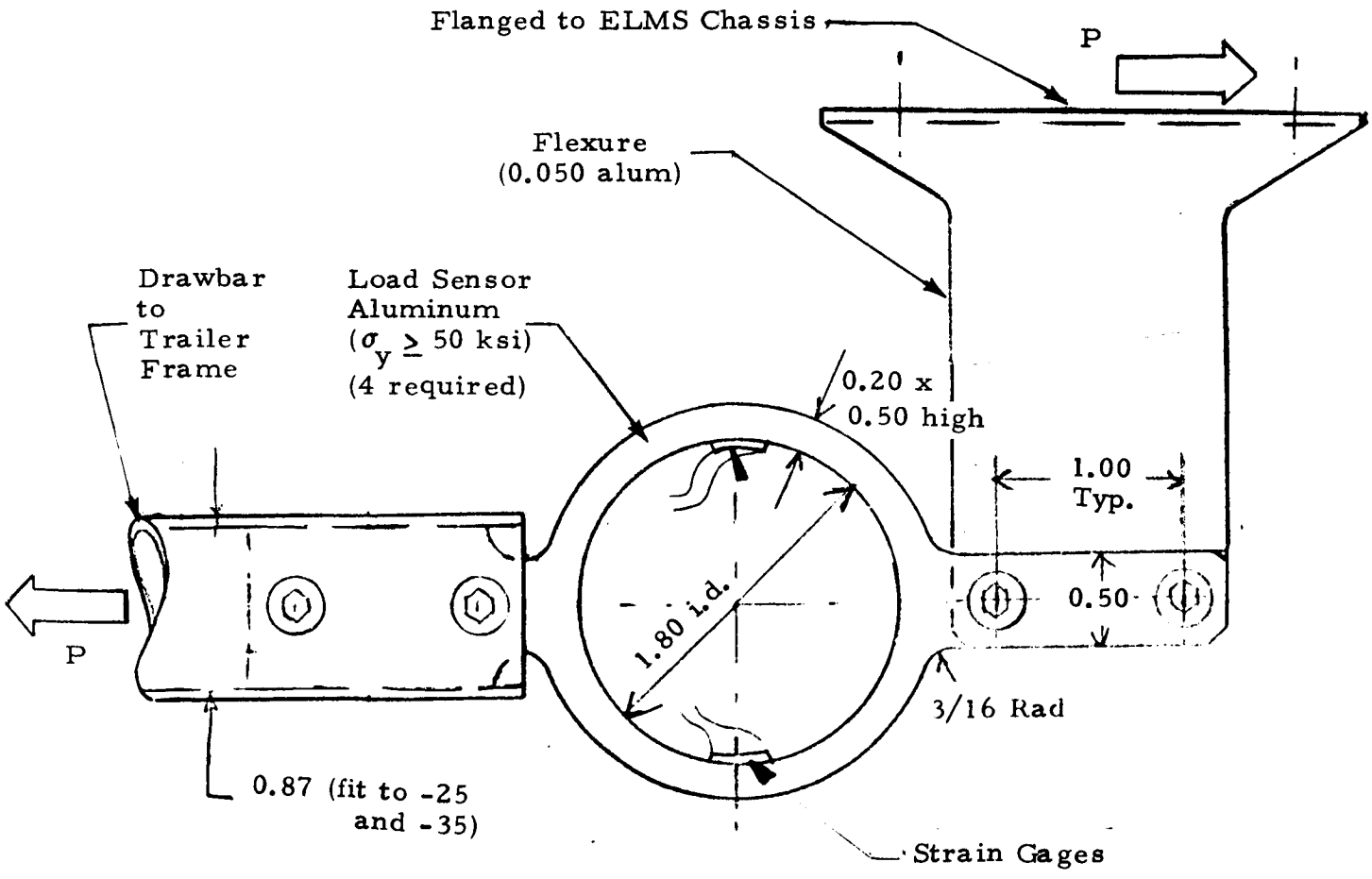

Fig. 7-4 - Ring Sensor Design to Measure Drawbar Pull and Pitch Torques. Ring dimensions as sized in Appendix O.

The location of the upper and lower sensors for measurement of drawbar pull and pitch torque are shown in Fig. 7-5. Calibration data for these sensors are tabulated in Table 7-1.

Table 7-1

ELMS TRAILER DRAWBAR PULL AND PITCH TORQUE SENSOR CALIBRATION DATA

Tensile Load (N)	Strain Gage Elongation (μ-in./in.)			
	Ring 1 (lower left)	Ring 2 (upper right)	Ring 3 (upper left)	Ring 4 (lower right)
0	0	0	0	0
333.8	920	920	910	920
823.3	2270	2275	2245	2268
1312.8	3615	3628	3580	3615
1802.3	4955	4970	4905	4955
2291.8	6295	6320	6235	6295
2781.3	7630	7657	7560	7632
Compressive Load (N)				
0	0	0	0	0
333.8	925	920	900	930
823.3	2275	2275	2215	2290
1312.8	3630	3640	3550	3640
1802.3	5000	5000	4890	5010

NOTE: Sensor locations are shown in Fig. 7.5.

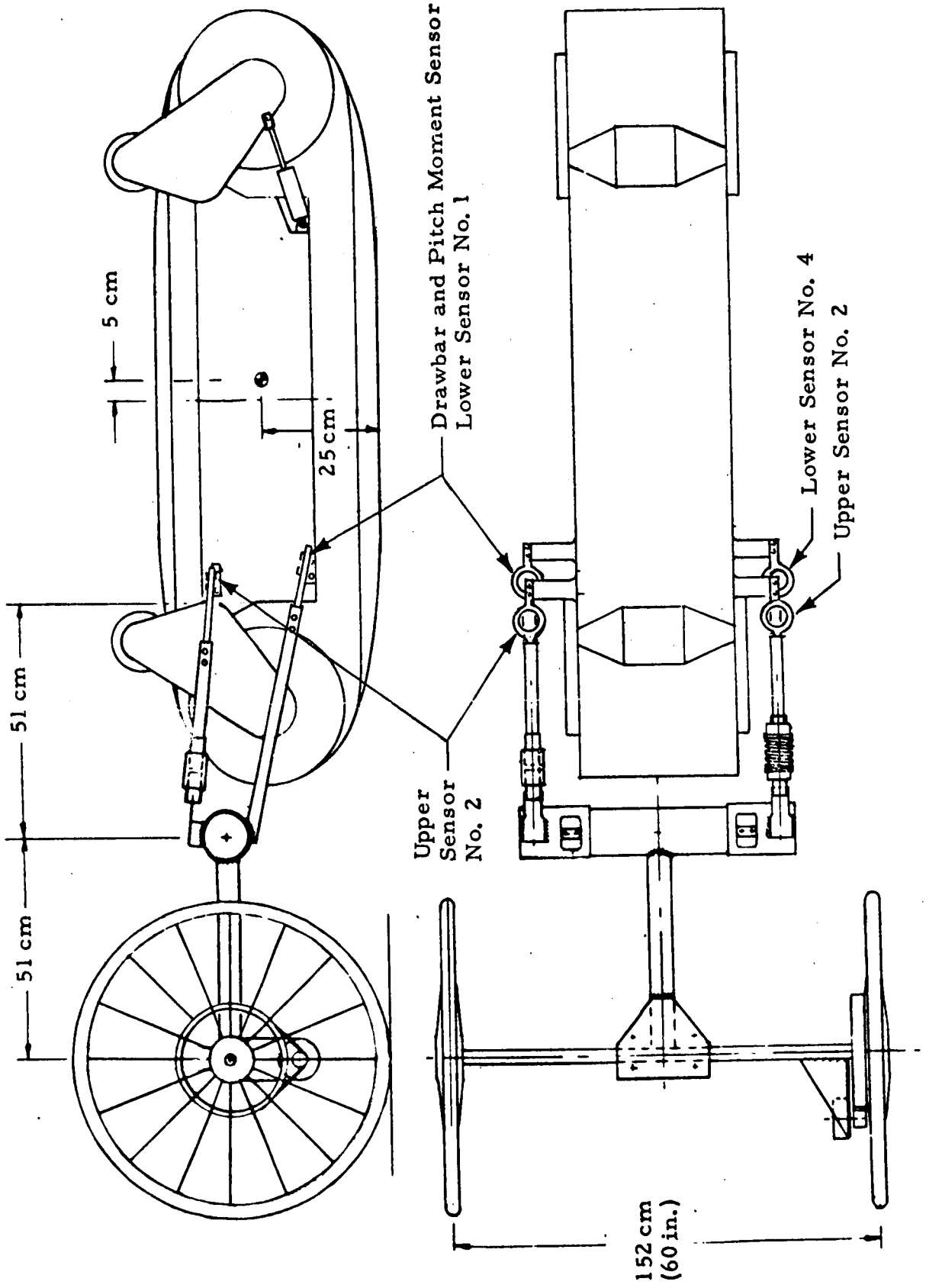

Fig. 7-5 - ELMS Trailer Instrumentation for Measurement of Drawbar Pull and Pitch Torques

7.6 INTERNAL ENERGY LOSSES

Input energy E_{in} is given by the product of battery current $I_{Bat.}$ and battery voltage $V_{Bat.}$; i.e.,

$$E_{in} = I_{Bat.} \times V_{Bat.}$$

To measure internal energy losses, strain gages are used. These gages are bonded to the left and right motor support tubes as shown in Fig. 3-1. Torque tube calibration for the drive motor supports is tabulated and shown in Table 7-2. The sum of the left sensor and the right sensor output yields the total torque of the motor. As a backup source for motor torque, input current and torque current calibration curves can be used to determine motor torque. The front and rear drive motor current versus torque characteristics for alternate output energy measurement is given in Figs. 7-6 and 7-7, respectively.

Table 7-2
TORQUE TUBE CALIBRATION FOR DRIVE MOTOR SUPPORTS

Torque (N-m)	Torque Tube							
	Strain Gage Elongation (μ-in./in.)				Shunt Resistance (10^3 ohm)			
	A	B	C	D	A	B	C	D
0	0	0	0	0				
4.07	30	35	30					
8.13	62	70	63	58	990	860	964	
12.20	92	116	93		670	530	664	
16.27	122	161	123	116	504	380	495	
20.34	152	203	154		406	304	397	
24.90	182	250	184	172	337	246	333	
28.47	212	295	215		291	209	285	
32.54	243	344	248	229	255	179	248	
36.60	272	384	276		227	160	222	
40.67	302	426	306	282	204	145	200	

Note: Torque Tubes A (right rear), B (left rear), C (right front), and D (left front)

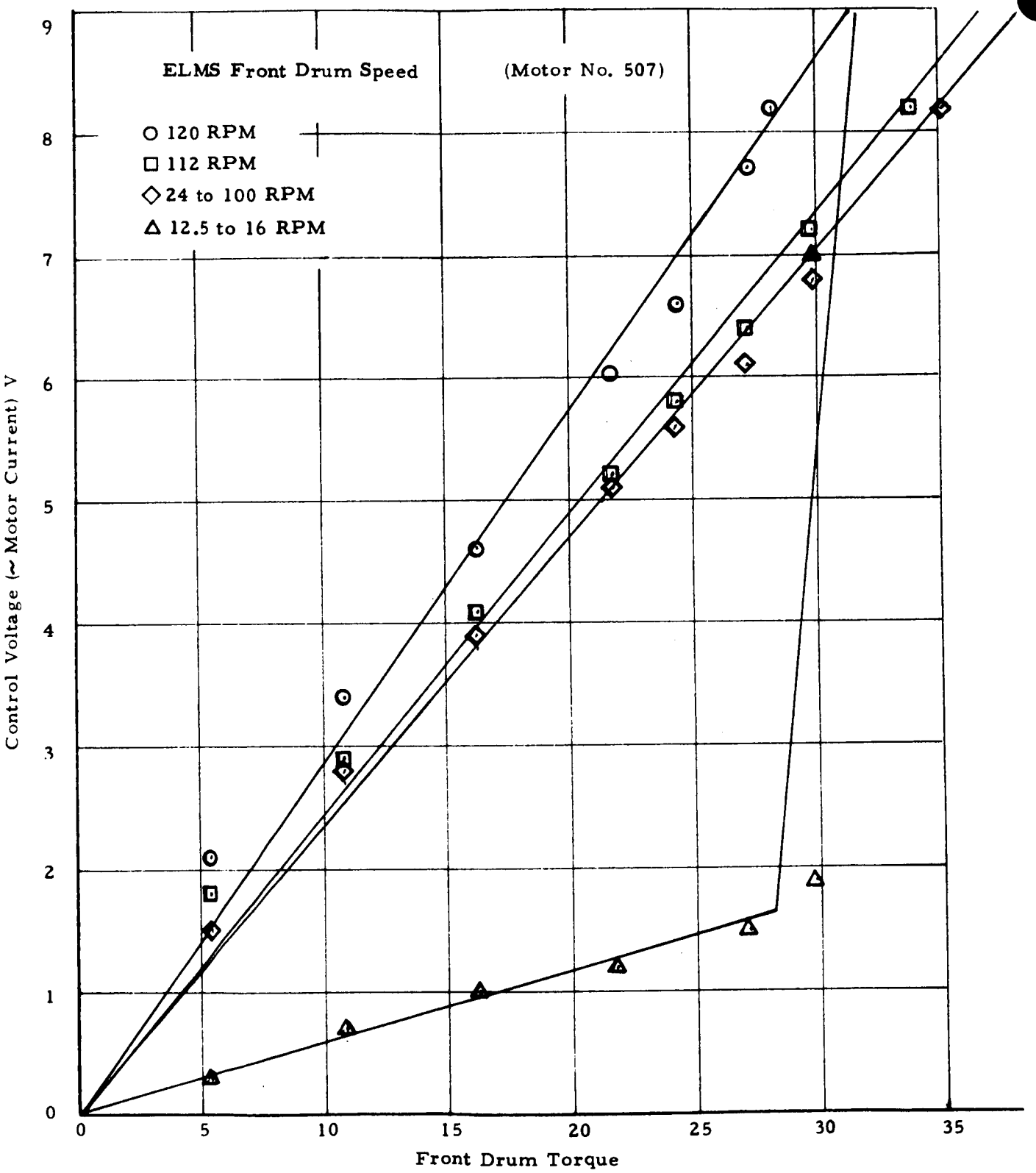

Fig. 7-6 - Front Drive Motor Current vs Torque Characteristics for Alternate Output Energy Measurement

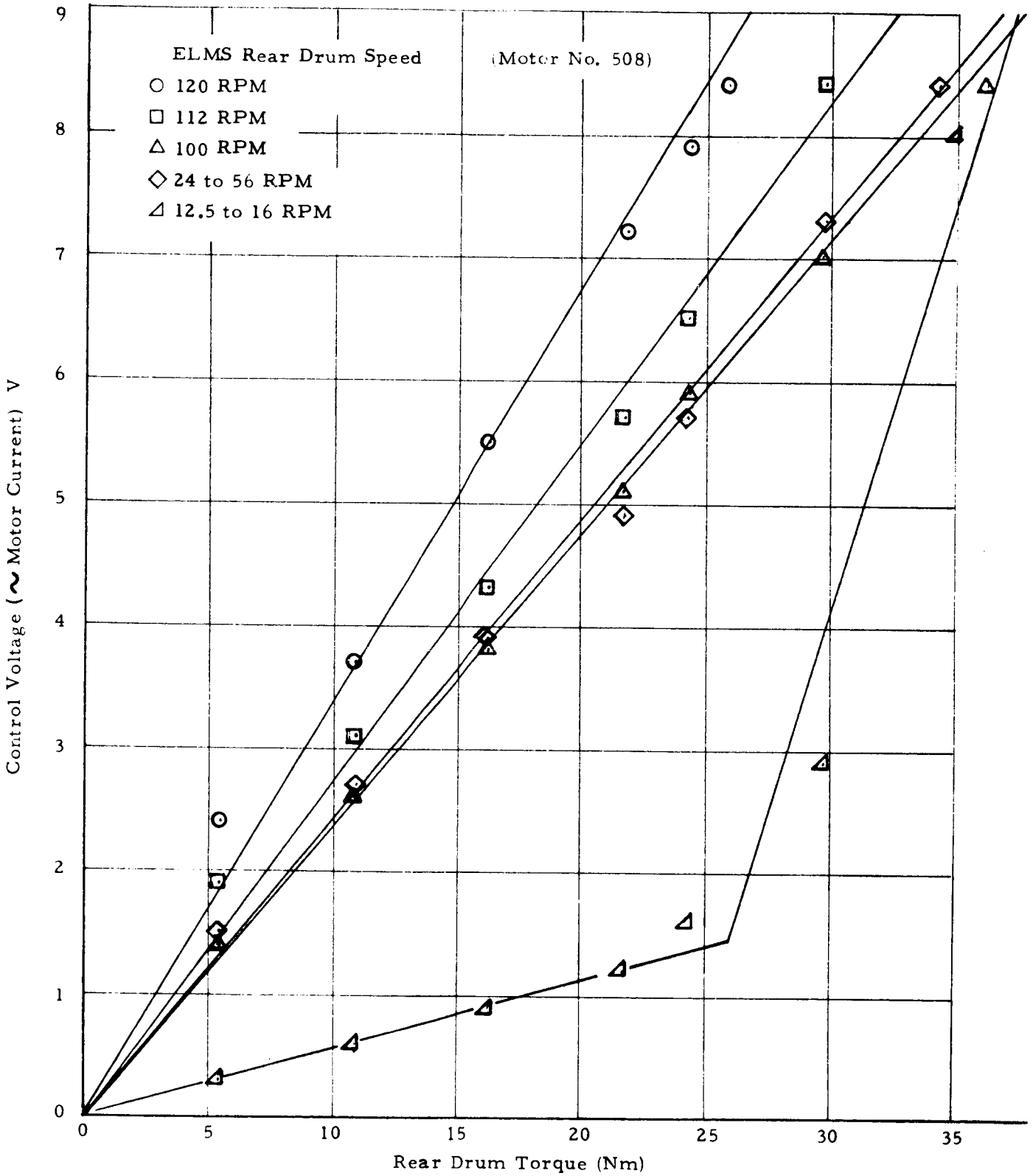

Fig. 7-7 - Rear Drive Motor Current vs Torque Characteristics for Alternate Output Energy Measurement

7.7 MEASUREMENT OF ENERGY DISSIPATED AT SHOCK ABSORBERS

Energy dissipated at the shock absorbers and dampers is determined through the measurement of piston force and piston travel. Piston force is measured by a strain gage clevis mounted on the piston rod. Calibration data for these clevises are shown in Table 7-3. Piston travel is measured by a potentiometer connected to the suspension arm. Calibration data for piston travel is given in Fig. 7-8.

Table 7-3

CLEVIS CALIBRATION FOR PISTON FORCE MEASUREMENT

Clevis No. 3*			Clevis No. 4*		
Force (N)	Strain Gage Elongation (μ-in./in.)	Shunt** Resistance (10^3 ohm)	Strain Gage Elongation (μ-in./in.)	Shunt Resistance (10^3 ohm)	Force (N)
0	0		0	0	0
336	315	195.0	368	168.0	425
434	400	153.0	792	77.6	917
926	836	72.9	1238	49.55	1410
1122	1015	60.1	1700	36.1	1900
1812	1666	36.63	2182	28.08	2400

*Clevis Nos. 1 and 2 replaced by reinforced Clevis Nos. 3 and 4.

**Shunt across black (Input "+") and red leads. Input "-" is green.

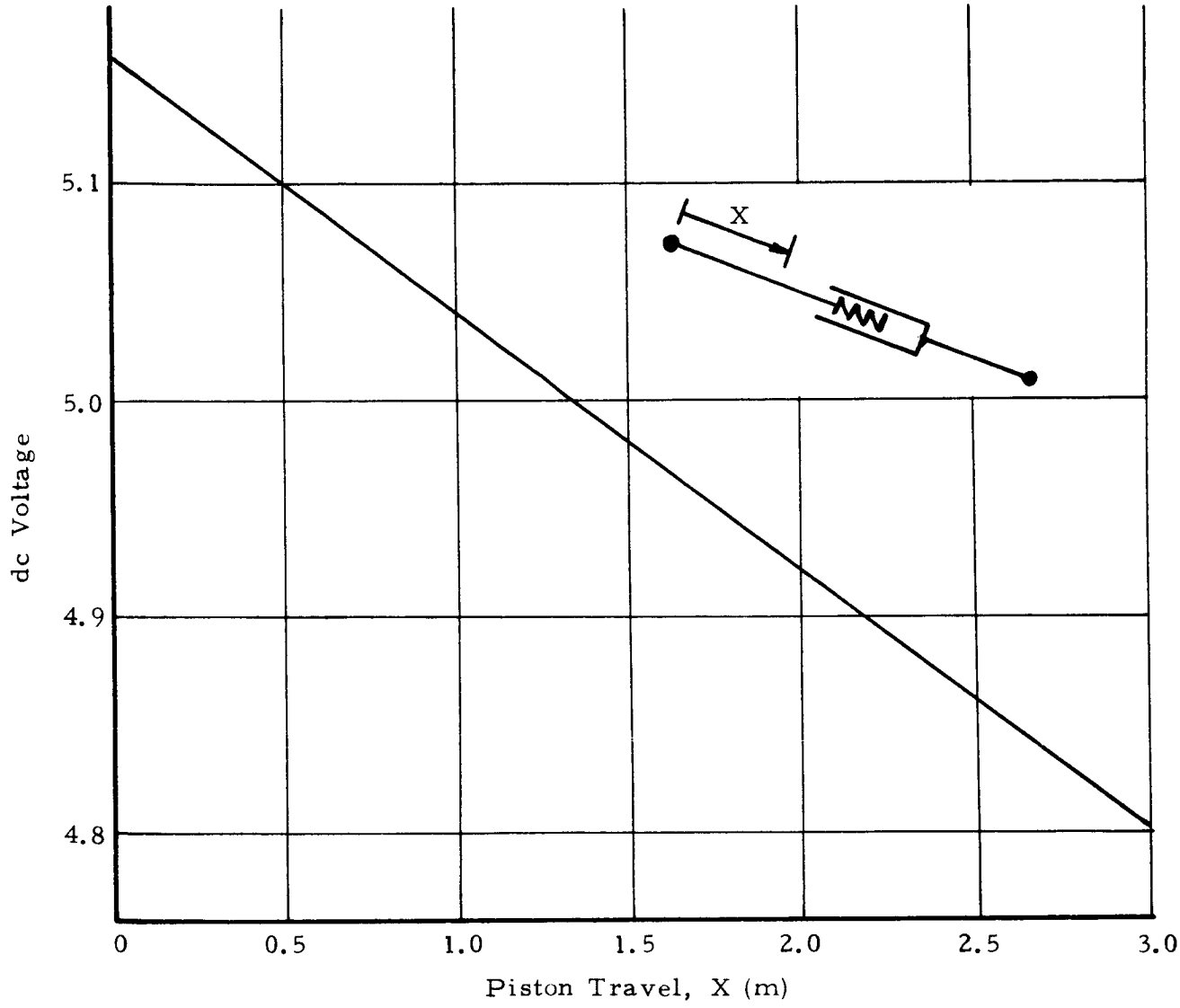

Fig. 7-8 - Voltage vs Piston Travel Characteristics for Measurement of Energy Dissipation

7.8 DISTRIBUTION OF CONTACT PRESSURE

Thin pressure transistors installed in special grousers are used to measure contact pressure distribution. The locations of these pressure transistors are shown in Fig. 7-9. Calibration data for these transistors are shown in Table 7-4. Specification and performance information are given in Figs. 7-10 and 7-11, respectively.

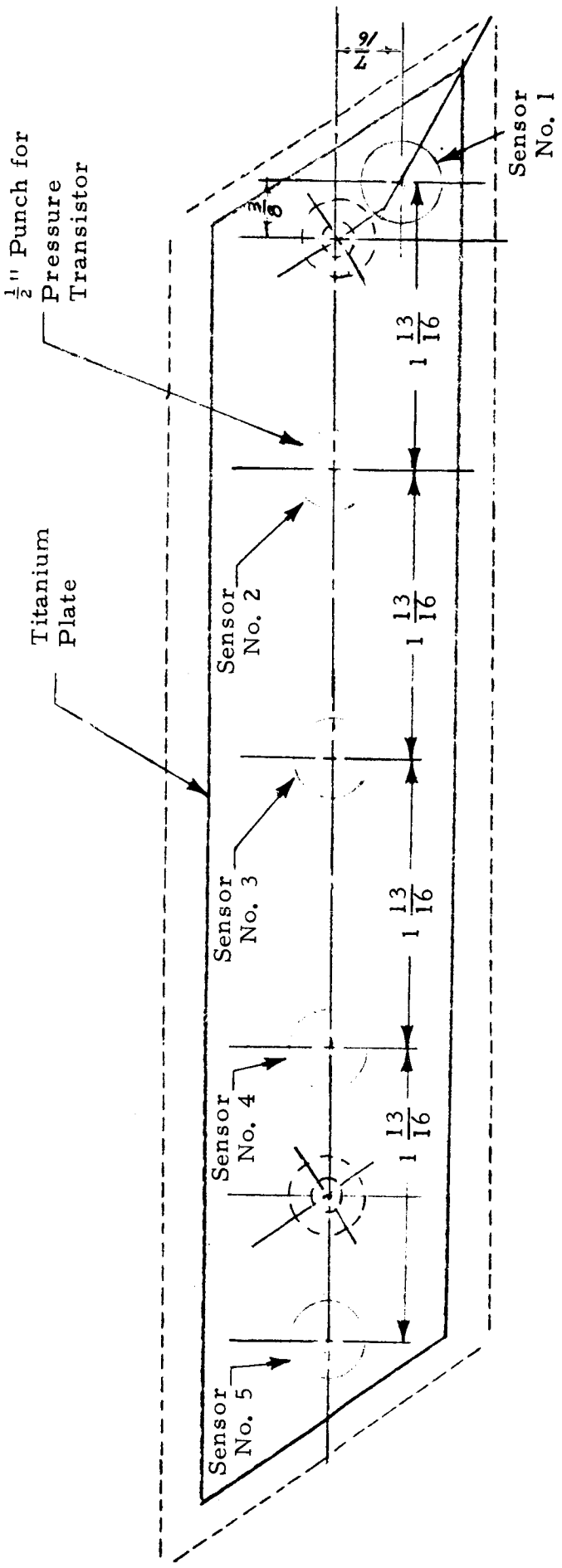

Fig. 7-9 - Location of Pressure Transistors in Special Grouser to Measure Contact Pressure Distribution

Table 7-4

PRESSURE TRANSISTOR CALIBRATION FOR CONTACT PRESSURE DISTRIBUTION

Pressure (N/cm^2)	Sensor No. 5 Base Current		Sensor No. 4 Base Current		Sensor No. 3 Base Current		Sensor No. 2* Base Current		Sensor No. 1 Base Current	
	64 μ-amp	58 μ-amp	175 μ-amp	161 μ-amp	162 μ-amp	152 μ-amp	207 μ-amp	197 μ-amp	112 μ-amp	107 μ-amp
	Output Voltage		Output Voltage		Output Voltage		Output Voltage		Output Voltage	
0	0.9259	2.905	1.85	3.86	1.98	3.99	1.99	3.87	1.98	3.01
0.138	1.7223	3.510	2.87	4.73	3.04	4.86	3.19	4.92	3.64	4.56
0.276	2.5516	4.108	3.72	5.53	4.08	5.65	4.33	5.84	5.10	5.87
0.414	3.2611	4.669	4.61	6.24	5.03	6.35	5.34	6.64	6.32	6.94
0.552	3.8393	5.166	5.41	6.86	5.83	6.94	6.20	7.31	7.29	7.78
0.689	4.3397	5.612	6.21	7.41	6.53	7.44	6.94	7.87	8.06	8.43
0.552	3.784	5.136	5.48	6.86	5.95	6.97	6.20	7.32	7.28	7.78
0.414	3.451	4.645	4.67	6.23	5.25	6.39	5.33	6.65	6.28	6.92
0.276	2.579	4.116	3.77	5.50	4.41	5.68	4.33	5.85	5.03	5.84
0.138	1.917	3.525	2.78	4.68	3.43	4.83	3.19	4.92	3.55	4.52
0	1.054	2.860	1.70	3.78	2.29	3.81	1.94	3.85	1.79	2.95

NOTE: Average of two runs.

*Sensor No. 2 has no stable base current. Adjust base current so that 3.87 volts output is obtained at $p = 0\ N/cm^2$. Do not exceed 300 μ-amp.

STOLAB

PITRAN®
Pressure Transistors

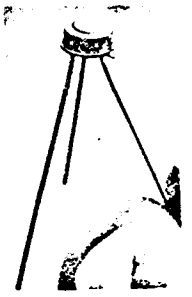

CONDENSED CATALOG

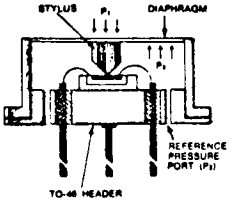

The PITRAN is a silicon NPN planar transistor that has its emitter-base junction mechanically coupled to a diaphragm. A differential pressure applied to the diaphragm produces a large, reversible change in the gain of the transistor.

LINEAR PRESSURE RANGES-PSID

MODEL	Min	Nom	Max
PT-L2	.07	.1	.17
PT-M2	.15	.25	.35
PT-H2	.3	.5	.7
PT-12	.65	1	1.5
PT-22	1.25	2	2.9
PT-52	2.8	5	6.5
PT-102	6	10	13
PT-152	12	15	18
PT-202	16	20	24

PRESSURE RANGE EQUIVALENTS

PSID	Inches H_2O	Torr (mm Hg)	dB (re 2 x 10^{-4} dynes/cm²)	Gram/cm²	Millibars
.1	2.77	5.17	151	7.03	6.89
.25	6.92	12.9	159	17.6	17.2
.5	13.8	25.9	---	35.2	34.5
1	27.7	51.7	---	70.3	69.0
2	55.4	103	---	141	138
5	138	259	---	352	345
10	277	517	---	703	690
15	415	776	---	1055	1035
20	554	1030	---	1410	1380

SPECIFICATIONS

	MINIMUM	NOMINAL	MAXIMUM	
Linear Output*	20			% of applied voltage
Linearity*		±0.5	±1.0	% deviation from best straight line
Hysteresis*		±0.5	±1.0	%
Overload Pressure Range See Note 1.	500	700		% of linear pressure range
Temperature Coefficient*				
Zero Shift		±150	±300	mV/°C
Sensitivity Change		-0.2	-0.5	%/°C
Noise*		0.3	1	mV
Dynamic Range	65			dB
Rise Time		10		microseconds
Volumetric Displacement		4×10^{-8}		in^3 for full scale pressure
Diaphragm Displacement		2	4	microinches
Mechanical Resonance Frequency	100	150		kHz
Life	10			billion cycles
h_{fe}*		10	40	at V_{CE} = 2 V, I_C = 800 μA, Δ P = 0
I_{CBO}*		0.1	1	μA at V_{CB} = 60 V
BV_{CEO}*	50	120		volts at I_C = 10 μA
Operating Temperature	-40		+75	°C
Acceleration			300	g
Vibration Sensitivity*		1		millivolt/g perpendicular to diaphragm
Weight, Including Leads			1/3	gram

*Measured in the Test Circuit shown on page 4.

Note 1: For 10, 15 and 20 PSID Models Maximum Overload Range is ± 35 PSID.

Fig. 7-10 - Manufacturer Specification Information

STOW LABORATORIES INC. KANE INDUSTRIAL DRIVE • HUDSON, MASS. 01749 • PHONE: (617) 562-9347

TYPICAL PERFORMANCE

The PITRAN is calibrated in the test circuit shown. The simple common-emitter configuration provides a linear dc output of at least 2 volts when rated pressure is applied to the PITRAN'S diaphragm.

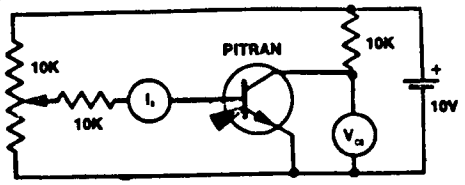

TEST CIRCUIT

PRESSURE CHARACTERISTICS

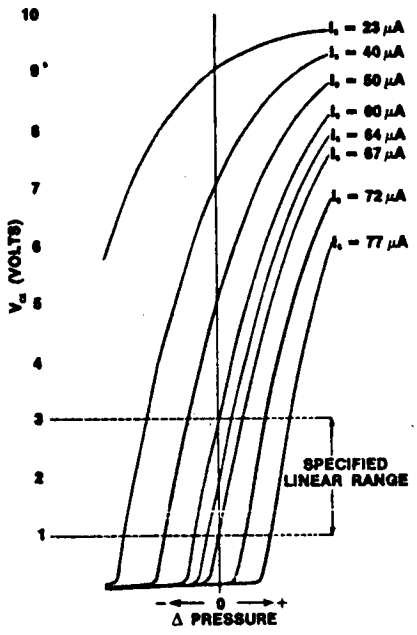

LINEAR PRESSURE RANGE AT V_{CE} = 2 V

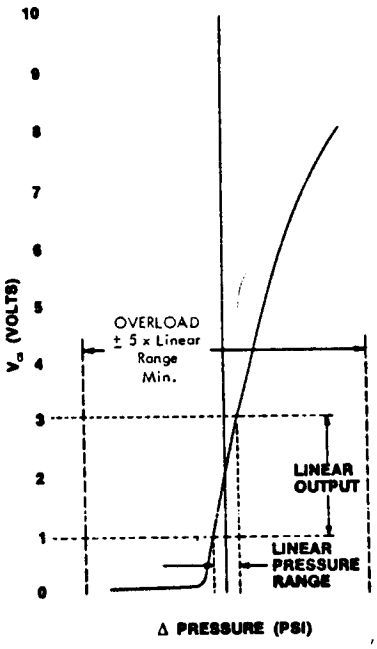

MECHANICAL SPECIFICATIONS

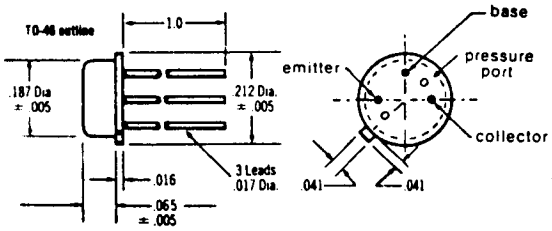

Diaphragm: Beryllium copper, nickel and gold plated
Case: Kovar, nickel and gold plated
Leads: Kovar, gold plated

(Note that the collector is connected directly to the case.)

The gold plated PITRAN diaphragm can measure pressure in almost any fluid. However, the reference side of the PITRAN is in contact with the NPN chip. Therefore, the pressure medium on the reference side must be nonconductive and noncorrosive.

NOISE VOLTAGE

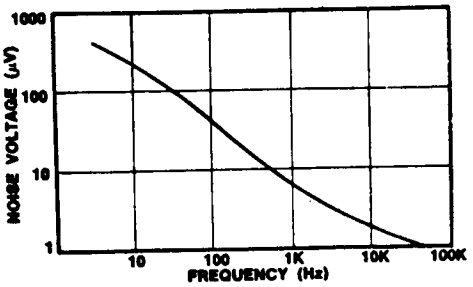

MECHANICAL FREQUENCY RESPONSE

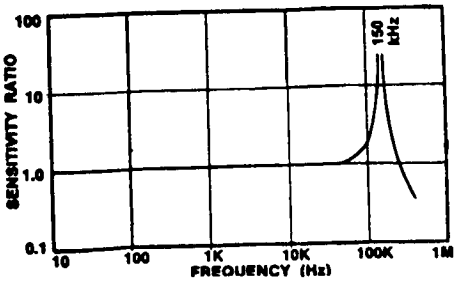

Fig. 7-11 - Manufacturer Performance Information

7.9 DRIVE TORQUE AND PITCHING MOMENT MEASUREMENTS

The drive torque T is given by the difference of the upper and lower drawbar pull, F_1 and F_2, respectively; i.e.,

$$T \approx \frac{1}{2} (F_1 - F_2) h$$

where h is the distance between the two drawbars as shown in Fig. 7-12.

7.10 DRY PARTICLE BRAKE MEASUREMENTS

Dry particle brake calibration is given in Fig. 7-13. The brake force at the tire-ground interface is based on 20.65 N/cm^2 (30 psi) tire pressure.

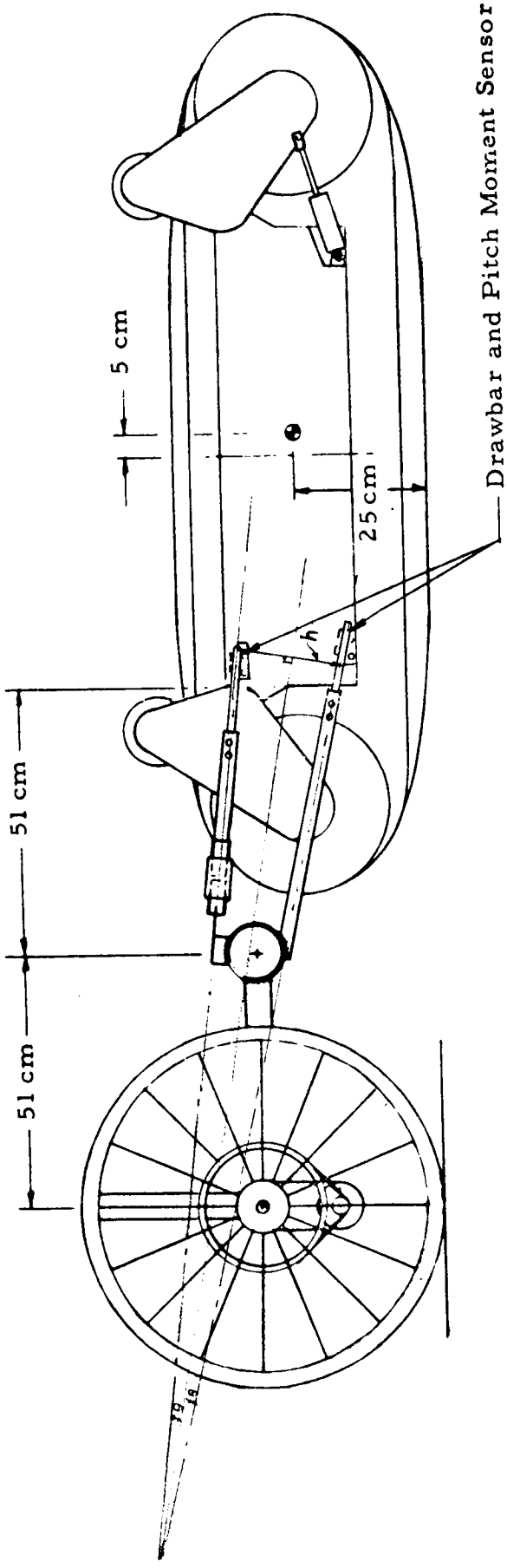

Fig. 7-12 - Drawbar Pull and Pitch Torques Measurements

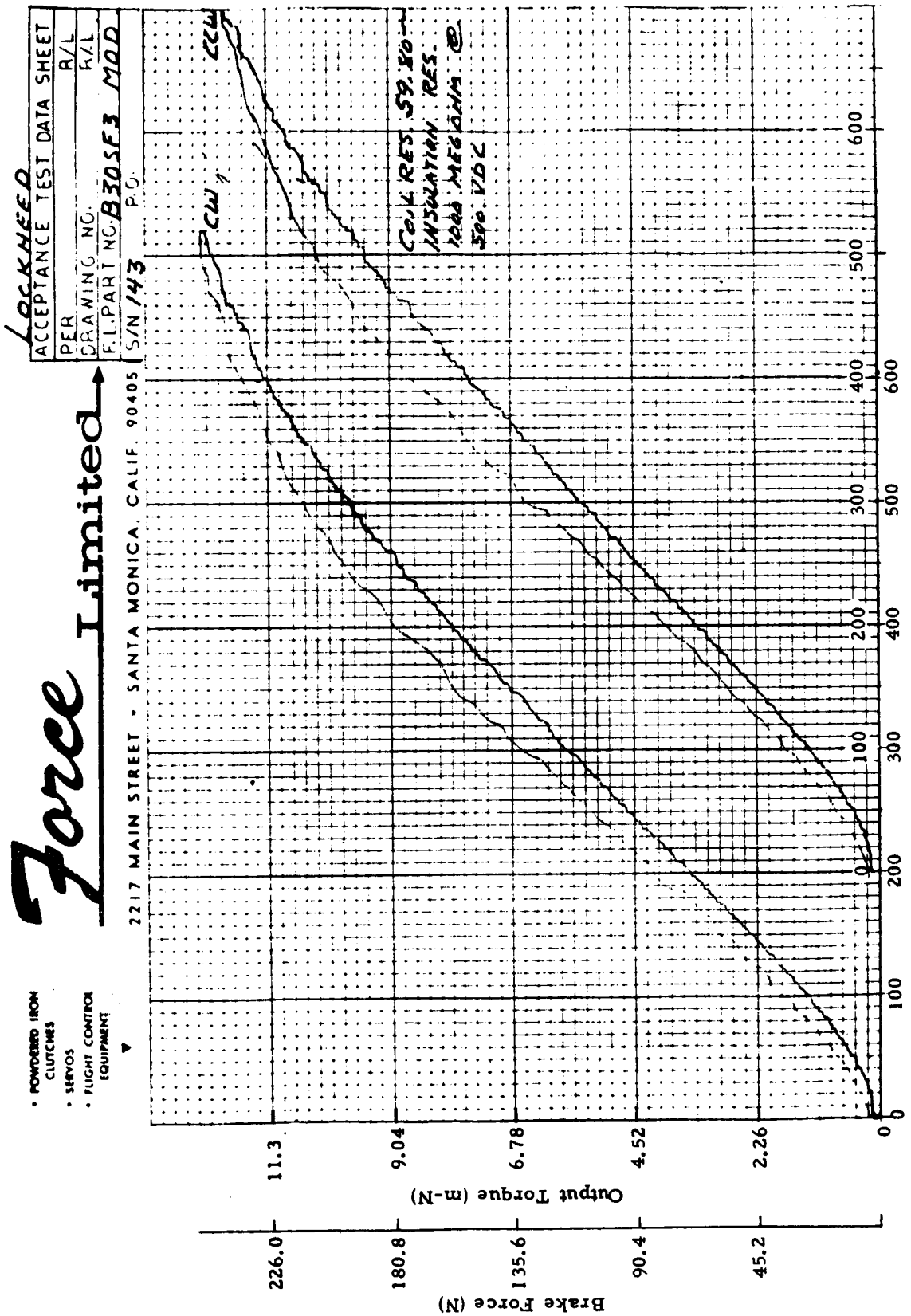

Fig. 7-13 - Dry Particle Brake Calibration

Appendix A

MAIN SECTIONS OF SCOPE OF WORK TO CONTRACT NAS8-27727

Appendix A

EXHIBIT "A"

SCOPE OF WORK

I. WORK STATEMENT: The contractor shall design; fabricate; check the structural integrity; calibrate the on-board instrumentation; and assure compatibility with GFE (including traction/drive system components, guidance control and data telemetry system), of an improved version of an existing "Loop-wheel," or "Loop track," mobility system, developed by the Lockheed Research & Engineering Center, Huntsville, Alabama. The improved version of said mobility system shall be designated, henceforth, as the "Elastic-Loop Mobility System (ELMS)." The Contractor shall, further, integrate all GFE components with the ELMS and assure compatibility for testing of the final assembled unit with the mobility performance testing apparatus of the U. S. Army Engineer Waterways Experiment Station (WES), Vicksburg, Mississippi. During the design and fabrication phase the Contractor will be required to visit the WES at Vicksburg, Mississippi, on an as needed basis as determined by the Contracting Officer's Technical Representative (COR). Travel to and from the WES facility will be provided by the Government. Upon completion of the foregoing tasks, the Contractor shall deliver the assembled ELMS to the Marshall Space Flight Center for a mobility performance evaluation testing program to be conducted by the WES.

The Scope-of-Work will include the tasks listed under the separate headings below.

II. SCOPE:

A. Basic Unit Design and Fabrication

1. General Considerations.

The design of the basic ELMS unit shall be compatible with the following considerations:

a. The mobility performance evaluation of the ELMS will be accomplished under two testing modes: (1) the ELMS will be attached to the WES mobility performance testing apparatus for the purpose of conducting controlled-slip tests on level, soft-soil surfaces; and (2) the ELMS will be subjected to soft-soil slope climbing, rigid obstacle negotiation and crevasse/depression bridging tests. Under this mode, the ELMS will be tested as a

EXHIBIT "A" (CONT'D)

self-contained, remote controlled unit, detached from any testing apparatus or any external power supply sources. For this mode a special trailer arrangement shall be constructed which will attach to the front part of the ELMS chassis with a vertical spring and damper, the position of which shall be made adjustable in a horizontal direction. Two each viscous (dashpot type) dampers will be provided by and at WES as GFE to the Contractor. The trailer dimensions shall be compatible with the rail dimensions and spacing of the WES soil bins.

b. Under the performance testing mode described in Item 1a.(1) above, the total contact load imposed by the ELMS on the soft surface including its dead weight, will be varied, by counterbalancing, between 60 lbs. and 150 lbs. Under the performance testing mode described in Item 1a(2) above, the dead weight of the ELMS, including the structure, the traction-drive system, batteries, onboard instrumentation, guidance and control and data telemetry systems, is estimated to be of the order of 125 lb.

c. The unit developed shall be provided with a sufficient instrumentation to assure that its mobility performance characteristics, power requirements and internal energy losses are determined in an unambiguous manner.

d. Provisions will be made in the design of the structure enveloping the traction-drive system and associated controllers and power source, as well as the instrumentation, guidance and control and data telemetry systems, as specified below, to ensure that all these components are easily accessible and can be repaired or replaced in-place without removing major structural components of the ELMS.

e. The unit developed under this contract shall be capable of being integrated, on a modularized basis, with a single or multiple ELMS units to form a manned, or an unmanned, remote controlled vehicle or a manned vehicle, if tested under a reduced gravity environment, with the understanding that the maximum speed under the "manned mode operation" will be governed by the limitation of the GFP motors.

Appendix B

SPRING CHARACTERISTICS AND STRESSES IN THE ELASTIC LOOP

Appendix B

B.1 FUNDAMENTAL RELATIONS

The deformations of the loop are inextensional bending distortions. The bending moment of an isotropic thin shell is given by

$$m^{\alpha\beta} = B\left[(1-\nu)\, k^{\alpha\beta} + \nu a^{\alpha\beta} k^{\lambda}_{\lambda}\right] \quad . \tag{B.1}$$

The coordinate system is chosen so that the metric tensor $a^{\alpha\beta}$ has the components

$$a^{11} = a^{22} = 1 , \qquad a^{12} = 0 \tag{B.2}$$

(See Fig. B-1.) $k^{\alpha\beta}$ is the change of curvature tensor and

$$B = \frac{Et^3}{12(1-\nu^2)} \tag{B.3}$$

is the bending rigidity of the shell. The maximum stresses are obtained from

$$\sigma^{\alpha\beta}_{max} = \frac{6}{t^2} m^{\alpha\beta} \quad . \tag{B.4}$$

B.2 FABRICATION OF THE LOOP

The flat strip is bent to form a circular ring and is welded together. The bending moment from $k^{11}=k_o$ is eliminated by heat treatment. Subsequently, a transverse curvature is introduced by bulge forming and rolling. In the unloaded condition (o) the loop assumes the characteristic flattened shape which is described by a transverse curvature $K_q^{(o)}$ in the straight segment

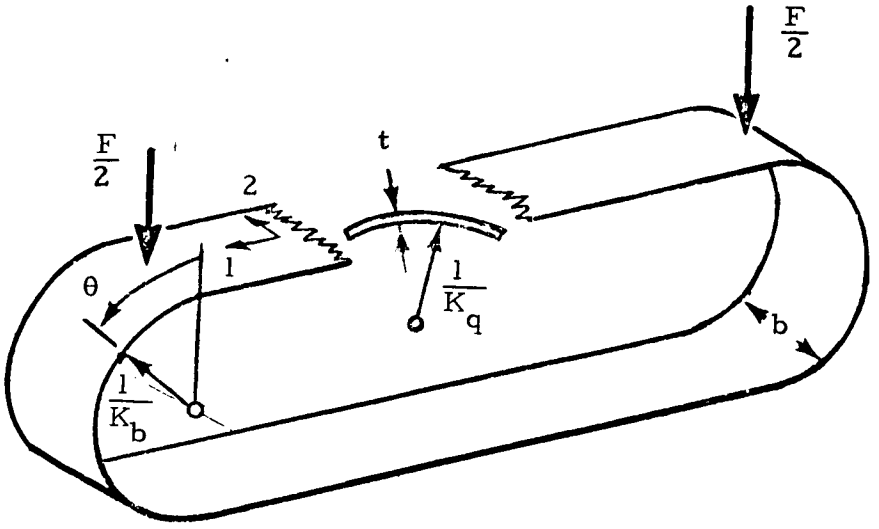

Fig. B-1 - Notations for Stress Analysis

and a longitudinal curvature $K_b^{(o)}$ in the curved segment. These quantities have to be measured after rolling because they are used in the further considerations. Depending on the rolling sequence, $K_q^{(o)}$ and $K_b^{(o)}$ can be different. They are assumed to be constant, thus neglecting the transition zones. In condition (o), a constant bending moment exists of magnitude

$$m^{11(o)} = B\,(K_b^{(o)} - \nu K_q^{(o)}) \quad . \tag{B.5}$$

B.3 LOOP UNDER LOAD

When a load F is applied on the loop, called condition (1), the curvatures $K_q^{(1)}$ and $K_b^{(1)}$ are caused. These are assumed in a first approximation also constant. They result in a bending moment of

$$m^{11(1)} = B\,(K_b^{(1)} - \nu K_q^{(1)}) \tag{B.6}$$

This is caused by the additional part

$$F \frac{\sin\theta}{2b\, K_b^{(1)}}$$

in the total bending moment,

$$m^{11(1)} = m^{11(0)} + F \frac{\sin\theta}{2b\, K_b^{(1)}} \quad . \tag{B.7}$$

Assuming an inextensional deformation,

$$b_1^1 b_2^2 = (b_1^1 + \delta b_1^1)(b_2^2 + \delta b_2^2) \quad ,$$

or in linearized form

$$b_1^1 \delta b_2^2 + b_2^2 \delta b_1^1 = 0 \quad , \tag{B.8}$$

where b_β^α is the curvature tensor, one can arrive at the statement

$$K_q^{(1)} - K_q^{(0)} \approx K_b^{(1)} - K_b^{(0)} \quad . \tag{B.9}$$

Although this cannot be mathematically proven, this relation is helpful in deriving the spring characteristic. Combining Eqs. (B.5), (B.6) and (B.7) and integrating over $0 \leq \theta \leq \pi$, one can see that the spring characteristic is

$$F = \pi b\, B (K_b^{(1)})^2 \left[1 - \frac{K_b^{(0)} + \nu(K_b^{(1)} - K_b^{(0)})}{K_b^{(1)}} \right] \tag{B.10}$$

At $F = 0$ the curvatures are

$$K_b^{(1)} = K_b^{(0)} \quad .$$

The maximum stress is given by

$$\sigma_{max}^{11(1)} = \frac{6}{t^2} B \left(K_b^{(0)} - \nu K_q^{(0)} + \frac{F \sin\theta}{2b B K_b^{(1)}} \right) \qquad (B.11)$$

having a peak at $\theta = \pi/2$.

B.4 COMPARISON OF THEORETICAL AND EXPERIMENTAL RESULTS

To check the validity of the formula for the spring characteristics, two existing loops were tested. The results of this comparison are given below.

Model A (1:6 scale model)

Material: Titanium Alloy Ti-6Aℓ-4V
Elastic Modulus $E = 11 \times 10^6$ N/cm^2
Poisson's Ratio = 0.3

Dimensions: Circumference 68 cm
Width b = 5.92 cm
Thickness t = 0.0318 cm

K_b (measured) (1/cm)	F (measured) (Newton)	F (computed) (Newton)	Error (%)
0.0996	0	0	0
0.1755	4.90	5.61	15
0.2245	9.79	11.89	21
0.2538	14.69	16.50	12

Model B: First Generation Loop

Material: Same as in Model A

Dimensions: Circumference 406 cm
Width b = 35.6 cm
Thickness t = 0.1295 cm

K_b (measured) (1/cm)	F (measured) (Newton)	F (computed) (Newton)	Error (%)
0.0248	0	0	0
0.0464	163	186	14
0.0543	291	276	- 5
0.0638	404	429	6

The results are shown on Fig. B-2. Considering the uncertainties in the material properties, the comparison between the theoretical and experimental results is satisfactory. This theoretical spring characteristic which has been derived under simplifying assumptions proves to be very useful in the design of elastic loops.

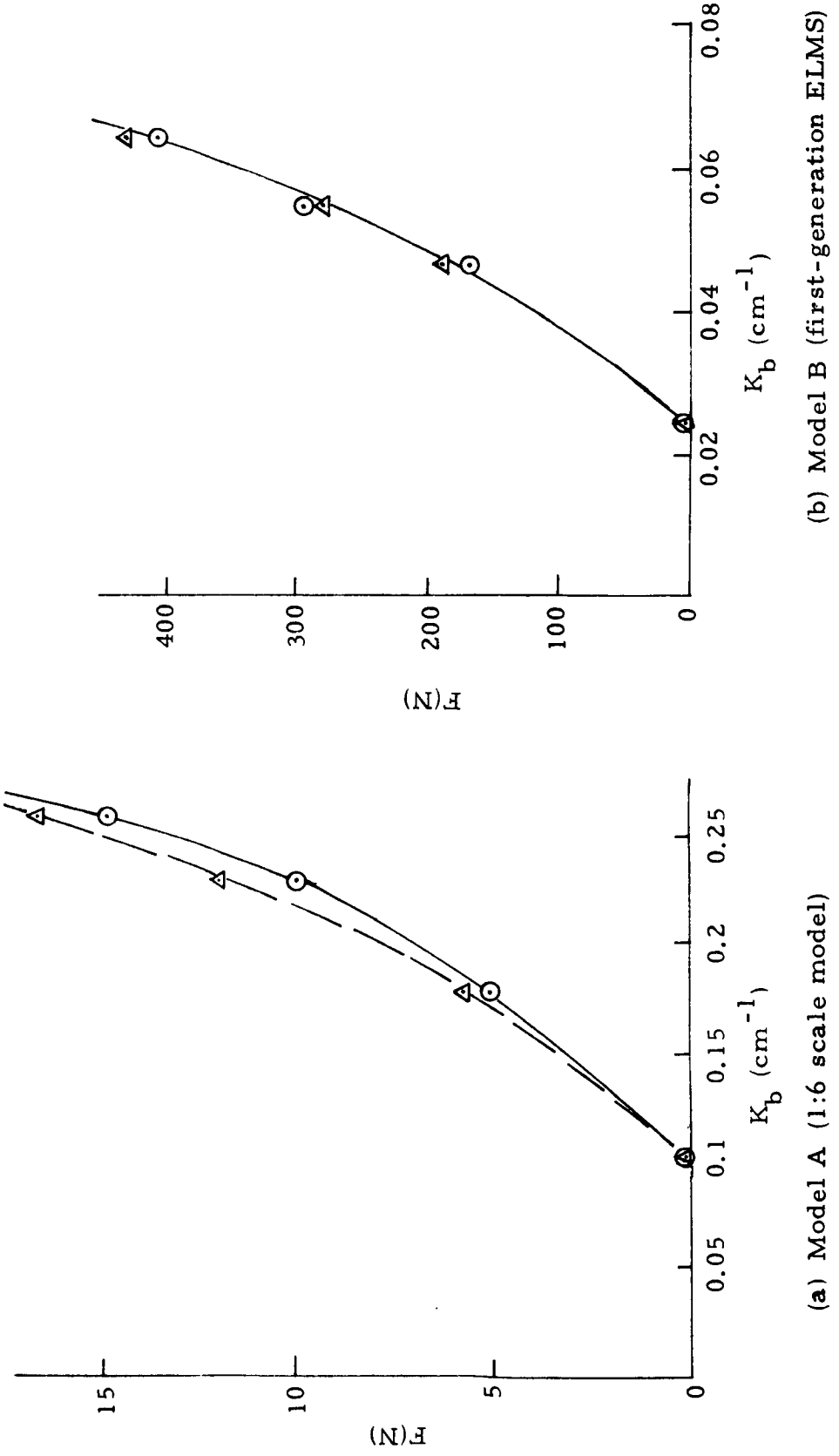

(a) Model A (1:6 scale model)

(b) Model B (first-generation ELMS)

Fig. B-2 - Comparison Between Measured ⊙ and Computed △ Applied Force vs Curvature

Appendix C

BULGE FORMING PROCEDURE

Appendix C

BULGE FORMING ELASTIC LOOP MOBILITY SYSTEM (ELMS) TITANIUM LOOPS

1. SCOPE

1.1 This Manufacturing Process Data covers the bulge forming ELMs Titanium Loops.

2. EQUIPMENT, ACCESSORIES, AND MATERIALS

2.1 Equipment

2.1.1 Lake Erie Press, MSFC 3994, in Bldg. 4704

2.1.2 Kobe Pump,. MSFC 28326, 6 gpm, 1000 psig maximum.

2.1.3 Vacuum Pump

2.2 Accessories

2.2.1 Bulge forming die assembly

2.2.2 Depth micrometer

2.2.3 Manifold and valve assembly

2.2.4 High pressure braided hose

2.2.5 Water fill hose

2.2.6 Water drain hose

2.2.7 Vacuum hose

NOTE: THIS DOCUMENT REFLECTS MANUFACTURING PROCESS DATA UTILIZED BY THE MANUFACTURING ENGINEERING LABORATORY AND SHALL NOT BE REFERENCED ON THE ENGINEERING DRAWINGS NOR CHANGED WITHOUT THE JOINT APPROVAL OF S&E-ME-D and S&E-ME-M.

APPROVAL

PROJECT ENGINEER	S&E-PT-D	S&E-PT-M
Vaughn H. Yost	F. Weckwarth	G. Parks W. Angele
ISSUE DATE	REVISION DATE	MPD NUMBER

S&E-PT-M	MANUFACTURING PROCESS DATA	SHEET 1 OF 4
MSFC	MANUFACTURING ENGINEERING LABORATORY	NASA

REVISIONS			
SYM	DESCRIPTION	DATE	APPROVAL

3. MATERIALS

3.1 Titanium (beta 3) loops (Source: Crucible Steel Corporation)

4. FORMING PROCEDURE

4.1 Schematic of System - Connect Equipment and Accessories as shown below.

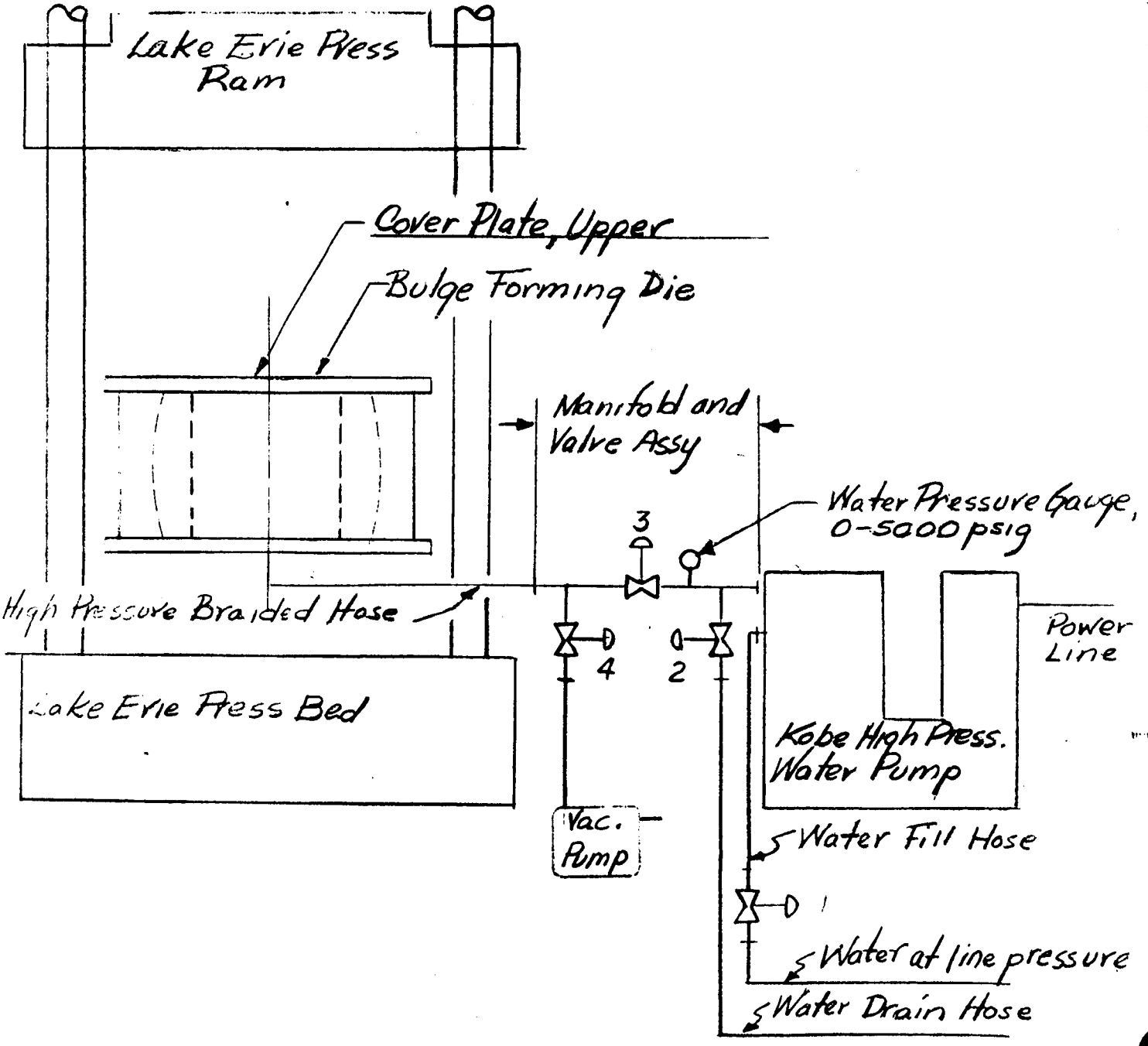

CODE IDENT NO	DWG SIZE	
	A	SHEET 2 of 4 sheets

4.2 Raise ram on Press.

4.3 Remove cover plate on die with fork lift.

4.4 Insert titanium loop in die.

4.5 Evacuation of system.

4.5.1 Close Valves 1 and 2.

4.5.2 Open Valves 3 and 4. Start vacuum pump.

4.5.3 Close Valves 2 and 4. Valve 2 should already be closed.

4.5.4 Turn vacuum pump off.

4.6 Fill bladder, inspect and adjust loop/bladder positioning, if necessary.

4.6.1 Open Valves 1 and 3. Valve 3 should already be open.

4.6.2 Turn Kobe pump on and fill forming die bladder with water.

4.7 Place cover plate on die with fork lift.

4.8 Lower ram on Press until it rests on die cover plate.

4.8.1 Start pump on Press and bring ram force to 200 tons.

4.9 Forming – Increase bladder pressure and ram forces according to following schedule to form titanium loop.

Lake Erie Press Ram Force (tons)	Manifold Gauge Pressure (psig)	Approximate Depth Micrometer Readings (inches)
200	Filling Bladder	3.00
250	200-300	3.00
300	300-400	3.00 to 2.50
350	400-500	2.50 to 2.30
400	500-700	2.30 to 2.277

Insert depth micrometer in hole in die. Start continuous measurement of titanium loop.

4.9.1 Water pressure rises rapidly once bladder is filled. As water pressure rises, increase ram force per schedule in 4.9. As water pressure approaches 400 psig, open Valve 2 to bleed off sufficient water to maintain 400 psig.

Caution: Gauge on Kobe pump does not work. Use gauge on manifold and valve assembly.

4.9.2 Increase bladder pressure to 500 psig by partially closing Valve 2. Titanium loop should start to move at this point.

4.9.3 Increase bladder pressure slowly letting it peak at 700 psig momentarily. Between 500 and 700 psig depth micrometer should read $2.277^{+\ 0.000}_{-\ 0.002}$. Once this measurement is reached, turn Kobe pump off, open Valve 2, and close Valve 1.

4.9.4 Decrease bladder pressure and ram forces according to schedule in 4.9.

4.9.5 Pump water from bladder. When bladder pressure reaches the point where the water runs slowly out of drain hose, disconnect high pressure braided hose from manifold and water drain hose from Kobe pump inlet, connect braided hose to pump inlet and drain hose to mainfold, start Kobe pump, and pump sufficient water from bladder to make it easy to remove from the die.

4.10 Raise ram on Erie Press.

4.11 Remove cover plate on die with fork lift.

4.12 Remove titanium loop from die.

Appendix D

NARRATIVE OF FAILURE ANALYSIS ON LOOP NO. 2

Appendix D

S&E-PE-MW-72-67 March 8, 1972

TO: S&E-SSL-N/Dr. N. C. Costes

FROM: S&E-PE-MW/P. G. Parks

SUBJECT: Failure Analysis on Elastic Loop

Please refer to the elastic loop mobility system for the Rover, being developed by Lockheed-Huntsville on contract NAS8-27737 for your office. In accordance withpprior arrangements, the PE Lab was to perform the welding and bulge forming on the loop.

During the recent bulge forming operation of one of the welded loops catastrophic failure occurred. In order to determine the cause of failure and thereby avoid future failures a failure analysis was undertaken. Included in the investigation were enlarged photos of the fractured part, spectrographic analysis of the base metal (Beta III Titanium), thickness and microhardness measurements optical microscopy of the microstructure, and scanning electron microscopy of the fractured surface. We found that the chemistry hardness, mechanical properties and microstructure of the Beta III titanium were normal. The weldment was of sound quality, without cracks porosity, or concentrated precipitates. As shown in the attached report (No. MW-72-9) failure was attributed to damage to the titanium near the weld by a hammer type blow. The resulting localized deformation and surface cracks caused brittle failure to be initiated. Continuation of the failure mode was in a ductile fashion, which is normal for a stressed component.

Recommendation

Precautions should be taken in bulge forming of subsequent elastic loops to insure that hammer blows, surface cracks or notches, or rough handling be avoided.

P. G. Parks
Chief, Metals Joining Development Branch

Inclosure
Lab Report No. MW-72-9

METALLURGICAL LABORATORY
WORK REQUEST COMPLETION REPORT

SREPTMM: MM-72-9

DATE: 2/22/72

NAME OF REQUESTOR: F. C. Parks

PROJECT NUMBERS: 8802 1/2

TOTAL HOURS:

SAMPLE IDENTIFICATION, MATERIAL AND HISTORY: Failure analysis - Lockheed supplied titanium. Sheet prewelded at MSFC.

METALLURGICAL SUPPORT FURNISHED

TEST MADE	NUMBER OF SPECIMENS	NAME	PHOTOGRAPHY TEST MADE	PHOTOGRAPHY NUMBER OF SPECIMENS	PHOTOGRAPHY NAME
X	3	SAMPLES PREPARED	X	16	POLAROID
X	30	MACROGRAPH POLAROIDS	X	8	NEGATIVES
X	20	MICROGRAPH POLAROIDS	X	15	CONTACT PRINTS
X	10	NEGATIVES	X	36	ENLARGEMENTS
X	11	TUKON MICROHARDNESS	X	36	WELD MEASUREMENTS
XX	5	OVERLAYS			

COMMENTS: METALLOGRAPHER's COMMENTS:

A Lockheed supplied titanium sheet with a fractured corner was submitted to the Laboratory to determine the cause of failure.

The sheets were welded by manual TIG process using titanium 6-4 filler wire. The sheet was then subjected to a bulge forming operation by Lockheed personnel.

Macroscopic examination of the sheet in the as-received condition showed deformation from forming, surface grinding marks at/and on both sides of the weld, and numerous indentations that appear to be hammer marks (Figures 1 & 2).

Microscopic examination showed surface cracks at the edge of the indentations (Fig.3). Numerous surface defects were evident in the sheet and weld zone (Figures 4 & 5). Examination also indicated that surface grinding of the weld and adjacent areas along with the forming operations caused variation in material thickness. Optical measurements were made on the sections shown in Fig. 6. Variations in thickness ranged from .05" to .06" in one weld. Micrometer measurements on the as-received sheet gave a range of .05" to .06" in thickness.

Examination of the fractured area showed that the initial failure occurred as a result of a direct blow at the surface as shown in Fig. 9 & 10. Arrow in Fig. 9 points to indentation that appears to be a hammer mark. Fractograph in Fig. 10 shows depression in surface that resulted from the blow. Fracture pattern indicates that initial failure was primarily intergranular or crystallographic in nature. Fractograph in Fig. 11 shows that secondary failure occurred after considerable necking at the center of the sheet as shown at arrow.

SIGNATURE OF [illegible]: D. F. Jackson

DATE: 2/23/72

MSFC - Form 3212 (Rev October 1971)

MW-72-9
Feb. 23, 1972

No evidence of welding defects was found or material defects in the base metal that could be contributed to the failure.

CONCLUSIONS:

Examination of the fractured area shows that the initial failure occurred as a result of a direct blow with a hammer or other object at the surface (Fig. 9 & 10).

Initial failure was primarily intergranular or crystallographic in nature with secondary failure occurring after considerable necking at the center of the sheet as shown in Fig. 11.

No evidence of welding defects were found or material defects in the base metal that could be contributed to the failure.

E. L. Goodwin, Sr. Assoc. Engr.

MF-72-9
Feb. 23, 1972

METALLURGICAL ENGINEER's COMMENTS:

A fractured sample of titanium was submitted for failure analysis. The sample was spectrographically analyzed and found to be Beta III titanium alloy. The failure analysis was performed using a scanning electron microscope (SEM) to obsure the fracture mode without metallographic polishing and etching of the fracture.

An overall view of the fracture is shown in Figure 12. In Figure 13 the impression left by a hammer type blow is shown. Figure 14 shows the intergranular or crystallographic fracture mode around the cracked area. This type fracture is typical of a brittle fracture mode. Figure 15 shows the dimple structure of a typical ductile fracture of areas adjacent to the brittle fracture zone shown in Figure 14.

CONCLUSIONS:

Failure was due to striking the metal with a hammer type blow and causing a brittle fracture. The part then failed in a ductile mode. Spectrograph chemical analysis and SEM/microprobe analysis showed no detrimental elements in the parent material or fractured surfaces.

J. N. Stokes, Metallurgical Engr.

Appendix E

FAILURE INVESTIGATION OF BETA III TITANIUM LOOP NO. 1

NATIONAL AERONAUTICS AND SPACE ADMINISTRATION
GEORGE C. MARSHALL SPACE FLIGHT CENTER
MARSHALL SPACE FLIGHT CENTER, ALABAMA 35812

REPLY TO ATTN OF: S&E-PE-MW-100-72 (eh)

April 17, 1972

TO: S&E-SSL-N/Dr. N. C. Costes

FROM: S&E-PE-MW/P. G. Parks

SUBJECT: Beta III Titanium Loop, Failed During Forming Operation

An elastic loop for the Rover, under development by Lockheed-Huntsville for your office, was investigated by our Weld Evaluation Lab to determine cause of failure.

The process history of the loop was determined to be as follows:

TIG Welded by MSFC (S&E-PE-DF, Bldg. 4705)

Bulge formed

Aged 12 hours at 950°F, air atmosphere furnace MSFC, Bldg. 4704 (8 hours first time, then one hour and 3 hours in successive treatments)

Roll Forming

During the roller forming operation to shape the loop to a deeper curvature, a fracture occurred in the circumferential direction through the weld.

Trim material from the loop was made available to this Branch for failure analysis and possible weld repair of the loop itself. A comprehensive investigation was conducted to determine the cause of failure. Methods of analysis included:

Hydrogen Analysis
Thickness measurement
Microhardness measurement
Optical microscopy
Scanning electron microscopy
Mechanical testing

Our analysis is detailed in the attached Metallurgical Laboratory reports MW-72-41 and -44. In brief the findings show that the production weld was of good quality, and was not contaminated during welding. Failure analysis in tensile specimens showed that approximately 50% of the area failed in a brittle mode. The percentage elongation in 2 inches on the tensile specimen was only 1%, because of excessive grain coarsening of the weld and heat affected metal during the ageing operation at 900°F. Surface oxidation was a contributing factor in the brittle failure.

Hydrogen analysis showed a concentration at the surface of material but the total concentration was within the values found acceptable in Phase II of the development of this alloy by Crucible, Inc. (Manufacturing Procedures for a New High Strength Beta Titanium Alloy having Superior Formability, AFML-TR-69-171 (III). Thickness measurements across the weld did not show any thin-out at the weld due to bulging or roll forming.

Conclusions

Ageing of the welded loop at 900°F caused the surface to be oxidized and the grains in and near the weld to grow excessively. Subsequent shear stresses from roll forming resulted in the elastic loop failing at a circumferential crack thru the weld. Weld repair was successful, but the shrinkage distortion from the weld was so great that the loop is of limited value to the testing for the loop mobility system.

P. G. Parks

1 Incl.
Lab Report MW-72-41 and 72-44

S&E-PE-M/Mr. Angele, Caruso w/o incl
S&E-PE-M/Mr. J. Williams w/o incl.
S&E-PE-MWP/Mr. V. Yost w/o incl.

MW-72-41 & MW-72-44

Pre-Production Welds

Pre-production welds made by S&E personnel MSFC were examined and documented as shown in Figure 13.
Microscopic examination in the as-polished and etched condition and at low and high magnification showed the welds to be sound and FREE of defects.

Microhardness conversion values ranged from Rc 20 - 21 in the parent material to Rc 21-24 in the weld nugget which shows that it was not embrittled in the welding (Figure 15). Figure 14 shows the microstructure of solution treated parent material. Grain boundary dileneation is poor due to the heat treatment. Grain size is greater than ASTM 7.5.
The welds were radiographically and metallurgically acceptable.

Pre-Repair Welds

Pre-Repair welds made by S&E personnel MSFC were also examined and documented as shown in Figure 16.
Microhardness values are comparable to values obtained on pre-production welds. Hardness values are super-imposed on macrograph in Figure 16.

The welds were sound and free of defects. They were radiographically and metallurgically acceptable.

CONCLUSIONS:

Loop Ring

Examination of the weld nugget showed that grain coarsening occurred which resulted in severe loss in ductility and consequent embrittlement. Weld nugget exhibited a grain size of ASTM 2.5 to 3 (Fig. 2 & 3).
Tensile test results showed a range of .5 to 1.5 % elongation on the weld tensile specimen in the aged condition compared to a range of 7.0 to 7.3% elongation on the aged parent material.
Examination of the edges of the tensile specimen revealed cracks and surface oxidation (Fig. 5). Figure 6 shows surface oxidation at the weld surface. Transverse and longitudinal sections of the parent material showed surface oxidation also.

Grain coarsening in the weld nugget and surface oxidation supported by loss of ductility in the mechanical test specimens is conclusive evidence that the material was degraded by heat treating.

Pre-Production and Pre-Repair Weld

Examination of the pre-production and pre-repair welds did not show any evidence of defects. The welds were radiographically and metallurgically acceptable.

E. L. Goodwin, Sr. Assoc. Engr.

METALLURGICAL ENGINEER's COMMENTS:

Two broken tensile specimens of Beta (B) 3 titanium were submitted for a Scanning Electron Microscope (SEM) fractography study to determine the fracture mode. One specimen was of non-welded material (parent material) and the other was welded before testing. The broken tensile specimens were examined and the results are given in Table No. 1.

CONCLUSIONS:

The conclusions are as follows:

(1) The parent material failed in a normal ductile fracture mode with about 25% of the fracture area being brittle in nature.

(2) The weld material failed primarily in the brittle mode. The fracture was both intergranular and transgranular which accounts for the low elongation values obtained in tensile testing.

RECOMMENDATION:

If Beta (B) -3 alloy is to be used as a thermal treatment, mechanical testing and metallurgical study should be made to determine if aging (thermal treatment) prior or after welding would be helpful in improving properties of this structure.

J. N. Stokes, Metall. Engr.,
Sr. Engr. Spec.

LOCATION OF TEST	FIGURE NO.	PRIMARY FRACTURE MODE	COMMENTS
Parent Material	17	Ductile	Brittle fracture mode Approx. 25% of sample
Heat Affected Zone	18	Brittle	Brittle fracture mode 50% of area
Weld Area	19	Brittle	Brittle fracture 50% of area - Transgranular and intergranular failure
Weld Area	20	Brittle	Brittle fracture 50% of area - Transgranular and intergranular failure

TENSILE TEST DATA

SHEET 1 OF 1

DATE: 3-29-72

LAB NUMBER: mcmm 8463

MATERIAL: Beta III Titanium .062" thick

IDENTIFICATION: Beta III Annealed (SSL)

REQUESTED BY: Parks

PROPERTIES REQUIRED

ULTIMATE: | YIELD: | PERCENT ELONGATION:

SAMPLE NUMBER	WIDTH	THICKNESS	AREA	ULTIMATE LOAD	ULTIMATE PSI	YIELD LOAD	YIELD PSI	PERCENT ELONGATION	REMARKS
Shoulder WT – 1	.4875	.0675	.0329	5460	170,625			.5	Dia. Over Bead = .0790
– 2	.4885	.0675	.0330	5900	178,788			1.5	" " " = .1003
PT – 1	.504	.0675	.0340	6610	194,412	6130	181,765	7.0	
" – 2	.505	.0675	.0341	6660	195,308	6240	182,991	7.3	Scratched Marks
AVERAGE									

GENERAL REMARKS:

WT = Weld Tensile

PT Parent metal Tensile.

" Scratch marks made intentionally: did not fail in marks

BY: [signature] 3-[illegible]

METALLURGICAL LABORATORY
WORK REQUEST COMPLETION REPORT

S&E-PT-MW: MW-72-41 & 72-44

DATE: 12 Anril, 1972

. C. Parks

PROJECT NUMBERS: Space Science Laboratory 8802

TOTAL HOURS:

SAMPLE IDENTIFICATION, MATERIAL AND HISTORY: Samples from the Lockheed-SSL loop ring trim material. Pre-production & pre-repair welds made by S&E personnel, MSFC. Beta III Ti sheet material (solution treated and aged) & (Solution treated condition).

METALLURGICAL SUPPORT FURNISHED

TEST MADE	NUMBER OF SPECIMENS	NAME
xx0	14	SAMPLES PREPARED
xx0	42	MACROGRAPH POLAROIDS
xx0	48	MICROGRAPH POLAROIDS
xx0	11	NEGATIVES
x0	39	TUKON MICROHARDNESS
xxx	15	Overlays

PHOTOGRAPHY

TEST MADE	NUMBER OF SPECIMENS	NAME
0		POLAROID
0		NEGATIVES
0		CONTACT PRINTS
0		ENLARGEMENTS
0		WELD MEASUREMENTS

COMMENTS:

METALLOGRAPHER'S COMMENTS:

Samples from the Lockheed-SSL loop ring were submitted to the laboratory for metallographic evaluation.
Pre-production and pre-repair welded samples by S&E-personnel, MSFC were examined also.

Loop Ring Samples

Microscopic examination of a section of a failed tensile specimen showed that failure was both inter and transgranular in nature (Figure 1). Micrograph in Fig. 4 shows that failure was primarily intergranular at Area 3 in Fig. 1.
The weld nugget showed grain coarsening with grain sizes of ASTM 2.5 to 3 (Fig. 2 & 3). According to information supplied by Crucible Inc. welds suffer a severe loss in ductility in age conditions and is attributed to grain coarsening in the weld nugget. This is supported by results obtained on tensile specimens taken through the weld area. The percent elongation on the weld tensile specimens ranged from .5 to 1.5 compared to a range of 7.0 to 7.3 percent on the aged parent material.
Oxidation of the weld surfaces were evident as shown in Figure 6. Examination of the edges of the weld tensile specimen also revealed cracks and surface oxidation (Fig. 5).
Longitudinal and transverse sections of the aged sheet material showed surface oxidation (Figure 7 & 8).
Microhardness surveys conducted in the weld nugget showed variations from Rc 34 to Rc 41 (Figure 9).
Hardness values obtained on the aged parent material ranged from Rc 36 to 38.
Variations in grain size of longitudinal and transverse sections of the aged material was minimal (Fig. 10).
A radiographic print of the circumferential crack in the loop ring is shown in Fig. 11. Photograph of the crack area after metal removal and cleaning operations was completed for repair weld is shown in Figure 12.

SIGNATURE OF SUPERVISOR: D. F. Jackson

DATE: 4/14/72

Form 321 (October 1971)

Appendix F
INSTRUCTIONS ON THE DRIVE MOTOR CONTROL

Appendix F

There is no protection against B+ reversals. All plus 36 volt leads are marked with red tape and with +36 V. All ground leads are marked with black tape and GND. Pull the circuit breaker out for off.

CCW rotation looking into the wire terminal end of the drum is forward. The torque in the reverse direction is limited to about 1/4 the forward torque.

If the battery is removed and the system is driven by an external battery through an umbilical, connect the two 960 uf capacitors in parallel and put them across the battery lines in the loop housing. This is to provide a low impendance drive source.

The $\pm$12 volt lines going to the pot are not short circuit protected. Avoid grounding or shorting.

The $\pm$12 volt out of one controller is not being used but is available. Pot excitation for both motors is supplied from the other controller and both speed input commands are tied together and are being driven from one pot.

The two signal grounds on the Jones strip may be commoned if desired. It should not be necessary since all telemetering signals can be referred to the power ground.

All leads are clearly marked. The leads of interest other than the +36 volt and power ground are torque tele (telemeter), tach tele, drive inhibit, plus 12 volt which is tied to one end of the speed input pot, minus 12 volt to the other end and speed command to the pot wiper.

The pot is a 3 turn pot. ±1.5 turn for forward and reverse.
Speed control from no load to full load is 5% of 120 rpm.
The tach gradient is 200 mV/rpm.

The no load speed may be set by the pot. To stop the system, short the two drive inhibit wires which are tied together to the plus 12 volts on the pot. This will inhibit the drive. Lift the inhibit wires and the speed will return to within 5% of the preset no load speed regardless of load. (Within limits of system.) This method for stop and go operation preferred over disconnecting the battery. The system can be back driven or forward driven up to 125 rpm as long as the battery is connected. Back driving by hand without the battery is okay. The system has regenerative braking and should have the battery connected to have a place to dump its braking energy. The system is internally protected should the battery be removed while commanded to brake and no damage will occur, but this condition should not be a part of the test requirements.

The drive system can turn approximately 120 rpm and put out 480 in.-lb only if the battery voltage is 36V or greater. At this power level, the battery current is about 30 amps; and due to internal impedance, a 35-volt battery may not be able to sustain its voltage. Hence, an external power source may be necessary for high torque at high speed.

The speed capability of the system is reduced by about 4 rpm per volt of drop in the supply.

With the system on and speed set at zero, the tach will cause the drive to oppose any back drive, unless the inhibit wires are connected to +12 V.

If an external supply is used, it does not have to be able to accept power from the drive system during braking. If the supply cannot accept power and braking is commanded at high speed, the circuit will inhibit itself in an oscillatory mode by sensing the line voltage and inhibit itself above 41 volts. This, however, should not have to be experienced during the test.

If external supply is used, the nominal voltage is 36 to 37 volts. Do not exceed 40 volts. The battery voltage should not be allowed to drop below 29 volts for safe operation of the controller. This includes drop due to loading and discharge.

Appendix G

STRESS ANALYSIS AND SIZING OF DRIVE MOTOR SUPPORT TUBES

Appendix G

Stress Analysis and Sizing of Drive Motor Support Tubes

$T_{MAX\ MOTOR}$ = 30 FT-LBS.
W_{MOTOR} = 11 LBS.
Applied Loads = 5 g Horizontal
5 g Vertical

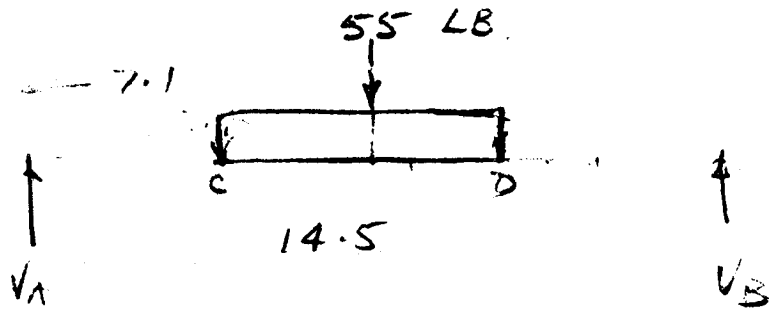

M_2 M_1

M. IN-LBS.

$$14.5\,V_A - 55(7.1) = 0$$

$$V_A = 55(7.1)/14.5$$

$$= 26.1$$

$$V_B = 55 - 26.1$$

$$= 26.9$$

$$M_2 = 26.1(4) = 112.4 \text{ IN-LBS.}$$

$$M_1 = 26.9(4.5) = 121.0 \text{ IN-LB}$$

T_{MAX} = 23 FT.-LB.

COMBINED BENDING & TORSION:

REF. MM P. 242

$$S_{s_{MAX}} = \frac{16}{\pi d^3}\sqrt{M^2 + M_t^2} \qquad (119a)$$

$$\frac{\pi d^3}{16} = Z \cdot \frac{I}{c} \qquad \frac{\pi d^3}{32} = \frac{I}{c}$$

$$I_p = 2 I_x \qquad Z = \frac{\pi d^3}{32}$$

FOR HOLLOW SHAFT:

$$I_x = \frac{\pi}{64}(d^4 - d_i^4)$$

$$Z_x = \frac{\pi}{32}\frac{(d^4 - d_i^4)}{d},$$

$$= \frac{\pi d^3}{32}\left[1 - \left(\frac{d_i}{d}\right)^4\right]$$

$$S_{s_{MAX}} = \frac{1}{2Z}\sqrt{M^2 + M_t^2}$$

$$= \frac{16}{\pi d^3\left[1 - \left(\frac{d_i}{d}\right)^4\right]}\sqrt{M^2 + M_t^2}$$

$$= \frac{16}{\pi (3.5)^3\left[1 - \left(\frac{3.4}{3.5}\right)^4\right]}\sqrt{(121)^2 + (23(12))^2}$$

$$= \frac{16}{\pi (43)\left[1 - .832\right]}\sqrt{14{,}600 + 76000}$$

=

$f_{s\ MAX}$ = 307 P.S.I.

L.H. SUPPORT TUBE # C-2002

ATTACH LUGS: 4 - 10-32 @ 2.861 B.C.D.

LOAD 23 FT-LBS. FACTOR 2X1.5 TO ULT.

$= 23(2)(1.5)(12)$

$= 828$ IN-LB.

ASSUME 2 LUGS CARRY LOAD

LOAD/LUG = 828/2.86

= 290 LB.

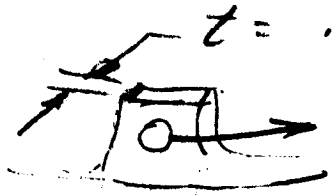

SHEAR OUT AREA = $\frac{.37-.19}{2}(.1)$

$= (.09)(.1)$

$= .009\ in^2$

F_{su} MAG AZ 31B = 17,000 P.S.I.

$f_{su} = \frac{290}{.009} = 30{,}000$ P.S.I.

TOO CONSERVATIVE.

∴ CONSIDER 40° TEAR OUT:

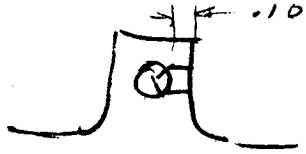

$A_s = 2 \times .1 \times .1 = .02$

$f_s = \frac{290}{.02} = 14{,}500$ PSI

M.S. $= \frac{17000}{14500} - 1 = .17$

CHECK OF B.M. DUE TO IMPACT WHEN DRIVE WHEEL HITS SOLID.

ASSUME 150 # @ 2 G = 300 # ON ONE SIDE.

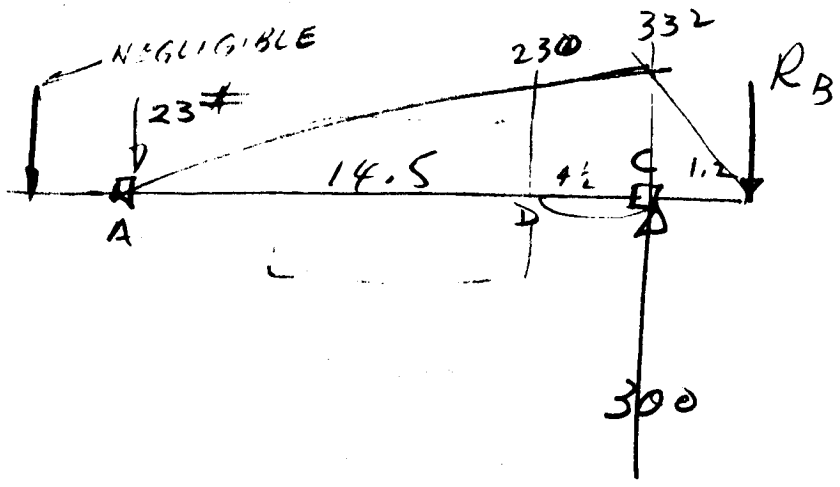

$\Sigma M_A = 0$

$$R_B = \frac{300(14.5)}{15.7} = 277\#$$

$M_C = 277(1.2) = 332$ IN-LB.

$M_D = 23(10) = 230$ IN-LB.

TOTAL $M = 230 + 121 = 351$ IN-LB

COMBINED WITH TORQUE:

$$S_{S\,MAX} = \frac{16}{\pi(3.5)^3\left[1-\left(\frac{3.4}{3.5}\right)^4\right]}\sqrt{351^2+(23\times12)^2}$$

$$= \frac{16}{\pi(43)(.118)}\sqrt{123{,}000+76000}$$

$S_{SMAX} = 1.01\,(446) = 452.$ P.S.I.

REF P. 4 7-2-71 (.050 WALL)

USING .040 WALL:

$$S_{S\,MAX} = \frac{16}{\pi (3.5)^3 \left[1 - \left(\frac{3.42}{3.5}\right)^4\right]} \sqrt{14{,}600 + 76{,}000}$$

$$= \frac{16}{\pi (43)(1 - .906)} \sqrt{90{,}600}$$

(.094; 301)

$= 380$ PSI.

USING .030 WALL

$$S_{SMAX} = \frac{16}{\pi (3.5)^3 \left[1 - \left(\frac{3.44}{3.5}\right)^4\right]} (301)$$

(43; .07)

$= 510$ P.S.I.

USING .020 WALL

$$S_{SMAX} = \frac{16}{\pi (43)\left[1 - \left(\frac{3.46}{3.5}\right)^4\right]} (301)$$

(.047)

$= 760$ P.S.I.

$f_s = \frac{M_t r}{I_p}$ CHECK FOR .020

$$= \frac{23 \times 12 \times 1.75 \,(3.2)}{\pi (3.5^4 - 3.46^4)}$$

$= 730 \text{ psi}$

Appendix H

DRIVE TORQUE TUBE ANALYSIS

GDR 5-6-71

Appendix H

MOTOR: GE HF 6-508

TORQUE: 30 FT-LB. @ 115 R.P.M.

WT 11 LBS. 2 OZ.

OUTPUT TORQUE TUBE:

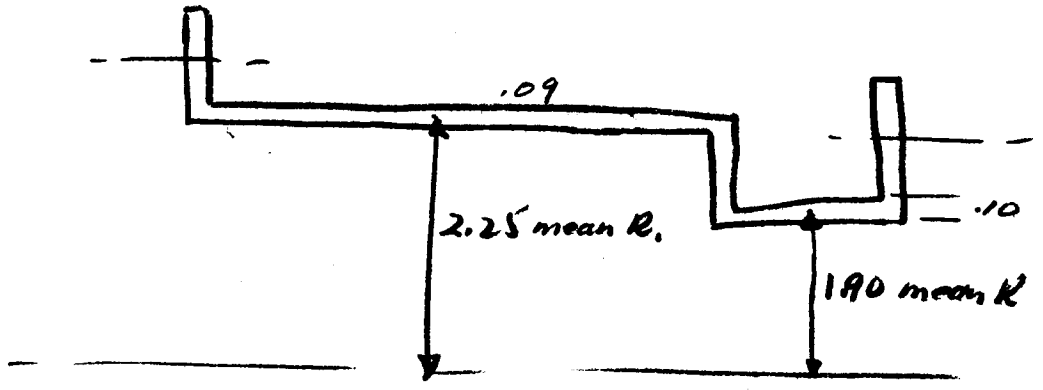

$f_s = \frac{M_t r}{I_p}$

$= \frac{276 \times 2.30}{6.487}$

$= 97.85$ psi

$M_t = 23$ FT-LB. $\times 12 = 276$ IN-LB

$r = 2.30$

$I_p = \frac{\pi}{2}(r_o^4 - r_i^4)$

$= \frac{\pi}{2}(2.30^4 - 2.21^4)$

$= 6.487$ IN.^{4}

M.S. DESIRED 1.5 ON YIELD

$f_s = 245$ psi.

$F_{sy} \approx 10{,}000$ P.S.I. A231B COND. F.

TRY $t = .050$

$T = \frac{2T}{\pi D^2 t}$

T = shear stress
T = torque
D = O.D.
t = thickness

$$T = \frac{2 \times 23 \times 12 \times 2.5}{\pi \times 2.3^2 \times .05}$$

$$= 1660 \text{ P.S.I.}$$

TRY $t = .030$

$$T = \frac{2 \times 23 \times 12 \times 2.5}{\pi \times 2.3^2 \times .03}$$

$$= 2780 \text{ P.S.I.}$$

TORSIONAL INSTABILITY REF. P. 243 NILES & NEWELL AIRPLANE STRUCTURES.

$$L^2 \frac{t}{D^3} = \frac{4.5^2 \times .03}{2.3^3}$$

$$= \frac{20.3 \times .03}{12.2} = .05 \quad \text{"short"}$$

CLAMPED EDGE (7.10a)

$$F_s = E \frac{t^2}{L^2} \left[3.0 + \sqrt{3.5 + .68 \frac{L^3}{(tD)^{1.5}}} \right]$$

$$= \frac{6.5 \times 10^6 \times .03^2}{4.5^2} \times \left[3.0 + \sqrt{3.5 + .68 \times \frac{4.5^3}{(.03 \times 2.3)^{1.5}}} \right]$$

$$= 17,750 \text{ P.S.I.}$$

HINGED $F_s = \frac{E t^2}{L^2} \left[1.8 + \sqrt{1.2 + .57 \frac{L^3}{(tD)^{1.5}}} \right]$ (7.10b)

$$= 15,980 \text{ P.S.I.}$$

EQN 7.11 For $\frac{L^2}{tD} > 20$

$$\frac{L^2}{tD} = \frac{4.5^2}{.03 \times 2.3} = 294$$

$$F_c = \frac{KE}{\left(\frac{D}{t}\right)^{5/4}\left(\frac{L}{D}\right)^{1/2}}$$

K = .80 CLAMPED
.75 HINGED

$$= \frac{.75 \times 6.5 \times 10^6}{\left(\frac{2.3}{.03}\right)^{5/4}\left(\frac{4.5}{2.3}\right)^{1/2}}$$

$$= 15,300 \text{ PSI.}$$

FROM FABRICATION STANDPOINT

t min. SHOULD BE .060 IN.

FLANGE THICKNESS .100 IN.

Appendix I

DRIVE DRUM CYLINDER STRESS ANALYSIS

Appendix I

DRUM CYLINDER AZ31B H24

.020 MAG. 10.813 I.D. 11.2" BETWEEN RIVET LINES

TORQUE (FACTORED) 57.5 FT-LB

$$T_{MAX} = \frac{2T}{\pi D^2 t}$$

$$= \frac{2(57.5)\times 12}{\pi (10.83)^2 (.020)}$$

$$= 15.6 \quad \text{PSI} \quad \times 12 = 187 \text{ PSI}$$

$$J = \frac{\pi}{4} D^3 t$$

$$= \frac{\pi}{4} (10.83)(.020)$$

$$= 20.05 \text{ IN}^4$$

$$\theta = \frac{TL}{JG}$$

$$= \frac{57.5 \times 11.2 \times 12}{20.05 \times 2.4 \times 10^6}$$

$$= 159.5 \times 10^{-6} \text{ RADIANS}$$

$$= .55'$$

BUCKLING ALLOWABLE OF SKIN

REF. LMSC STR. METHODS 6.12.2.

$$F_{scr} = \frac{K_s \pi^2 \eta E}{12(1-\mu^2)} \left(\frac{t}{L}\right)^2$$

t = thickness = .020"

L = length = 11.2"

E = Young's Modulus = 6.5×10^6

η = plasticity redn fact. = 1

K_s = Buckling Coeff. = 130

Ref. Fig. 6.12-1

$$Z_L = \frac{L^2}{Rt}\sqrt{1-\mu^2}$$

$$= \frac{11.2^2}{5.4 \times .02}\sqrt{1-.35^2}$$

$$= \frac{125}{5.4 \times .02}(.937)$$

$$= 1085.$$

$$F_{scr} = \frac{130 \times \pi^2 \times 1 \times 6.5 \times 10^6}{12(1-.35^2)}\left(\frac{.020}{11.2}\right)^2$$

$$= 253 \text{ PSI}$$

COMPRESSIVE LOAD ON DRUM DUE TO TILT OF ELMS :

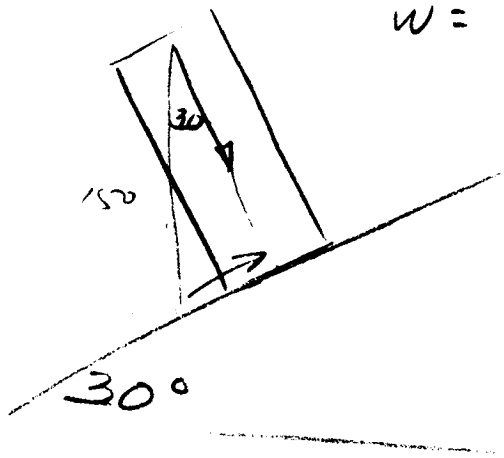

$W = 150\#$

$W \sin 30 = 75\#$

2 ROLLERS

LOAD - 1 ROLLER $= \frac{75}{2} = 37.5\#$

FACTOR 2.5

FACTORED LOAD = 94 #

REF LMSC ST. M. HDBK FIG 6.11-1

$L/R = \frac{11.2}{10.81} \times 2 = 2.07$

$R/t = \frac{5.40}{.02} = 270$

$\frac{.5\ F_{cy}}{E_c} = \frac{.5\ (12000)}{6.5 \times 10^6} = .923 \times 10^{-3}$

$K = 1.14$

$F_{c\,cr} = \frac{K}{2\pi} E_c \frac{t}{R}$

$= \frac{1.14}{2\pi} \quad 6.5 \times 10^6 \times \frac{.02}{5.4}$

$= 4370$ P.S.I.

GDR 6-4-71

COMBINED AXIAL & TORSION

$$R_c + R_t^2 = 1$$

$$R = \frac{f}{F}$$

$$R_c = \frac{4370}{12000} = .366$$

$$(R_t)^2 = 1 - .366$$

$$= .634$$

$$R_t = \sqrt{.634} = .797$$

$$R_t = \frac{f}{F}$$

$f = 187$ psi

$F = 253$ psi.

$$R_t = \frac{187}{253}$$

$$= .739$$

$$R_c + R_t^2 = .366 + .739^2 = .901$$

Ref. MIL HDBK 5 P. 8-2 1.5.3.5

$$M.S. = \frac{2}{R_1 + \sqrt{R_1^2 + 4R_2^2}} - 1$$

$R_1 = R_c$ $R_2 = R_t$

$$= \frac{2}{.366 + \sqrt{.366^2 + 4(.739)^2}} - 1$$

EOR

M. S. = 1.065 - 1

= .065

THIS INCCUDES LOAD FACTOR OF 2.5 ON YIELD.

ATTACHMENT OF DRUM CYLINDER TO RING

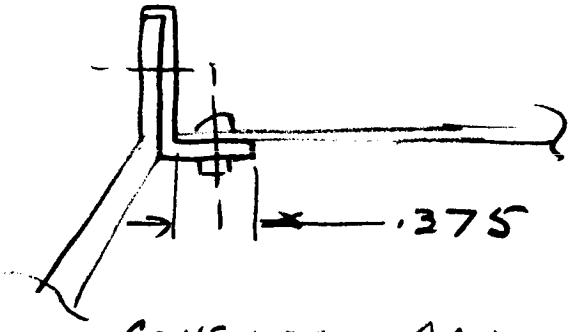

CONSIDER ALL TORQUE TO ONE SIDE

REF. SH. 1 LOAD = 56 x 2 = 112 LBS.

USE 3/32 RIVETS - ALUM. ed. on

Mag = .20

Appendix J

DRIVE LUG AND SPROCKET RING ENGAGEMENT ANALYSIS

EDK 7-29-71

Appendix J

DRUM DIA. - MINIMIZED

D_{MIN} = 11.850 PRACTICAL D_{MIN} = 12.00

(1) 36 ROLLERS 10°

66 LUGS/SIDE

LOOP 145" CIRCUM.

LUG SPACING = $\frac{145}{66}$ = 2.19697

$R_{LOOP} = \frac{S}{\theta_{20°}} = \frac{2.19697}{.3490659} = 6.2938$

D = 12.587

(2) 36 ROLLERS
67 LUGS

$\frac{145}{67} = 2.16418$

$R = \frac{2.16418}{.3490659} = 6.1999$

D = 12.3998

(3) D = 12.00

R = 6.00

$S = R\theta = 6(.3490659) = 2.0943954$

$N_{LUGS} = \frac{145}{2.094} = 69.3$

4) [illegible]

36 ROLLERS

64 LUGS

$$\text{LUG SPACES} = \frac{145}{69} = 2.10145''$$

$$R_{loop} = \frac{S}{\theta_{20°}} = \frac{6.0202}{.349065}$$

$$D = 12.04''$$

$t_{loop} = .066$

$$R_{INNER} = 6.020 - .033 = 5.187$$

$$L_{MIN} = 11.974''$$

ROLLER ℓ = 11.320 DIA

RADIUS = 5.660

$$11.974 - 11.320 = .654 \text{ IN.}$$

ROLLER DIAM. =

BASE RADIUS OF ROLLERS .25

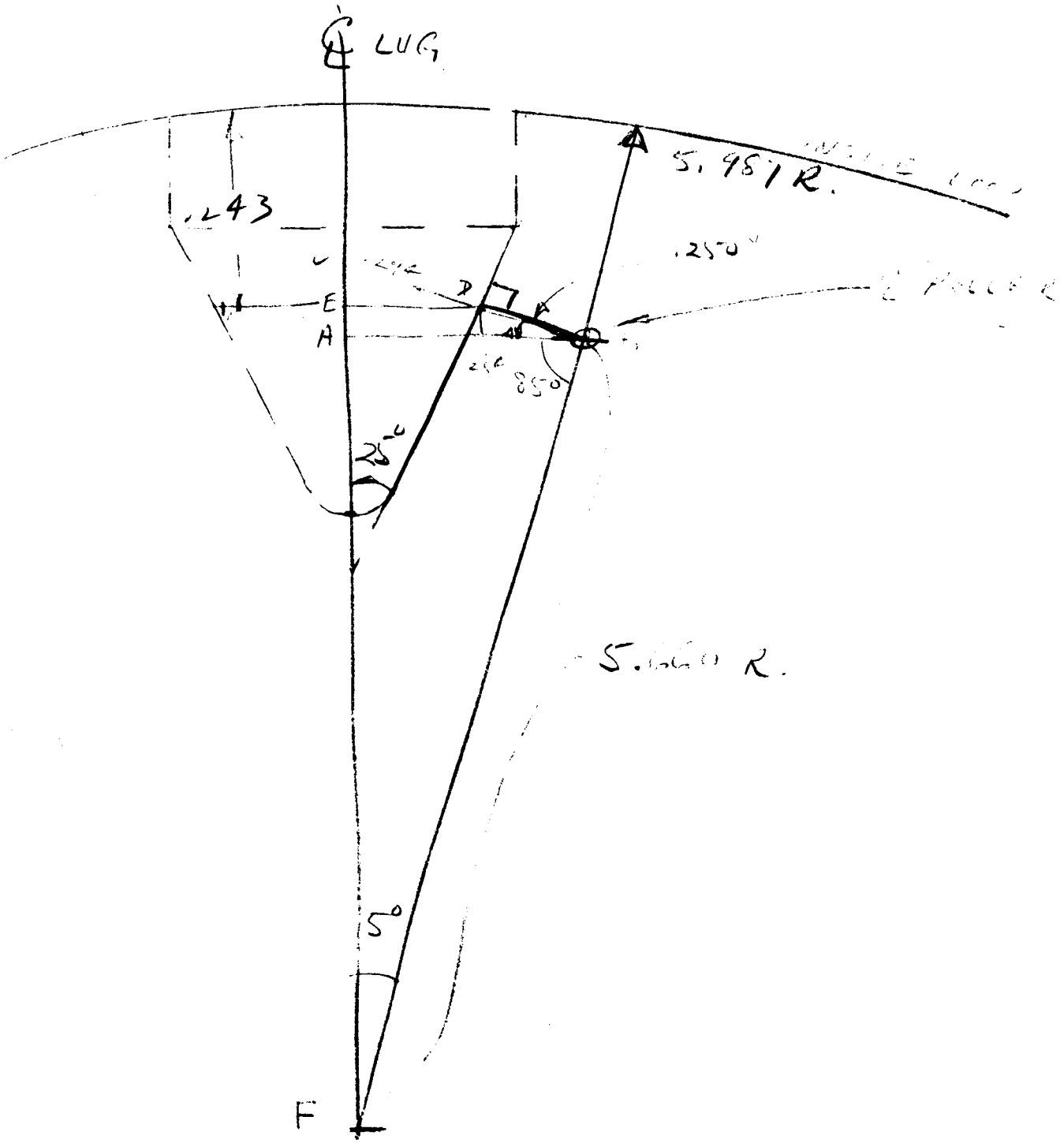
℄ LUG
.243
E
A
5.951 R.
.250
25°
85°
5°
F

AB = 5.660 sin 5° sin 5° = .087156

= .49330

BC = AB / cos 25° = .49330 / .906308

= .54429

RADIUS OF ROLLER GROOVE = .544 − .250 = .294 = CD

DE = CD cos 25° = .294(.906308)

= .26645 IN.

AL = .25 sin 25° = .25(.422618)

= .10565

AF = 5.660 cos 5° = 5.660(.996195)

= 5.63806

LUG HT. @ E = 5.987 − 5.744 = .243

5.63806 + .10565 = 5.74411

LOC. DIA @ E = 2DE = 2(.26645)

= .5329

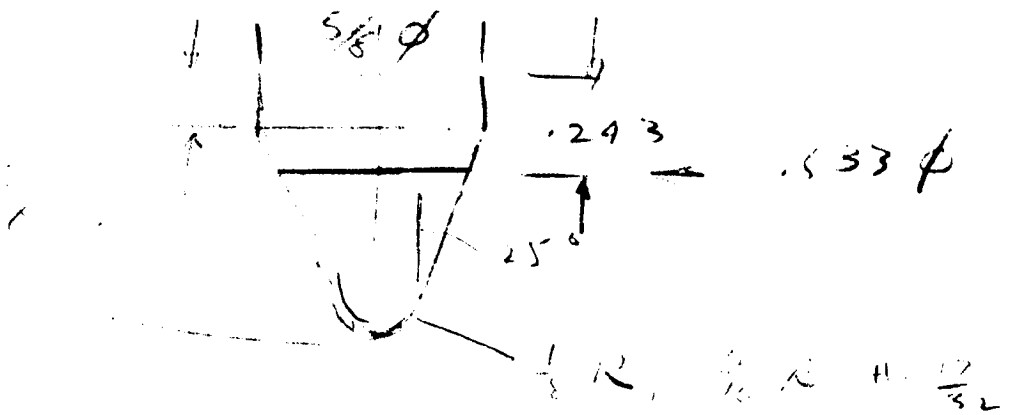

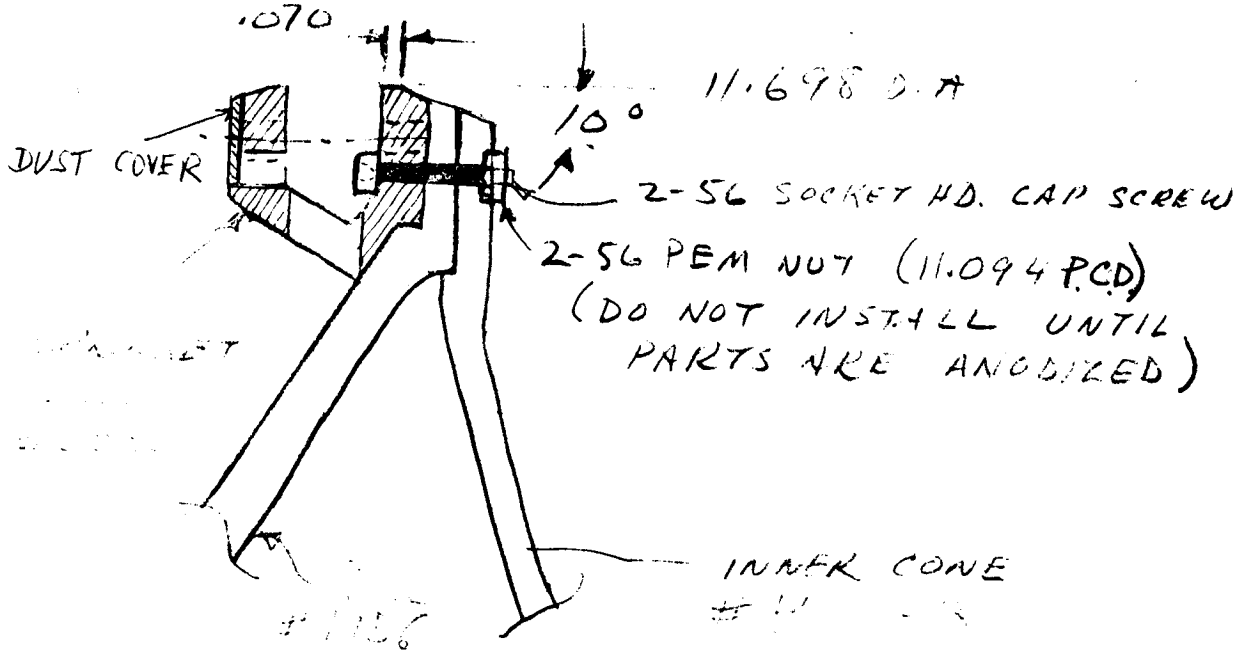

Fig. J-1 - Assembly Details of Sprocket Ring-Drive Drum Interface

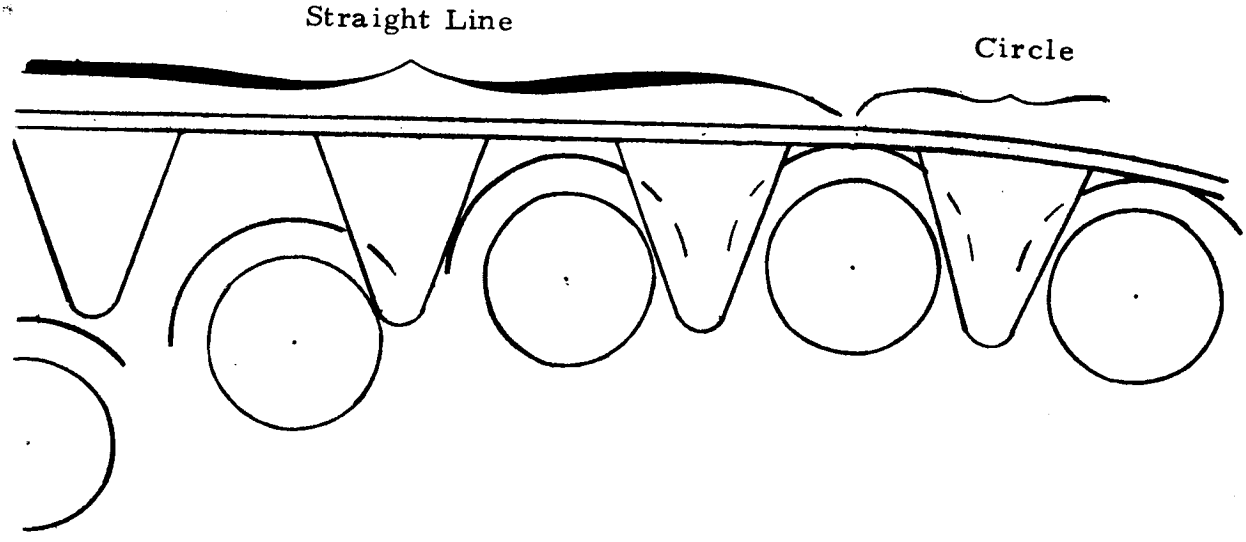

Fig. J-2 - Worst Case for Drive Lug Engagement: Loop Approaches Drive Drum in Straight Line which Defines Minimum Cone Angle of Drive Lugs for Safe Clearance. Calculation is given in Appendix I.

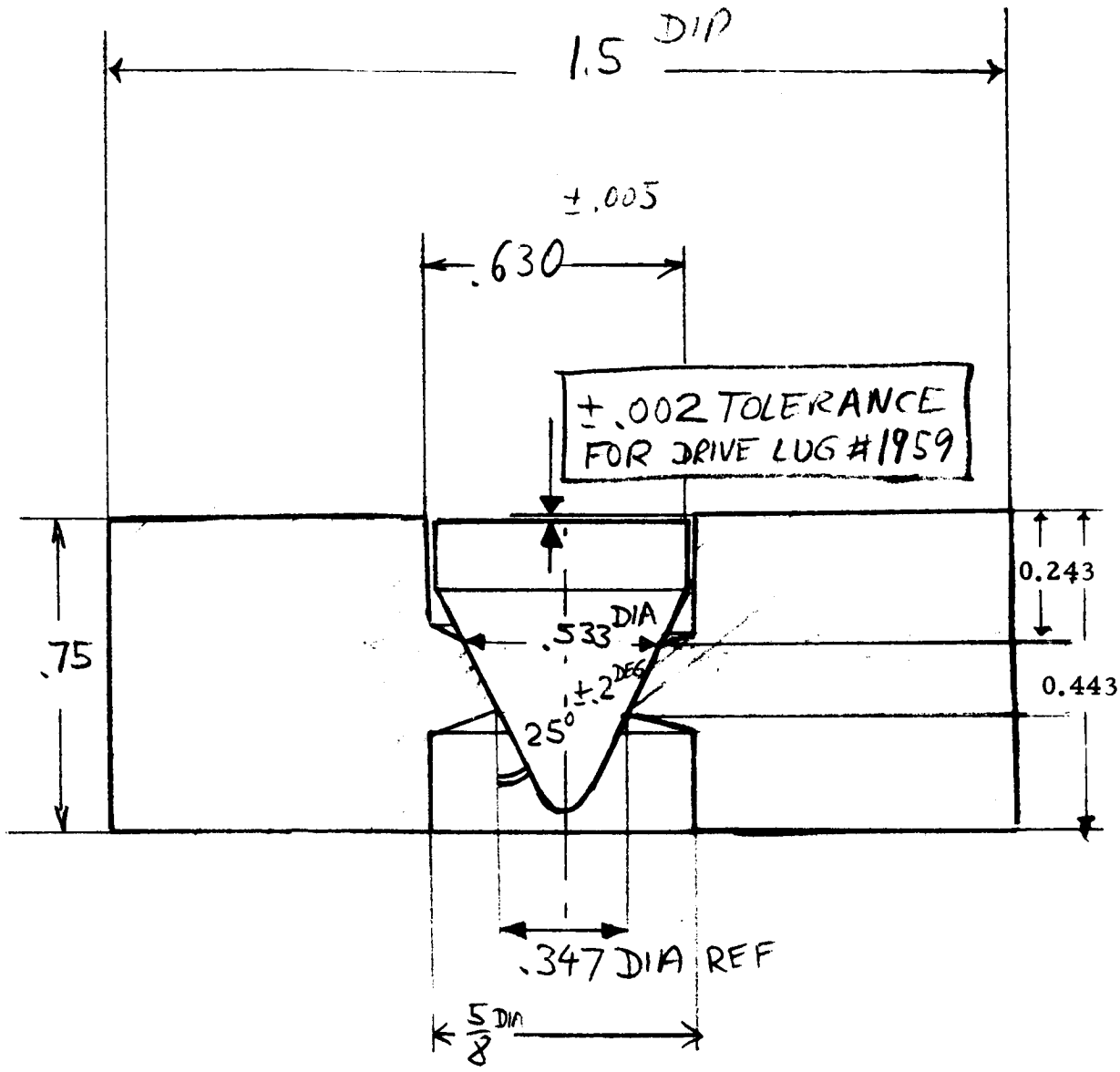

Fig. J-3 - Ring Gage for Drive Lug No. 1959 Quality Control

Appendix K

ANALYSIS OF FLEXURAL PIVOT LOADS

Appendix K

The loads acting on the roller bearings were predicted as follows:

Tangential Forces Due to Drive Torque:

Assumption: Minimum of two rollers per drum share drive torque (one per side or two on one side only)

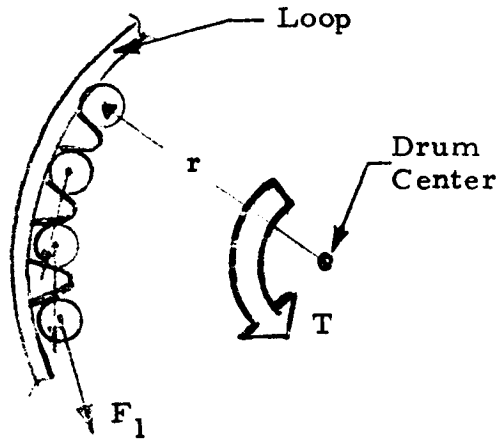

Maximum Torque per Drum:

$T \leq 41$ Nm (30 ft-lb)

$r = 0.143$ m

Tangential Force per Roller:

$$F_1 \leq \frac{T}{2r} = 144 \text{ N } (32 \text{ lb})$$

Flexural pivots have highest strength for loads that tend to stretch the springs (V_t in Fig. K-1). Strength is lowest if the springs are under compression (V_c). The best orientation on the drive drum is therefore as shown in Fig.

V_c = Compression Load

Load applied to one section of cantilever or center section of double end that tends to compress the spring.

V_t = Tension Load

Load applied to one section of cantilever or center section of double end that tends to stretch springs.

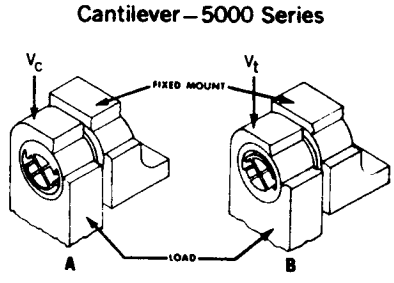

Fig. K-1 - Basic Loading Conditions for Cantilevered Flexural Pivots. Two cantilevered pivots of standard stock size are required per planetary roller.

Appendix L

INSTALLATION INSTRUCTIONS FOR BENDIX FLEXURAL PIVOTS

Appendix L

Materials Required per replaced pair:

Name	PN	Quantity
Bendix Flexure	5006-600	2
Locktite Retaining Compound	75	
Locktite Primer	N	
Dust Seal	Lockheed 72111-29	2

Refer to LMSC Dwg. No. 72111 - Drum Drive System Details & Assy. ELMS.

The steps required in removing and replacing a Bendix flexure pair are as follows:

1. Remove 72111-23 cover, Item No. 45 on drawing number 72111, and sprocket ring (Item 2 below).
2. Heat sprocket ring, PN 2005, Item 44 on drawing number 72111, locally and press out pair of defective flexures, PN 5006-600. The temperature at which the retaining compound fails begins
3. about 400°F.
3. Discard old flexures if defective.
4. Discard old dust seals, LMSC PN 72111-29 if defective.
5. Clean the following surfaces with a chlorinated solvent such as 1, 1, 1-trichloroethane.
   a. Outside surface of 2 Bendix flexures, PN 5006-600.
   b. The inside surface and the faces of the planetary roller, LMSC PN 2006, Item 46 on Dwg. 72111.
   c. Inside surface of the holes in sprocket ring.

6. Apply any common glue to attach one dust seal to each side of the planetary roller, keeping the smooth side of the seal out.

7. Spray Locktite primer N on surfaces to be bonded.

8. Apply a very thin film of Locktite 75 retaining compound to surfaces to be joined. Assemble immediately.

9. Orient as shown in Fig. 3-4 with the outside edge of the flexure flush with the outside edge of the sprocket ring (Fig. 3-5).

10. Heat cure for 30 seconds at 250 to 300°F.

11. Reassemble cover, PN 72111-23, Item 45 on Dwg. 72111.

Manufacturer Recommendations:

INSTALLATION AND HANDLING PRECAUTIONS

1. Do not touch cross flexures with tools or probing instruments.
2. Do not apply excessive force to install pivots in mounting holes. Slip fits should be used wherever possible.
3. Do not deflect beyond normal intended operating angle where hysteresis is important.
4. When tightening mounting screws be sure that wrench or screwdriver forces are not transmitted through flex pivot from its fixed to movable member or vice versa.
5. Where instrument cleanliness or sensitive operation characteristics are specified, protective oil should be removed by normal [illegible] cleaning solvents.
6. Installation should provide for [illegible] travel stops external to the flexure.
7. Consult technical publication for proper orientation relative to applied forces.
8. Mounting should not permit the unrestricted application of moments to the flexure through the cylindrical axis. Consult manufacturer for [illegible].
9. Under no conditions should an attempt be made to deflect a flex pivot beyond the maximum rated deflection angle.

Compliance with the above precautions will insure maximum life and best performance of this product.
For Bendix Corporation's Flight Power Division, 21 Seward Avenue, Utica, New York 13503

Appendix M

ELASTIC LOOP SUSPENSION ARM TORSIONAL AND BENDING STIFFNESS

Appendix M

FIRST GENERATION ELMS:

Open Section

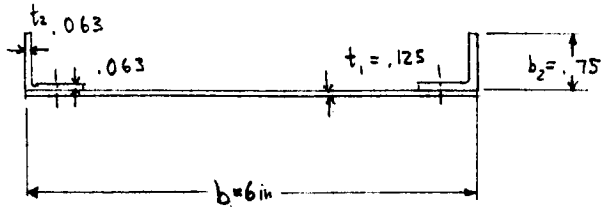

torsional constant $J_t = \frac{1}{3} \sum b_i t_i^3$

i	t_i	t_i^3	b_i	$t_i^3 b_i$
1	.125	.00195	4.5	.00877
2	.065	.000275	1.5	.00041
3	.190	.00687	1.5	.01040
				.01958

$$J_t = \frac{1}{3} (.01958) = .00653 \text{ in}^4$$

NEW DESIGN:
Closed Section

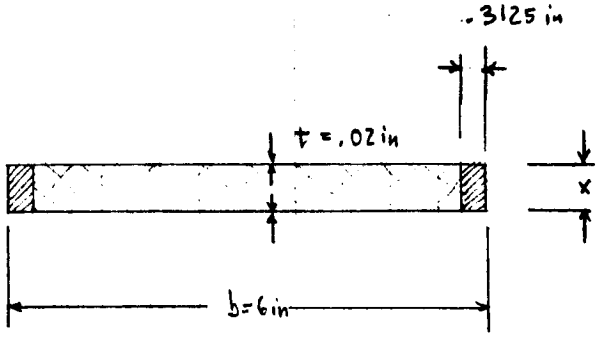

torsional constant $J_t = \dfrac{4 A_e^2}{\oint \frac{ds}{t}}$

$$4 A_e^2 = 4(6 - .3125)^2 x^2 = 4(32.3) x^2 = 129.2 x^2$$

5.6875

$$\oint \frac{ds}{t} = \frac{2(5.6875)}{.02} + \frac{2x}{.3125} =$$

$$= 568.75 + 6.4x$$

$$J_t = .00653 \text{ in}^4 = \frac{129.2 x^2}{568.75 + 6.4x} = \frac{x^2}{4.4 + .0495x}$$

quadratic equation

$$x^2 - (4.4 + .0495x)(.00653) = 0$$

$$x^2 - .323 \times 10^{-3} x - .0287 = 0$$

$$x_{1,2} = \frac{1}{2}(.323 \times 10^{-3}) \pm \sqrt{\frac{1}{4}(.323 \times 10^{-3})^2 + .0287}$$

$$x \approx .170 \text{ in}$$

$$1.5\, J_t = .00980 \text{ in}^4 = \frac{x^2}{4.4 + .0495x}$$

$$x^2 \approx \sqrt{(4.4)(.00980)^1} = \sqrt{.0431^1}$$

$$\underline{x \approx .208 \text{ in}}$$

LMSC-HREC D225600-II

ELMS Suspension Arm Stiffness

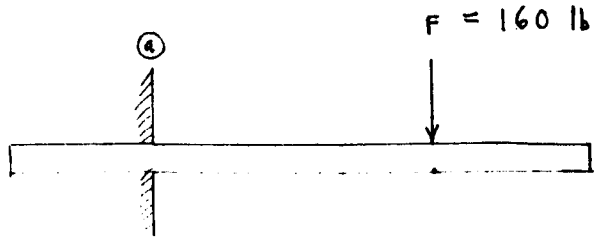

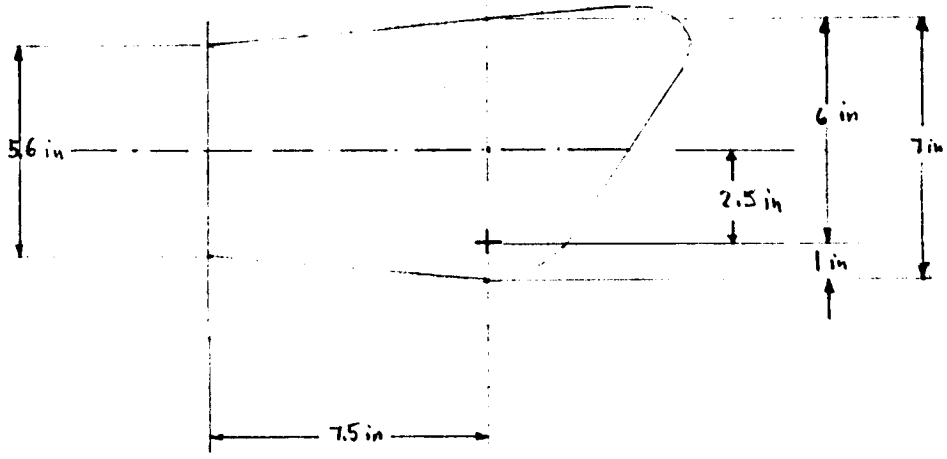

bending moment @ @

$M_B = 160 \times 7.5 = 1200$ in-lb

twisting moment @ @

$M_T = 160 \times 2.5 = 400$ in-lb

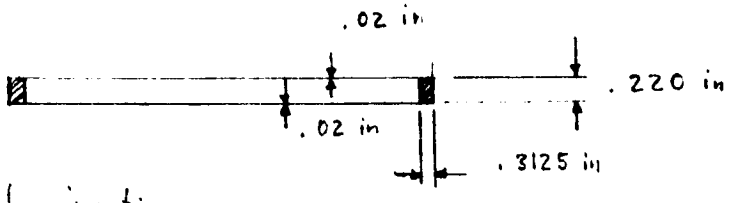

moment of inertia

$$I = 2\left[\frac{(.3125)(.200)^3}{12} + \frac{(.02)(5.6)(.200)^2}{2}\right] =$$

K R. Leimbach 6-23-71

ELMS Suspension Arm Stiffness

$$I = \frac{(.3125)(.008)}{6} + (.01)(5.6)(.04) =$$

$$= .417 \times 10^{-3} + 2.240 \times 10^{-3} = 2.657 \times 10^{-3} \text{ in}^4$$

check stress from bending moment

$$\sigma_{max} = \frac{My}{I} = \frac{(1200 \text{ in-lb})(.100 \text{ in})}{2.657 \times 10^{-3} \text{ in}^4} =$$

$$= 45.2 \times 10^3 \text{ psi} > \sigma_{yield}$$

ELMS Suspension Arm Stiffness

increase to .250 in.

$$I = 2\,\frac{(.3125)(.250)^3}{12} + \frac{(.02)(5.6)(.250)^2}{2} =$$

$$= \frac{(.3125)(.0156)}{6} + (.01)(5.6)(.0625) =$$

$$= .812 \times 10^{-3} + 3.500 \times 10^{-3} = 4.312 \times 10^{-3}\ in^4$$

check stress from bending moment

$$\underline{\sigma_{max}} = \frac{My}{I} = \frac{(1200\ in\text{-}lb)(.125\ in)}{4.312 \times 10^{-3}\ in} = \underline{34.7\ ksi}$$

check shear stress from twisting moment

shear flow $T = \dfrac{M_t}{2A_e}$

enclosed area $A_e = (5.6)(.250) = 1.40\ in^2$

$$T = \frac{400\ in\text{-}lb}{(2.)(1.40\ in^2)} = 143\ lb\text{-}in^{-1}$$

$$\underline{max\ \tau} = \frac{T}{t_{min}} = \frac{143\ lb\text{-}in^{-1}}{.02\ in} = \underline{7.2\ ksi}$$

Appendix N

ELMS DAMPING REQUIREMENTS

	NAME	DATE	LOCKHEED MISSILES & SPACE COMPANY A GROUP DIVISION OF LOCKHEED AIRCRAFT CORPORATION	Page 1	TEMP.	PERM
Prepared	W. Tr.					
Checked			TITLE Appendix N	Model		
Approved				Report No.		

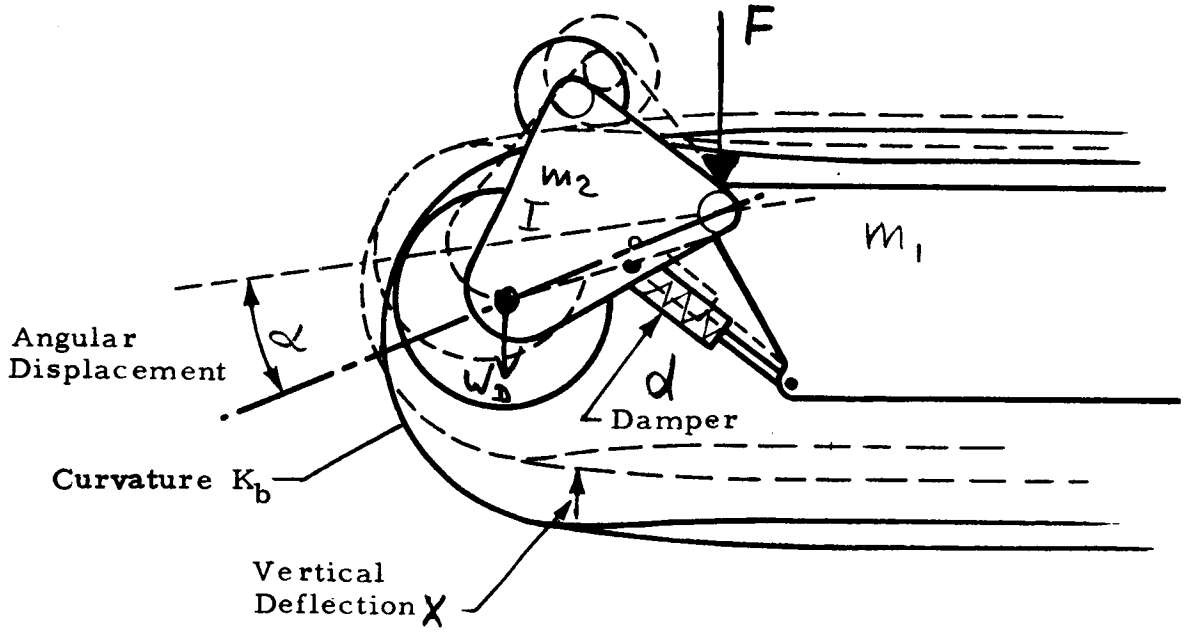

Assume a linear relation

$$\alpha \approx C X$$

Loopwheel Spring Characteristic (Appendix B)

$$F = \pi b B K_b^{(1)2}\left[1 - \frac{K_b^{(0)} + \nu\left(K_b^{(1)} - K_b^{(0)}\right)}{K_b^{(1)}}\right]$$

where $B = \dfrac{E t^3}{12(1-\nu^2)}$

Local Spring Rate for nominal deflection X_N:

$k_1 = \left(\dfrac{dF}{dx}\right)_N$ from plot 2-6

(A) Simplified Analysis assuming negligible I_{Arm}, k_2 and $m_2 << m_1$, where $m = m_1 + m_2$:

Equation of vertical motion

$$m\ddot{x} + a d \dot{x} + k_1 x = 0$$

$$\ddot{x} + \frac{ad}{m}\dot{x} + \frac{k_1}{m} x = 0$$

$$\omega_o = \frac{k_1}{m}$$

Damping coefficient

$$\zeta = \frac{ad}{2\omega_o m}$$

$$\boxed{d_{opt} = \frac{2\omega_o m}{a}\zeta_{opt}}$$

ω_o Natural Frequency (rad/sec) (Undamped)

Prepared	NAME	DATE	LOCKHEED MISSILES & SPACE COMPANY A GROUP DIVISION OF LOCKHEED AIRCRAFT CORPORATION	Page 3 TEMP PERM
Checked			TITLE	Model
Approved				Report No.

Numerical Data:

Ratio $a = \frac{\alpha}{x} = \frac{17 \text{ Deg}}{8.6 \text{ cm}} = 1.98 \frac{\text{Deg}}{\text{cm}}$

Elastic Loop: $K_{b_{NOM}}^{(1)} = .053 \text{ cm}^{-1}$; $b = 38.8 \text{ cm}$; $t = 1.6 \text{ mm}$

$E = 10.3 \cdot 10^6 \text{ N/cm}^2$; $\nu = .3$

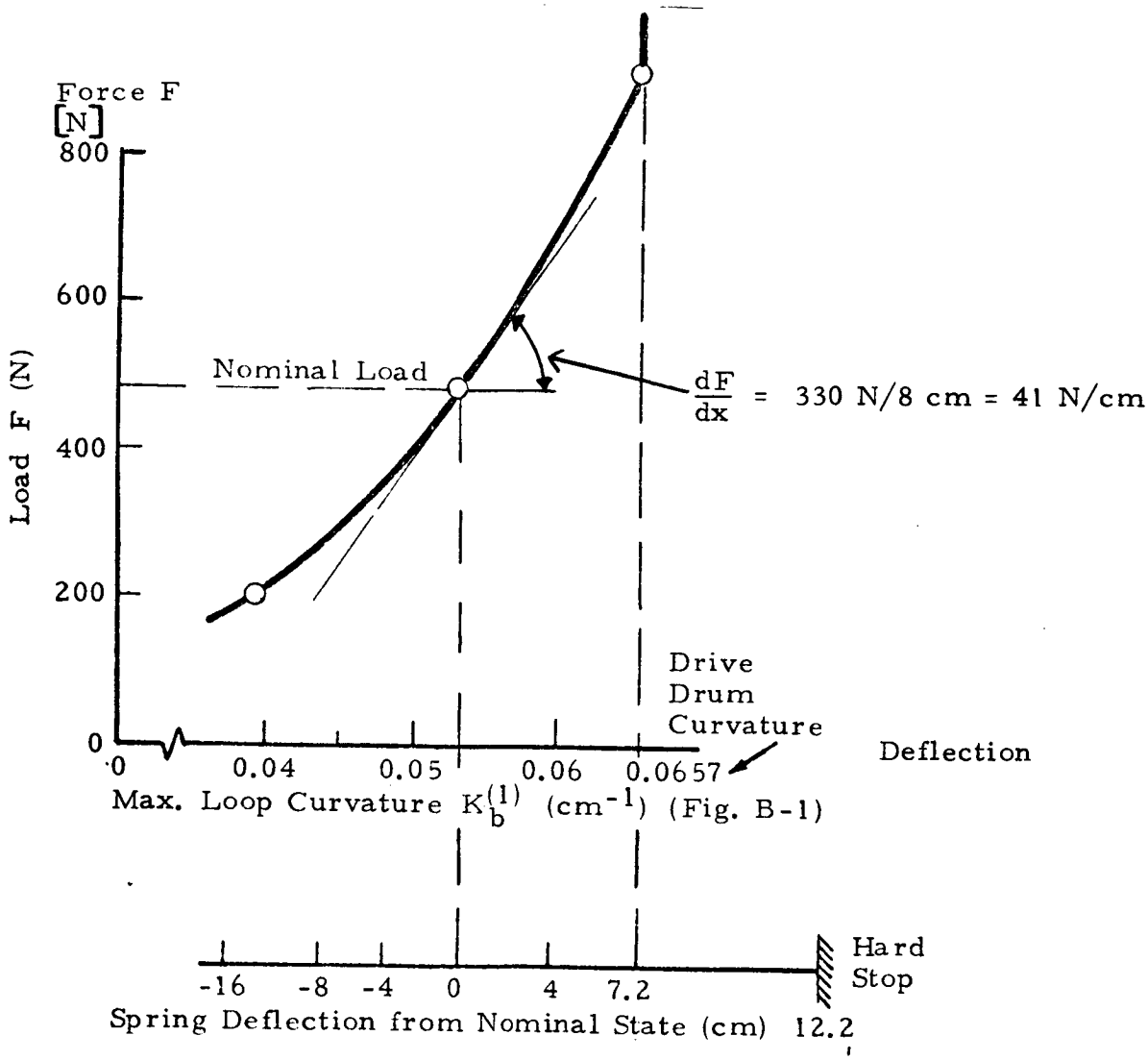

Prepared	NAME	DATE	LOCKHEED MISSILES & SPACE COMPANY A GROUP DIVISION OF LOCKHEED AIRCRAFT CORPORATION	Page 4	TEMP	PERM
Checked			TITLE	Model		
Approved				Report No.		

$$k_1 = \frac{dF}{dx} = \frac{330}{8}\ \frac{N}{cm} = 41\ N/cm$$

Nominal Mass per half Loop: $m = \frac{241\ N}{9.81\ m/s^2} = 24.6\ Kg$

$$\omega_0 = \sqrt{\frac{k_1}{m}} = \sqrt{\frac{4100}{24.6}} = 12.9\ \frac{1}{s} = 2.06\ Hz$$

$167\ 1/s^2$

[In a lunar flight version the mass would be 6 times greater. Thus $\omega_{0_{Moon}} = \frac{\omega_0}{\sqrt{6}} = .41\omega_0$
$= .8\ Hz$]

Required Damper for $\zeta_{opt} = .7$:

$(1/s)$ (Ns^2/m)

$$d = \frac{2\omega_0 m}{a}\zeta_{opt} = \frac{2 \cdot 12.9 \times 24.6}{198\ (°/m)} .7$$

$$= 2.24\ \frac{N}{Deg/sec}$$

Max. Expected Rate: $\dot{x} \leq 50$ Deg/sec

Max. Damper Force: $F_D \leq 112\ N$ (25 lb)

Appendix O

SELECTION OF TRAILER SPRINGS TO SIMULATE FLEXIBLE JOINT

ELMS

TRAILER SPRINGS

REF. IMPROVED ELMS SPRING & STRESS DATA.

FOR TOTAL WT (F) OF 100 LB., DEFLN = 4.5"

FOR 1° PITCH, SPRING TRAVEL:

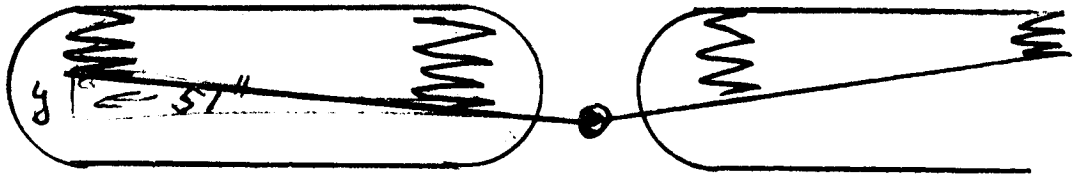

.01745

$y = 51 \sin 1° = .89$

DEFL'N @ EACH END = ±.45"

RATE = $\frac{50\#}{.45}$ = 111 #/"

TORSIONAL MOMENT = 50 # (51")

= 2550 IN-LB

MOMENT ON TRAILER LINK:

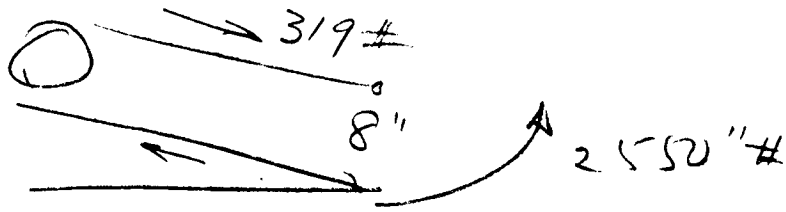

$\frac{2550"\#}{8"}$ = 319 LB

LOAD/SIDE = 319/2 = 160 LBS.

1° PITCH = 8(.01745) = .14 IN DEFLN

160# / .14" = 1140#/"

GDR 9-9-71

ELMS SPRING

FROM MIL STD 29A P. 73

2" O.D. .250 ϕ WIRE

351 # / .344" = 1020 #/"

END LOAD ON TUBE (LWR) = 160 LB.

TUBE ℓ = 24" 1.0 O.D. x .065

$$\ell/\rho = \frac{24}{1.331} = 72.4$$

Use Column Curve ρ = 51

F_c = 18,500 psi. AVCO V 6.1.5-2

$$f_c = \frac{160}{.1909} = 840 \text{ psi.} \quad \text{O.K.}$$

LOAD = 388# (REF P3)

.063 x 1½ x 2"

$$\frac{L}{\rho} = \frac{2}{\sqrt{\frac{I}{A}}} = \frac{2.000}{.0182} \qquad \sqrt{\frac{.0000313}{.095}} = \sqrt{.00033} = .0182$$

$$I = \frac{bh^3}{12} = \frac{1.5 \times .063^3}{12} = .0000313 \qquad A = .063 \times 1.5 = .095$$

$$L' = \frac{L}{\sqrt{4}} = 1$$

$$\frac{L'}{\rho} = 55$$

$$f_c = \frac{388}{.095} = 4080 \text{ psi}$$

f_{cr} = 24,000 psi

.250 $\frac{351}{.346}$ = 1020

.312 $\frac{661}{.295}$ = 2210

.281 $\frac{509}{.295}$ = 1700

.312 $\frac{710}{.256}$ = 2770 #/"

Coarse Spring Rate. (Ref. W.T. 9-13-11)

2 R = 2 (1140) = 2280 #/"

5/16 SPRING, 2" O.D. @ 2770 #/" selected

±6° TRAVEL BY ADJUSTMENT - 11 RATE

TURNS 1.75 LONG.

SPRING DEFLN: .14" FOR 1° PITCH

USE .50" (3½°)

4 TURNS @ 1/8 GAP

Defln/coil = $\frac{.256}{710}$ = .000361 "/#

Load @ solid = $\frac{4 \times .125"}{.000361"}$ = 1385. #

$f_c = \frac{1385}{.1909}$ = 7260 PSI

Fc = 185000 Ref. sh 2

Load @ .14" defln = $\frac{.14"}{.000361}$ = 388 #

Stress = 100 000 $\frac{388}{710}$ = 54,700 PSI

Appendix P

RING SENSOR DESIGN FOR DRAWBAR PULL MEASUREMENT

Prepared	NAME K.R. Leimbach	DATE 11-30-71	LOCKHEED MISSILES & SPACE COMPANY A GROUP DIVISION OF LOCKHEED AIRCRAFT CORPORATION	Page	TEMP 1	PERM
Checked			TITLE Lead Measuring Device	Model		
Approved				Report No.		

Appendix P

$$p = r\left(1 - \cos\frac{\alpha}{2}\right)$$

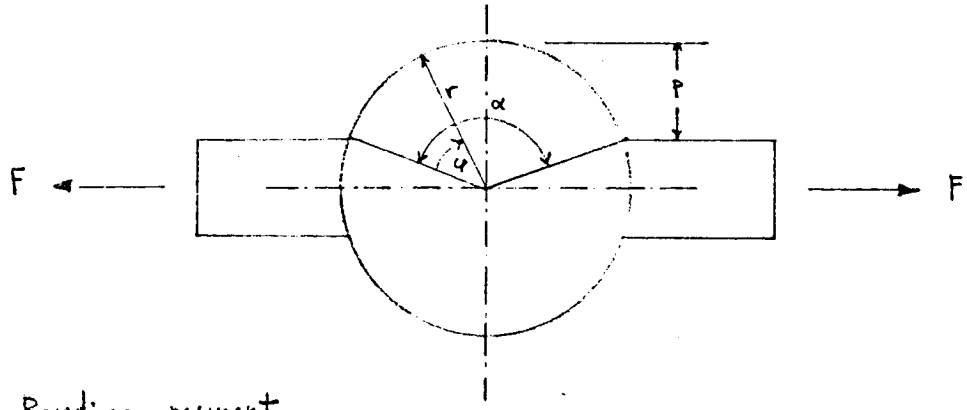

1. Bending moment.

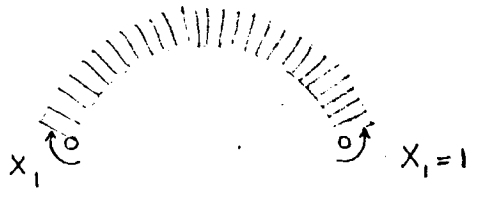

$$M_1(\varphi) = 1$$

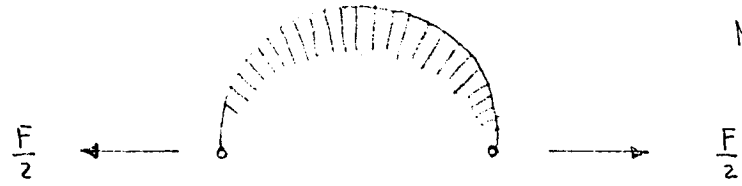

$$M_L(\varphi) = \frac{F}{2} p \sin\frac{\pi\varphi}{\alpha}$$

$$E I \delta_{11} = \int_0^{\alpha} M_1^2 \, r \, d\varphi = r\varphi$$

$$E I \delta_{1L} = \int_0^{\alpha} M_1 M_L \, r \, d\varphi = \frac{Fpr}{2} \int_0^{\alpha} \sin\frac{\pi\varphi}{\alpha} \, d\varphi = \frac{Fpr\alpha}{\pi}$$

$$X_1 = -\frac{\delta_{1L}}{\delta_{11}} = -\frac{Fpr\alpha}{\pi} \frac{1}{r\alpha} = -\frac{Fp}{\pi}$$

$$M(\varphi) = M_L(\varphi) + X_1 M_1(\varphi) = \frac{Fp}{2}\left(\sin\frac{\pi\varphi}{\alpha} - \frac{2}{\pi}\right)$$

Prepared	NAME K. R. Leimbach	DATE 11-30-71	LOCKHEED MISSILES & SPACE COMPANY A GROUP DIVISION OF LOCKHEED AIRCRAFT CORPORATION	Page	TEMP 2	PERM
Checked			TITLE Load Measuring Device	Model		
Approved				Report No.		

$$M(0) = M(\alpha) = -\frac{F_p}{2}\left(\frac{2}{\pi}\right) = -.64\,\frac{F_p}{2}$$

$$M\left(\frac{\alpha}{2}\right) = \frac{F_p}{2}\left(1 - \frac{2}{\pi}\right) = +.32\,\frac{F_p}{2}$$

2. Stresses (approximate)

$$\underline{\sigma_{max}} = \frac{F}{2bh} \pm \frac{6M(0)}{bh^2} = \frac{F}{2bh} \pm \frac{6(-.64)\frac{F_p}{2}}{bh^2}$$

$$= .5\,\frac{F}{bh} \mp 1.92\,\frac{F_p}{bh^2}$$

3. Deflection from bending in the direction of F

$$\bar{M} = \frac{P}{2}\sin\frac{\pi\varphi}{\alpha}$$

$$EI\,\delta_l = \int_0^{\alpha} M\bar{M}\,r\,d\varphi =$$

$$= \frac{Fp^2}{4}\,r \int_0^{\alpha}\left(\sin^2\frac{\pi\varphi}{\alpha} - \frac{2}{\pi}\sin\frac{\pi\varphi}{\alpha}\right)d\varphi$$

$$= \frac{Fp^2}{4}\,r\,\frac{\alpha}{\pi}\left[\frac{\pi}{\alpha}\,\frac{\alpha}{2} - \frac{4}{\pi}\right] =$$

$$= \frac{Fp^2 r\alpha}{4\pi}\left[\frac{\pi}{2} - \frac{4}{\pi}\right]$$

$$\delta_l = \frac{1}{EI}\,\frac{Fp^2 r\alpha}{4\pi}\left[\frac{\pi}{2} - \frac{4}{\pi}\right]$$

Prepared	NAME K R Leimbach	DATE 11-30-71	LOCKHEED MISSILES & SPACE COMPANY A GROUP DIVISION OF LOCKHEED AIRCRAFT CORPORATION	Page	TEMP. 3	PERM
Checked			TITLE Load Measuring Device	Model		
Approved				Report No		

4. Numerical results

(a) max pull $F_p = 120$ lb

(b) max moment

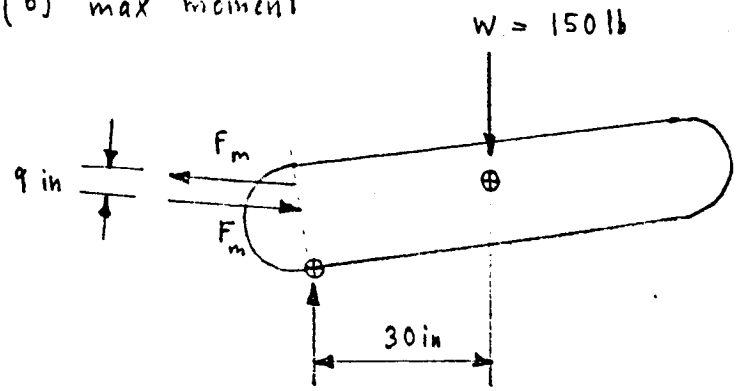

$$F_m = \frac{150 \times 30}{9} = 500 \text{ lb}$$

(c) total force $F = F_p + F_m = 120 + 500 = 620$ lb

(e) dimensions of the device

$r = 1.0$ in
$b = 0.5$ in
$p = 0.75$ in

$E = 10^7$ lb/in^2 (Aluminum)

want h, max ε, δ_L

$$\cos\frac{\alpha}{2} = 1 - \frac{p}{r} = 1. - \frac{.75}{1.0} = .25$$

$$\frac{\alpha}{2} = 1.32$$

$$\alpha = 2.64$$

Prepared	NAME K. R. Leimbach	DATE 11-30-71	LOCKHEED MISSILES & SPACE COMPANY A GROUP DIVISION OF LOCKHEED AIRCRAFT CORPORATION	Page	TEMP 4	PERM
Checked			TITLE Load Measuring Device	Model		
Approved				Report No.		

let $h = .2$ in

$$\sigma_{max} = .5\,\frac{620}{(.5)(.2)} + 1.92\,\frac{(620)(.75)}{(.5)(.04)} =$$

$$= 3100 + 44700 = 47800\ \text{lb/in}^2 < 53\,000$$

O.K.

$$\varepsilon_{max} = \frac{\sigma_{max}}{E} = \frac{47\,800}{10^7} = .0048\ \frac{\text{in}}{\text{in}} = 4800\ \frac{\mu\,\text{in}}{\text{in}}$$

$$I = \frac{bh^3}{12} = \frac{(0.5)(.008)}{12} = 3.33 \times 10^{-4}$$

$$\delta_L = \frac{1}{(10^7)(3.33 \times 10^{-4})}\,\frac{620\,(.75)^2\,(1.0)\,(2.64)}{4\,\pi}\left(\frac{\pi}{2} - \frac{4}{\pi}\right) =$$

$$= \frac{620}{3.33 \times 10^3}\,(.118)(1.57 - 1.27) =$$

$$= \frac{620}{3.33 \times 10^3}\,(.0354) =$$

$$= .0066\ \text{in}$$

Appendix Q

REFERENCES

Appendix Q
REFERENCES

1. Costes, N. C., W. D. Carrier, J. K. Mitchell, and R. F. Scott, "Apollo 11 Soil Mechanics Investigation," NASA SP-214, Sec. 4, Apollo Preliminary Science Report, 1969.

2. Scott, R. J., W. D. Carrier, N. C. Costes, and J. K. Mitchell, "Mechanical Properties of the Lunar Regolith - Apollo 12 Preliminary Science Report," NASA SP-235, 1970, pp. 161-188.

3. Costes, N. C., G. T. Cohron, and D. C. Moss, "Cone Penetra-Resistance Test – An Approach to Evaluating the In-Place Strength and Packing Characteristics of Lunar Soils," Proc. of the Second Lunar Science Conf., Vol. 3, 1971, pp. 1973-1987.

4. Mitchell, J. K., L. G. Bromwell, W. D. Carrier, N. C. Costes, and R. F. Scott, "Soil Mechanics Experiment," NASA SP-272, Sec. 4, Apollo 14 Preliminary Science Report, 1971.

5. Freitag, D. R., A. J. Green, K.-J. Melzer and N. C. Costes, "Wheels for Lunar Vehicles," Proceedings of Off-Road Mobility Symposium, International Society for Terrain Vehicle Systems (ISTVS) - TRW Systems, El Segundo, Calif., 1970.

6. Green, A. J., and K.-J. Melzer, "Performance of the Boeing LRV Wheels in a Lunar Soil Simulant; Effect of Wheel Design and Soil," TR M-71-10, Report 1, U. S. Army Engineer Waterways Experiment Station, Corp of Engineers, Vicksburg, Miss., 1971.

7. Melzer, K.-J., "Performance of the Boeing LRV Wheels in a Lunar Soil Simulant, TR M-71-10, Report 2, U. S. Army Engineer Waterways Exe Experiment Station, Corp of Engineers, Vicksburg, Miss., 1972.

8. Mitchell, J. K., R. F. Scott, W. N. Houston, N. C. Costes, W. D. Carrier, and L. G. Bromwell, "Mechanical Properties of Lunar Soil: Density, Porosity, Cohesion, and Angle of Internal Friction," Proceedings, Third Lunar Science Conference, Houston, Texas, 10-13 January 1972.

9. Costes, N. C., J. E. Farmer, E. B. George, "Mobility Performance of the Lunar Roving Vehicle Terrestrial Studies – Apollo 15 Results," Proceedings of the 4th International Conference of the International Society for Terrain-Vehicle Systems, Stockholm, Sweeden, 1972.

10. Mitchell, J. K., L. G. Bromwell, W. D. Carrier, N. C. Costes, W. N. Houston, and R. F. Scott, "Soil Mechanics Experiment — Apollo 15 Preliminary Science Report," NASA SP 289, Cahpter 7, 1972.

11. Lessem, A. S., "Operations and Maintenance Manual for a Scale-Model Lunar Roving Vehicle," Misc. Paper M-72-3, U. S. Army Engineer Waterways Experiment Station, Corp of Engineers, Vicksburg, Miss., April 1972.

12. Melzer, K.-J., and A. J. Green, "Performance Evaluation of a First-Generation Elastic Loop Mobility System," TR M-71-1, U. S. Army Engineer Waterways Experiment Station, Vicksburg, Miss., May 1971.

13. W. Trautwein, "Elastic Loop with Uniform Longitudinal Ground Pressure Distribution," Disclosure of Invention No. D-03-5917, Lockheed Missiles & Space Company, Huntsville, Ala., 3 May 1971.

14. Chang, J. C., "Fabrication Study of Beta III Titanium Alloy Sheet and Foil," WESTEC Paper W 71-23.1, Los Angeles, Calif., March 1971.

15. Technical Proposal, "Produce an Improved Single Elastic Loop Mobility System and Submit for Testing," LMSC-HREC D225075, June 1971.

16. Jones, C. S., Jr., B. J. Doran, and F. J. Nola, "Traction Drive System Design Considerations for a Lunar Roving Vehicle," NASA TMX-53972, November 1969.

17. Jones, C. S., Jr., and F. J. Nola, "Mobility Systems Activity for Lunar Rovers at MSFC," NASA TMX-64623, September 1971.